

Award Number:

W81XWH-08-1-0358

TITLE:

Multiadaptive Plan (MAP) IMRT to Accommodate Independent Movement of the Prostate and Pelvic Lymph Nodes

PRINCIPAL INVESTIGATOR:

Ping Xia, Ph.D

CONTRACTING ORGANIZATION:

Cleveland Clinic~|^ää\↔~^,
Cleveland, OH 44195

REPORT DATE:

June 2013

TYPE OF REPORT:

Final Report

PREPARED FOR: U.S. Army Medical Research and Materiel Command
Fort Detrick, Maryland 21702-5012

DISTRIBUTION STATEMENT: (Check one)

- ☒ Approved for public release; distribution unlimited
- ☐ Distribution limited to U.S. Government agencies only;
report contains proprietary information

The views, opinions and/or findings contained in this report are those of the author(s) and should not be construed as an official Department of the Army position, policy or decision unless so designated by other documentation.

REPORT DOCUMENTATION PAGE

Form Approved
OMB No. 0704-0188

Public reporting burden for this collection of information is estimated to average 1 hour per response, including the time for reviewing instructions, searching existing data sources, gathering and maintaining the data needed, and completing and reviewing this collection of information. Send comments regarding this burden estimate or any other aspect of this collection of information, including suggestions for reducing this burden to Department of Defense, Washington Headquarters Services, Directorate for Information Operations and Reports (0704-0188), 1215 Jefferson Davis Highway, Suite 1204, Arlington, VA 22202-4302. Respondents should be aware that notwithstanding any other provision of law, no person shall be subject to any penalty for failing to comply with a collection of information if it does not display a currently valid OMB control number. **PLEASE DO NOT RETURN YOUR FORM TO THE ABOVE ADDRESS.**

1. REPORT DATE June 2013		2. REPORT TYPE Final Report		3. DATES COVERED (From - To) 1 May 2008-12 May 2013	
4. TITLE AND SUBTITLE Multi-Adaptive Plan (MAP) IMRT to Accommodate Independent Movement of the Prostate and Pelvic Lymph Nodes				5a. CONTRACT NUMBER W81XWH-08-1-0358	
				5b. GRANT NUMBER W81XWH-08-1-0358	
				5c. PROGRAM ELEMENT NUMBER	
6. AUTHOR(S) Ping Xia Email: xiap@ccf.org				5d. PROJECT NUMBER	
				5e. TASK NUMBER	
				5f. WORK UNIT NUMBER	
7. PERFORMING ORGANIZATION NAME(S) AND ADDRESS(ES) Cleveland Clinic Foundation, Cleveland, OH 44195;				8. PERFORMING ORGANIZATION REPORT NUMBER	
9. SPONSORING / MONITORING AGENCY NAME(S) AND ADDRESS(ES) U.S. Army Medical Research and Material Command Fort Detrick, Maryland 21702-5012				10. SPONSOR/MONITOR'S ACRONYM(S)	
				11. SPONSOR/MONITOR'S REPORT NUMBER(S)	
12. DISTRIBUTION / AVAILABILITY STATEMENT Approved for public release; distribution unlimited					
13. SUPPLEMENTARY NOTES					
14. ABSTRACT: Because of the challenge of the independent movement of the prostate relative to the lymph nodes, this research is to develop a novel method using multi-adaptive plan (MAP) IMRT to accommodate independent movement of the two targeted tumor volumes. In this project, we evaluated two adaptive strategies: strategy A creates a set of IMRT plans individually optimizing on a series of possible prostate positions in the planning CT; and strategy B creates a set of multi-adaptive plans by dynamically adjusting the radiation apertures to accommodate the daily position of the prostate. Using dual imaging registration method, we found that the bi-directional prostate movement in relative to the pelvic lymph nodes, particular in anterior-posterior and superior-inferior directions, must be considered with strategy A, which increases the number of prepared IMRT plans. Using implanted markers as a surrogate for the location of the prostate gland may mis-interpret the rotation of the gland and a special caution is needed when a large rotation is detected. The prostate rotation can be compensated with translational shifts of the radiation portals. With current clinical planning margins of 8mm/6mm posterior to the prostate and 5 mm to the pelvic lymph nodes, the MLC tracking strategy is not necessary. Further reduction in the planning margins to the both targets may require MLC tracking method or real time planning.					
15. SUBJECT TERMS : Adaptive Radiotherapy, Image guided Radiotherapy, Prostate cancer, Pelvic Lymph nodes					
16. SECURITY CLASSIFICATION OF:			17. LIMITATION OF ABSTRACT UU	18. NUMBER OF PAGES 15	19a. NAME OF RESPONSIBLE PERSON USAMRMC
a. REPORT UU	b. ABSTRACT UU	c. THIS PAGE UU			19b. TELEPHONE NUMBER (include area code)

Standard Form 298 (Rev. 8-98)
Prescribed by ANSI Std. Z39.18

PC073349 Final Report

November 13, 2009 to May 12, 2013

Contact Information

Ping Xia, Ph.D
Department of Radiation Oncology
Cleveland Clinic
9500 Euclid Ave/T28
Cleveland, OH 44195
Tel: 216-444-1398
Email: xiap@ccf.org

Table of Contents

	Page
Cover	1
SF 298	2
Table of Content	3
Introduction.....	4
Body.....	4
Task 1-1. Atlas-based Segmentation.....	4
Task 1-2. Pattern of prostate motion and effect of prostate rotation	5
Task 1-3: Magnitude of prostate motion during treatment	6
Task 2: Practical considerations for the novel multiple adaptive planning strategy.....	6
Task 3-1: Comparison of ideal MAP plans with MLC-MAP plans	7
Task 3-2: Progressive planning margin reductions.....	7
Task 3-3: Shifting the planned daily dose matrix	9
Task 3-4: Sensitivity and verification of MLC positions.....	10
Task 4-1: Overcome MLC leaf width limitations.....	11
Key Research Accomplishments	12
Reportable Outcomes.....	13
Abstracts:	13
Peer reviewed Publications	14
References:.....	14
Personnel supported by this award	15
Appendices.....	16
Appendix A-L	16

Introduction

It is estimated that 40% or more of patients with intermediate to high risk prostate cancer will relapse locally and systemically within five years after definitive radiotherapy. We hypothesize that this high rate of failure is partly due to under-irradiation of the pelvic lymph nodes. One of the challenges when using intensity modulated radiation (IMRT) in concurrent treatment of the prostate and the pelvic lymph nodes is the independent movement of the prostate relative to the lymph nodes, rendering the conventional iso-center shifting method of tracking prostate movement inadequate. The purpose of this research is to develop a novel method using multi-adaptive plan (MAP) IMRT to accommodate independent movement of the two targeted tumor volumes. In order to evaluate effectiveness of the MAP IMRT approach, we first established a baseline benchmark by creating a set of ideal IMRT plans for each patient based on the daily acquired mega-voltage (MV) or kilo-voltage (KV) cone beam computed tomography (CBCT), which represents the ideal case of daily online treatment planning. Based on this established benchmark, we can further evaluate two adaptive strategies: strategy A creates a set of IMRT plans individually optimizing on a series of possible prostate positions in the planning CT; and strategy B creates a set of multi-adaptive plans by dynamically adjusting the radiation apertures to accommodate the daily position of the prostate.

Body

Task 1-1. Atlas-based Segmentation

To validate MAP strategy, we recognized that task of delineating the prostate, rectum, and bladder on daily verification images can be time consuming. We sought to develop a computer assisted, atlas-based segmentation method for target volume delineation in whole pelvic IMRT for prostate cancer. This work was reported in the annual report of 2010. The manuscript has been published (1) and in Appendix A. Briefly, from an IRB approved registry at the University of California-San Francisco (UCSF), we selected planning data from 44 patients. From 44 planning CTs and the associated contours of the pelvic lymph nodes, prostate, rectum, and bladder, we constructed a general atlas. This atlas was then applied to a separate set of planning data from fifteen patients (also selected from an IRB approved registry of UCSF) to test utility of the atlas-based segmentation method. From the atlas, we found that there are significant inter-physician differences among the target volumes contoured by different physicians, particularly for pelvic lymph nodal volume. The atlas-based segmentation for pelvic lymph node delineation can serve as an initial guideline for physicians, potentially improving both consistency and efficiency in contouring.

Using the atlas-based segmentation, we found that the average overlap between the manually drawn and atlas-based contours for the prostate, pelvic lymph nodes, and rectum was 60%, 51%, and 64%, respectively. The volume differences were significant in the rectum and pelvic lymph nodes ($p = 0.049$ and $p = 0.016$, respectively); this was not true for the prostate. These results were also reported in the annual report of 2010.

Because the atlas-based auto-segmentation tool achieved a modest success (1), we hypothesized that a patient specific atlas-based segmentation tool can improve the overlap indices between the manually drawn and automatic contours significantly when compared to the general patient atlas method (1). The preliminary results of using the patient specific atlas were reported in in the

annual report of 2011, and a manuscript is in Appendix B. Using a planning CT as a single image-set atlas, we found the overlap indices were 86.9%, 82.9%, and 91.4% for the prostate, rectum, and bladder.

Task 1-2. Pattern of prostate motion and effect of prostate rotation

As reported in the annual reports of 2010 and 2011, we encountered large rotations of the prostates from eight patients when aligning the implanted markers as stated in SOW Task 1. Due to the limited soft tissue contrast in mega-voltage cone beam CT (MV- CBCT), the source of the rotation such as the migration of the markers or a true rotation of the prostate, could not be determined. From an IRB approved registry of prostate cancer at Cleveland Clinic, we identified five patients, with 43 kilo-voltage cone beam CT (KV-CBCT) and implanted markers. With these KV-CBCTs, we were able to manually delineate the prostate, bladder, and rectum on each KV-CBCT to quantify geometric and dosimetric effects if the prostate rotations are not corrected and if they can be compensated with translational shifts. To eliminate potential setup errors, we first co-registered each CBCT with its corresponding planning CT based on the pelvic bony alignment. Subtracting these shifts from other alignment methods, we obtained the prostate displacements relative to the bone. This work was reported in the annual report of 2011. The manuscript has been published (2) and listed in Appendix C.

Briefly, the prostate contours from the planning CT and CBCT were aligned manually to achieve the best overlaps. This contour registration served as the benchmark method for comparison with two marker registration methods: (a) using six degrees of freedom but rotations were not corrected (ROT_NC); and (b) using three degrees of freedom while compensating rotations into the translational shifts (ROT_C). The center of mass distance (CMD) and overlap index (OI) were used to evaluate these two methods. The dosimetric effects were also analyzed by comparing the dose coverage of the prostate clinical target volume (CTV) in relation to the planning margins. According to our analysis, the detected rotations dominated in the left-right axis with systematic and random components of 4.6° and 4.1° , respectively. When the rotational angle were greater than 10° , the differences in CMD between the two registrations were greater than 5 mm in 85.7% of these fractions; when the rotational angle were greater than 6° , the differences of CMD were greater than 4 mm in 61.1% of these fractions. With 6 mm/4 mm posterior planning margins, the average difference between the dose to 99% (D99) of the prostate in CBCTs and the planning D99 of the prostate was $(-8.0 \pm 12.3) \%$ for the ROT_NC registration, and $(-3.6 \pm 9.0) \%$ for the ROT_C registration ($p = 0.01$). When the planning margin decreased to 4 mm/2 mm posterior, the average difference in D99 of the prostate was $(-22.0 \pm 16.2) \%$ and $(-15.1 \pm 15.2) \%$ for the ROT_NC and ROT_C methods, respectively ($p < 0.05$).

In conclusion, we found that that the rotation of the prostate resulting from marker registration may be substantial. Without correcting the rotational error, inadequate dosimetric coverage to the prostate may result, especially when the rotations are large. Purposely placing the iso-center, which is presumed to be the rotation center of the image registration method, close to the centroid of the implanted markers can minimize the potential rotational error when an automatic marker registration method is applied without a six-degree couch. Otherwise, manually registering the implanted markers with translational shifts, which partially compensates rotations, is recommended, especially when the magnitude of the rotation is large.

Task 1-3: Magnitude of prostate motion during treatment

We studied the prostate motion between treatments in previous task (task 1-2). Using collected data from an IRB approved registry from Cleveland Clinic, we studied magnitude of prostate motion during treatment. We retrospectively analyzed 1,045 fractions of real-time prostate tracking data from 31 patients. For patients treated without real time tracking, we investigated the relationship imaging frequency during treatment and planning margin to account for intrafraction prostate motion by simulating online intrafraction position correction at various imaging frequencies. The result of this study showed that the magnitude of intrafraction prostate motion along the superior-inferior and anterior-posterior directions is comparable and the smallest magnitude is in the left-right direction. Under ideal position correction circumstances, 1 mm, 2 mm, and 3 mm vector planning margins require an imaging frequency of every 15 seconds, 60 second, and 240 seconds to account for intrafraction prostate motion, respectively. This work has been published (3). The manuscript is listed in Appendix D

Task 2: Practical considerations for the novel multiple adaptive planning strategy

Based on the results from Task 1, we recognized that most significant prostate movements are along the longitudinal and vertical directions. Failure to accommodate simultaneous movements in these two directions may result in inadequate dose coverage for the prostate as we showed in the published paper [4] (appendix E). The question is how many plans can adequately account for multi-directional movements of the prostate (task 2-3 in SOW). In this study, we provided a guideline for the minimum number of plans required for clinically implementing the MAP technique. This work was reported in the annual report of 2010. The manuscript is in appendix F.

Briefly, from data of six patients, who received concurrent irradiation of the prostate and PLNs, nine IMRT plans were created for each patient with nine presumed prostate movements: 5 mm in either the anterior-posterior (A-P), or superior-inferior (S-I), or simultaneous 5 mm movements in these two directions. From treatment data of the six patients, thirty three fractions with usable megavoltage (MV) cone-beam CT (CBCT) images were identified. Through a process of dual image registrations between simulation CT and MV-CBCT: by aligning to the implanted markers inside the prostate and by aligning to the pelvic bones, large prostate displacements (> 3 mm in any directions) with respect to pelvic bones were found in 17 of these 33 fractions. For each of these 17 fractions, one MAP plan was selected and applied to the corresponding MV-CBCT images for fraction dose calculation. For comparison, an isocenter shifted plan and an adaptive plan based on the MV-CBCT were also created for each of these 17 fractions. The dose to 95% (D95) of the prostate and PLNs, and the dose to 5% (D5) of the rectum and bladder were calculated and analyzed.

For the prostate, D95 $> 97\%$ of the prescription dose was achieved in 16, 16, and 17 of 17 fractions for the MAP, iso-shifting, and ART plans, respectively. For PLNs, D95 $> 97\%$ of the prescription doses was achieved in 10, 3, and 17 of 17 fractions for the MAP, iso-shifting, and rART plans, respectively. The average (± 1 SD) D5 of the rectum was 45.78 ± 5.75 Gy, 45.44 ± 4.64 Gy, and 44.64 ± 2.71 Gy, and the average (± 1 SD) D5 of the bladder was 45.18 ± 2.70 Gy, 46.91 ± 3.04 Gy, and 45.67 ± 3.61 Gy for the MAP, iso-shifting, and rART plans, respectively.

Although extra planning effort is required, we found that the MAP strategy with nine IMRT plans achieved similar dose coverage to the prostate but improved dose coverage to PLNs when

compared to the conventional iso-shifting technique. The MAP approach can be immediately used in clinical practice without requiring extra hardware and software.

Task 3-1: Comparison of ideal MAP plans with MLC-MAP plans

To establish evaluation criteria for our proposed adaptive strategies, we created a set of IMRT plans, which retrospectively simulate real-time planning based on the acquired daily verification images. These sets of simulated real-time plans are referred to as ideal MAP plans. Because of real time planning is yet clinically practical, we proposed an adaptive strategy by shifting multi-leaf collimator (MLC) leaves without requiring real-time planning or dose recalculation. The plans created with this method are referred to as MLC-MAP plans. This work is now accepted for publication (5) and the major results were reported in the annual report 2011 and 2012. The manuscript is in appendix G.

Briefly, a total of 124 kilo-voltage cone-beam computed tomography (kV-CBCT) images from six patients were studied. For each KV-CBCT, four plans were retrospectively created using an iso-center shifting methods with two different alignment focuses (prostate, PLN), MLC shifting method, and the adaptive real-time planning (ART) method. The selected dosimetric endpoints were compared among these plans.

For the iso-shift-contour, iso-shift-bone, MLC-shift, and ART plans, D99 of the prostate was $\geq 97\%$ of the prescription dose in 97.6%, 73.4%, 98.4%, and 96.8% of 124 fractions, respectively. Accordingly, D99 of the PLN was $\geq 97\%$ of the prescription dose in 98.4%, 98.4%, 98.4%, and 100% of 124 fractions, respectively. For the rectum, D5 exceeded 105% of the planned D5 (and D5 of ART plans) in 11% (4%), 10% (2%), and 13% (5%) of 124 fractions, respectively. For the bladder, D5 exceeded 105% of the planned D5 (and D5 of ART) plans in 0% (2%), 0% (2%), and 0% (1%) of 124 fraction, respectively.

We concluded that for concurrent treatment of the prostate and PLN, with a planning margin to the prostate of 8mm/6mm posterior and a planning margin of 5mm to the PLN, aligning to the prostate soft tissue can achieve adequate dose coverage to the both target volumes; aligning to the pelvic bone would result in underdosing to the prostate in 1/3 of fractions. With these planning margins, MLC tracking and ART methods have no dosimetric advantages. Further reduction of the planning margins to less than 5 mm, MLC tracking and ART method may indicated, especially for stereotactic body radiotherapy (SBRT) of prostate.

Task 3-2: Progressive planning margin reductions

From Task 3-1, we found MLC tracking is not necessary when a planning margin for the prostate is 8mm/6mm posterior. When the planning margins to the prostate while keeping 5 mm planning margin to the PLN are further reduced, we designed a study to investigate the advantage of the MLC tracking method. The abstract of this work has been accepted by the annual meeting of AAPM 2013 and listed in Appendix H.

Briefly, ninety-four daily CBCTs from five patients who received concurrent IMRT treatment for the prostate and PLN with a clinical planning margin to the prostate of 8mm/6mm posterior (M(8,6)), and 5mm to the PLN, were selected. Using the same planning beam directions, three additional IMRT plans were created retrospectively for each patient with prostate planning margins of 6mm/4mm posterior (M(6,4)) , 4mm/2mm posterior (M(4,2)) and 2mm uniform

margin (M(2,2)). The PLN planning margin remained 5mm. Subsequently, each plan was applied to the daily CBCT using MLC and iso-center-contour shifting methods. D95 of the prostate and D95 of the PLN, and D5 of the rectum and D5 of the bladder were compared.

Table 1 lists the detailed results. For both MLC and iso-center-contour shifting method, D95 of the prostate was $\geq 97\%$ of the prescription dose in 97.8%(100%), 98.9%(97.9%), 95.8%(97.9%), and 93.7%(96.8%) of 94 fractions, for M(8,6), M(6,4), M(4,2), and M(2,2) respectively. Accordingly, D95 of the PLN was $\geq 97\%$ of the prescription dose in 98.9% (100%), 100% (98.9%), 98.9%(98.9%), and 100%(98.9%) of 94 fractions, for M(8,6), M(6,4), M(4,2), and M(2,2) respectively. Figure 1 and Figure 2 show dose volume histograms of the bladder and rectum for a selected patient. Quantitatively, D5 of the rectum exceeded 105% of the original IMRT D5 for the MLC-shift (and iso-shift-contour) plans in 16%(14.9%), 14.9%(16.4%), 5.4%(12.2%) and 4.3%(12.2%) of 94 fractions for M(8,6), M(6,4), M(4,2), and M(2,2) respectively. D5 of the bladder exceeded 105% of the original IMRT D5 for the MLC-shift (and iso-shift-contour) plans in 0%(1.1%), 6.4%(3.2%), 13.9%(4.3%), and 8.6%(4.3%) of 94 fractions, for M(8,6), M(6,4), M(4,2), and M(2,2) respectively.

In conclusion, With 5 mm planning margin to the PLN, both MLC tracking and iso-center shifting method can achieve adequate dose coverage to the both target when the planning margin to the prostate reduced to 4mm/2mm posterior.

Table 1: Dose coverage to the prostate and PLN with four different planning margins

	Daily D95 normalized to D95 of the original IMRT plans		Daily D95 normalized to the prescription dose		Daily D95 normalized to 97% of the prescription dose	
	Prostate(%)	LN(%)	Prostate(%)	LN(%)	Prostate(%)	LN(%)
MLC						
M(8,6)	97.9	98.9	96.8	92.7	97.9	98.9
M(6,4)	96.8	100	95.8	89.5	98.9	100
M(4,2)	91.9	98.9	83.3	85.4	95.8	98.9
M(2,2)	89.5	100	86.4	89.5	93.7	100
Iso-Contour						
M(8,6)	100	100	97.9	90.6	100	100
M(6,4)	97.9	98.9	96.8	91.6	97.9	98.9
M(4,2)	93.7	98.9	82.2	90.6	97.9	98.9
M(2,2)	90.6	98.9	88.5	96.8	96.8	98.9

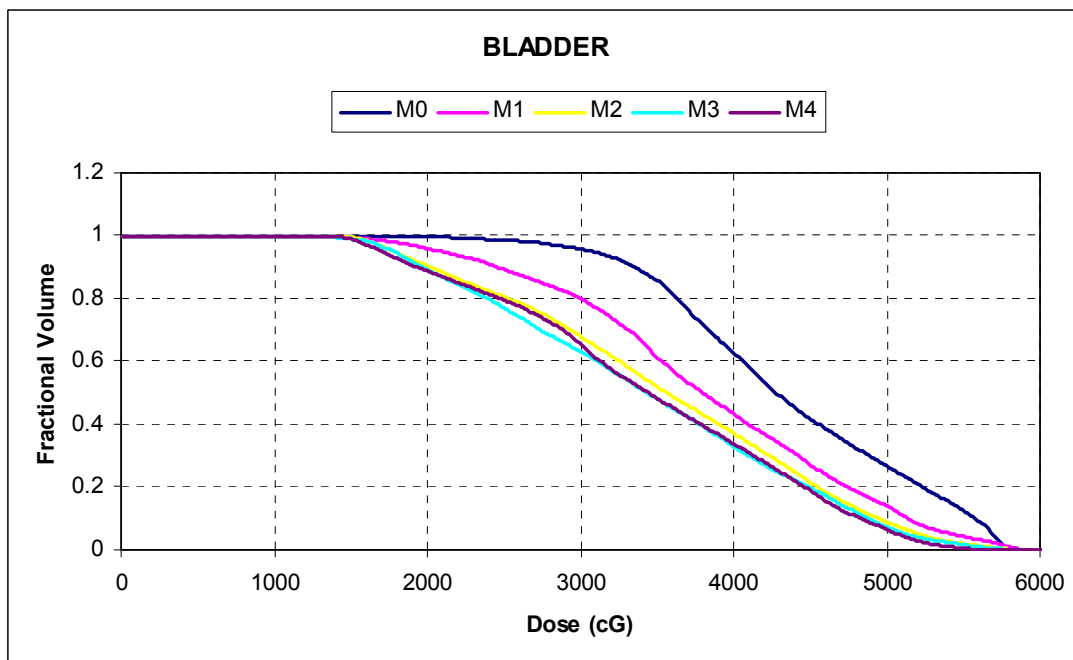


Figure 1: DVHs of the bladder with four different planning margins for a selected patient. (M0(8mm/6mm posterior); M1(6mm/4mm posterior); M2(4mm/2mm posterior); M3(2mm uniform); M4 (0 uniform))

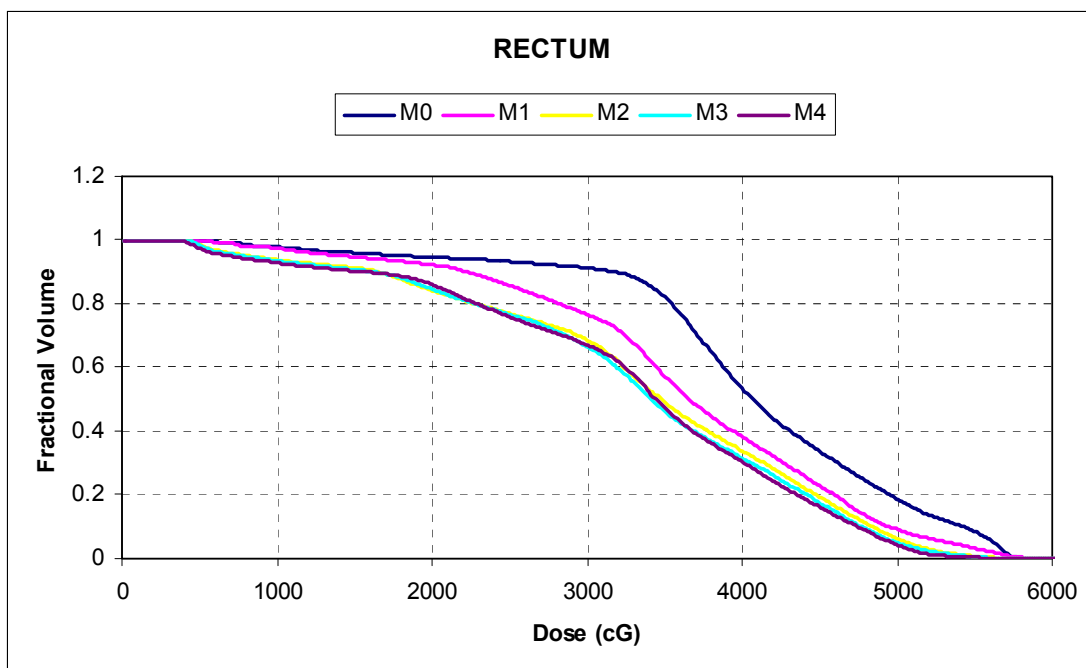


Figure 2: DVHs of the rectum with four different planning margins for a selected patient. (M0(8mm/6mm posterior); M1(6mm/4mm posterior); M2(4mm/2mm posterior); M3(2mm uniform); M4 (0 uniform))

Task 3-3: Shifting the planned daily dose matrix

As reported from the annual report of 2012, we applied the shifted MLC portals to the corresponding KV-CBCT or MV-CBCT and calculated daily dose distribution using the commercial treatment planning system (Pinnacle, Philips Medical Systems). The calculated daily dose provided us dosimetric information for each fraction. To assess the impact of treatment outcomes, we want to know the cumulative treatment effect – the total dose from all treatment days. Because of different reference frames from daily images, we could not obtain cumulative doses from the daily calculated dose without using deformable image registration. The uncertainty in deformable imaging registration might lead to erroneous cumulative dose. Alternatively, knowing the daily iso-center shift from aligning to the prostate contour, we could shift the planned dose matrix on the opposite directions of the iso-center shift. Because the shifted planned dose matrices were from the same reference frame, we could sum these dose matrices together to obtain a cumulative dose. For this purpose, we developed an in-house program written in MATLAB to shift the planned daily dose matrix according to the iso-center shifts by aligning to the prostate contours. The shifted matrices were input to the Computational Environment for Radiotherapy Research (CERR) software for display and other analysis. The preliminary result of this work has presented in the annual meeting of American Association of

Task 3-4: Sensitivity and verification of MLC positions

To experimentally verify accuracy of MLC position shift, we designed a series of experiments to investigate the detection sensitivity of a commercially available two-dimensional ionization chamber array (MatriXX) for MLC leaf positioning errors. The abstract of this work has been accepted by the Annual Meeting of American Association of Physicists in Medicine (AAPM) of 2013 and is listed in Appendix J.

Briefly, a single square field ($10 \times 10 \text{ cm}^2$) and a clinical IMRT plan for a prostate case with 5 fields (0° , 50° , 100° , 260° , 310°) were evaluated in this study. Systematic MLC leaf positioning errors (± 1 , ± 2 , $\pm 3 \text{ mm}$) for one side of the leaf bank in the square field and the IMRT fields were purposely introduced into the plan in the treatment planning system (TPS). To test the effect of the ion chamber resolution (7.62 mm), the center of the square field was shifted to different locations at 1 mm interval in relationship to the ion chamber positions. Both treatment plans with and without leaf positioning errors were delivered and measured with a commercial MatriXX device. To eliminate potential beam modeling errors from the TPS, the Gamma index of each measured planar field was directly calculated between with and without errors.

For the square field, the Gamma indices of 3%/3mm were 99.8% and 98.8% for 1mm and 2 mm leaf positioning error, respectively; the Gamma indices of 2%/2mm were 98.8% and 97.5% for 1mm and 2 mm error, respectively. The Gamma index was independent of the error positions relative to the chamber positions. For the clinical prostate treatment plan, the average Gamma indices of 3%/3mm for 5 fields were 100%, 99.8%, and 98.6% for 1 mm, 2 mm, and 3 mm error, respectively; the average Gamma indices of 2%/2mm were 99.8%, 98.3%, and 96.6% for 1 mm, 2 mm, and 3 mm error, respectively.

Figure 3 showed the measured dose map from a selected beam angle. From two selected directions, the measured profiles with no MLC positional error, and with 2mm and 3mm purposely introduced MLC positional errors were compared with the calculated profiles without MLC positional errors.

In conclusion, using the Gamma passing rate of 99% for 3%/3mm as a criterion, the MatriXX 2D array can detect 2 mm leaf positioning error for a single field, and 3 mm error for composited multiple fields.

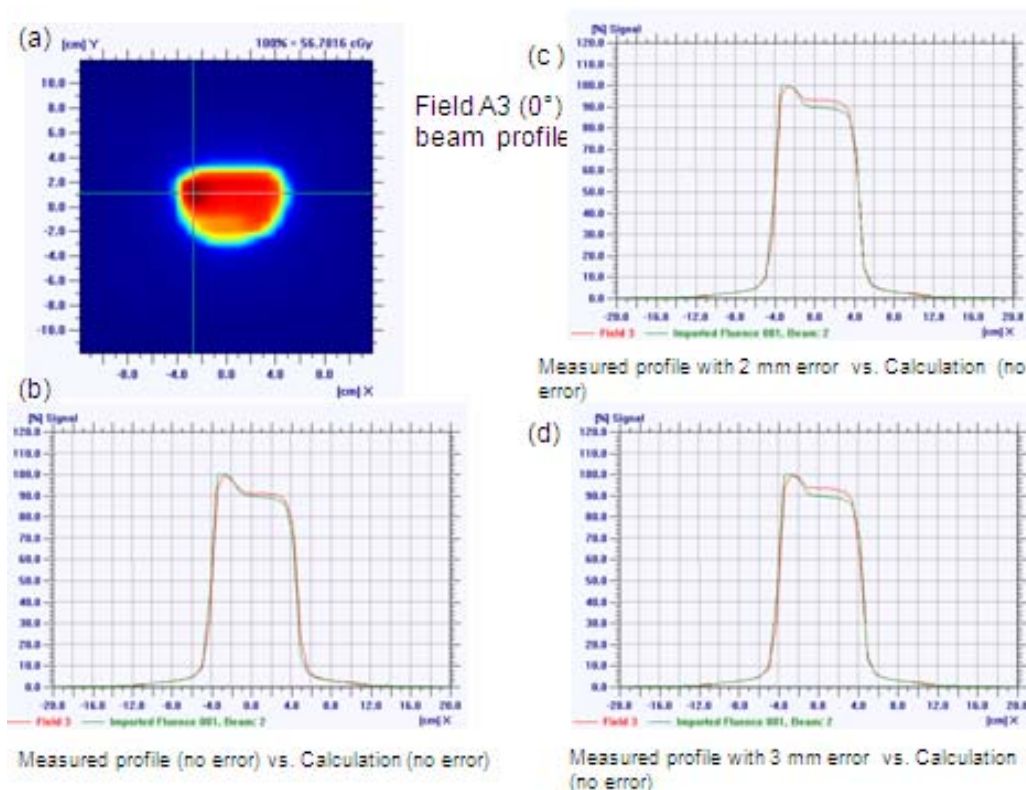


Figure 3: The measured dose map from a selected beam angle. From two selected directions, the measured profiles with no MLC positional error, and with 2mm and 3mm purposely introduced MLC positional errors were compared with the calculated profiles without MLC positional errors.

Task 4-1: Overcome MLC leaf width limitations

Our previous study (3) showed that adjusting selected MLC leaf pairs to follow prostate movement is an effective strategy to account for daily prostate displacement during concurrent treatment with the pelvic lymph nodes. The MLC leaf width affects quality of MLC shifting plans for the longitudinal prostate motion compensation. This study is to investigate the effect of the MLC leaf width in compensation of the prostate movement. This work has been published (6). The preliminary results were reported in the annual report of 2012. The manuscript is in appendix K.

Briefly, seventy-five kilo-voltage cone beam CTs (KV-CBCT) from six patients were included for this retrospective study. For each patient, three different IMRT plans were created based on a planning CT using three different MLC leaf widths of 2.5 mm, 5 mm, and 10 mm, respectively. For each CBCT, the prostate displacement was determined by a dual image registration. Adaptive plans were created by shifting selected MLC leaf pairs to compensate for daily prostate movements. To evaluate the impact of MLC leaf width on the adaptive plan for each daily CBCT, three MLC shifted plans were created using three different leaf widths of MLCs (a total of 225 adaptive treatment plans). Selective dosimetric endpoints for the tumor volumes and organs at risk (OARs) were evaluated for these adaptive plans. Using the planning CT from a selected patient, MLC shifted plans for three hypothetical longitudinal shifts of 2 mm, 4 mm, and

8 mm were delivered on the three linear accelerators to test the deliverability of the shifted plans and to compare the dose accuracy of the shifted plans with the original IMRT plans.

Adaptive plans from 2.5mm- and 5mm-MLCs had inadequate dose coverage to the prostate ($D_{99} < 97\%$, or $D_{\text{mean}} < 99\%$ of the planned dose) in 6% ~ 8% of the fractions, while adaptive plans from 10mm-MLC led to inadequate dose coverage to the prostate in 25.3% of the fractions. The average $V_{56\text{Gy}}$ of the prostate over the six patients was improved by 6.4% (1.6% ~ 32.7%) and 5.8% (1.5% ~ 35.7%) with adaptive plans from 2.5mm- and 5mm-MLCs, respectively, when compared with adaptive plans from 10mm-MLC. Pelvic lymph nodes were well covered for all MLC adaptive plans, as small differences were observed for D_{99} , D_{mean} and $V_{50.4\text{Gy}}$. Similar OAR sparing could be achieved for the bladder and rectum with all three MLCs for treatment adaptation. The MLC shifted plans can be accurately delivered on all three linear accelerators with accuracy similar to their original IMRT plans, where Gamma (3%/3mm) passing rates were 99.6%, 93.0%, and 92.1% for 2.5mm-, 5mm-, and 10mm-MLCs, respectively. The percentages of pixels with dose differences between the measurement and calculation being less than 3% of the maximum dose were 85.9%, 82.5%, and 70.5% for the original IMRT plans from the three MLCs, respectively.

In conclusion, dosimetric advantages associated with smaller MLC leaves were observed in terms of the coverage to the prostate, when the treatment was adapted to account for daily prostate movement for concurrent irradiation of the prostate and pelvic lymph nodes. The benefit of switching the MLC from 10 mm to 5 mm was significant ($p < 0.01$); however, switching the MLC from 5 mm to 2.5 mm would not gain significant ($p = 0.15$) improvement. IMRT plans with smaller MLC leaf widths achieved more accurate dose delivery.

Key Research Accomplishments

- (a) We found that the rotation detected by registering implanted markers may not reflect true rotation of the prostate. Ignoring these detected rotation may lead to erroneous errors of determining the true prostate position.
- (b) We found that compensating for the prostate rotations detected based on marker registration can be compensated with translational shifts. Such compensation will significantly improve geometric and dosimetric indices.
- (c) We found that iso-center shifting based on the bony alignment plans achieved adequate dose coverage for the pelvic lymph nodes, but not sufficient for the prostate. In contrary, the iso-center shifting based on the prostate contour alignment plans achieved adequate dose coverage for the prostate, but not sufficient for the pelvic lymph nodes. MLC-shifting plans provide the best compromised solution.
- (d) Using dual imaging registration method, we found that the bi-directional prostate movement in relative to the pelvic lymph nodes, particular in anterior-posterior and superior-inferior directions, must be considered with strategy A, which increases the number of prepared IMRT plans.
- (e) We concluded that depending on the prostate displacement patterns, aligning daily images to the pelvic bones would require a planning margin of the prostate greater than 8 mm/6 mm posterior. Aligning to the prostate soft tissue, a planning margin of 5 mm to the PLN is adequate and the planning margin to the prostate can be further

- reduced. With reduced planning margins or greater magnitudes of the prostate displacement, MLC-shifting method may be beneficial.
- (f) According to the studied prostate motion pattern, we found that using a leaf width of 5 mm is sufficient to accommodate MLC-shifting method in compensation of the prostate movement in the longitudinal direction.

Reportable Outcomes

Abstracts:

- 1 Shang Q, and Xia P: “*Sensitivity of MatriXX 2D Array in Detection of MLC Leaf Positioning Errors*”, abstract, accepted by the Annual Meeting of American Association of Physicist in Medicine, 2013.
- 2 Li W, Vassil A, Muieddine Mossilly L, Shang QY, and Xia P: “*Diagnostic Quality Images Used for IGRT Can Safely Reduce Planning Margins Using Soft Tissue Alignment For Prostate Cancer: Implication For SBRT*”, abstract, accepted by the Annual Meeting of American Association of Physicist in Medicine, 2013.
- 3 Ferjami S, Stephans, KL, and Xia P: “*Planning Margins Validation for Concurrent Treatment of Prostate and Pelvic Lymph Nodes under Daily Image Guided Delivery*”, abstract, accepted by the Annual Meeting of American Association of Physicist in Medicine, 2013.
- 4 Ferjami S, Huang G, Shang QY, and Xia P: “*Shifting MLC to Follow the Prostate Movements While Concurrently Treating Pelvic Lymph Nodes*”, abstract, Med. Phys. Vol 39, No.6, 3904 (2012).
- 5 Ferjami S, Huang G, Shang QY, and Xia P: “*Using Shifting Planned Dose Matrix to Evaluate Daily Dose Changes for IMRT Prostate Treatment*”, abstract, Med. Phys. Vol. 39, No.6, 3659 (2012).
- 6 Shang QY, Qi P, Vassil A, Huang G, Xia P: “*Effect of MLC Leaf Width on MLC Leaf Shifting Algorithm for Concurrent Treatment of Prostate and Pelvic Lymph Nodes*”, abstract, Med. Phys. Vol. 39, No.6, 3657 (2012).
- 7 Shang QY, Sheplan L, Stephans KL, Tendulkar R, and Xia P: “*Daily Prostate Rotation should be Compensated in Translational Correction and not to be Ignored*”, abstract, Med. Phys. Vol 38, No.6, 3450 (2011).
- 8 Huang G, Yu N, Stephans KL, Tendulkar R, and Xia P: “*Assessing Planning Margins Using Shifting Dose Matrix Method to Calculate Daily and Cumulative Doses Under Imaging Guided Radiotherapy (IGRT).*” abstract, Med. Phys. Vol 38, No.6, 3612 (2011).
- 9 Huang G, Qi P, Shang, QY, Shephan Olsen L, Stephans KL, Tendulkar R, Xia P: “*Shifting MLC to follow the prostate Movement While Concurrently Treating Pelvic Lymph Nodes*”, Vol 38, No.6, 3631 (2011).
- 10 Qi P, Pouliot J, Roach M, Xia P: “*Practical considerations for the novel multiple adaptive planning strategy for patients concurrently treated with the prostate and pelvic lymph nodes*”, Vol 37, No.6, 3375 (2010).
- 11 Xia P, and Qi P, “*Multi-Adaptive Plan (MAP) IMRT to Accommodate Independent Movement of the Prostate and Pelvic Lymph Nodes*” Accepted by the second Innovative Minds in Prostate Cancer Today (IMPACT) conference, sponsored by prostate cancer research program of USAMRMC (Appendix L).

Peer reviewed Publications

1. Pejavar S, Yom SS, Hwang A, Speight J, Gottschalk A, Hsu, IW, Roach III M, Xia P: “*Computer-Assisted, Atlas-Based Segmentation for Target Volume Delineation in Whole Pelvic IMRT for Prostate Cancer*”, Technol Cancer Res Treat, Vol. 12, 199 (2013).
2. Shang QY, Sheplan LJ, Stephans KL, Xia P: “*Prostate rotation detected from implanted markers can affect dose coverage and cannot be simply dismissed*”, J. App. Clin. Med. Phys. Vol. 14(3), 4262 (2013).
3. Curtis W, Khan M, Magnelli A, Stephans K, Tendulkar R, Xia P: “*Relationship of Imaging Frequency and Planning Margin to Account for Intrafraction Prostate Motion: Analysis Based on Real-Time Monitoring Data.*” Int J Radiat Oncol Biol Phys, 85(3),700-6 (2013).
4. Xia P, Qi P, Hwang A, Kinsey E, Pouliot J, Roach III M: “*Comparison of Three Strategies in Management of Independent Movement of the Prostate and Pelvic Lymph Nodes*”, Med Phys. 37(9), 5006-13. (2010).
5. Ferjami S, Huang G, Shang QY, Stephans KL, Zhong Y, Qi P, Tendulkar R, and Xia P: “*Alignment focus of Daily Image Guidance for Concurrent Treatment Of Prostate and Pelvic Lymph Nodes*”, Int J Radiat Oncol Biol Phys (2013, in press)
6. Shang QY, Qi P, Ferjami S, and Xia P: “*Effect of MLC leaf width on treatment adaptation and accuracy for concurrent irradiation of prostate and pelvic lymph nodes*”, Med. Phys. Vol. 6, 061701 (2103).

References:

1. Pejavar S, Yom SS, Hwang A, Speight J, Gottschalk A, Hsu, IW, Roach III M, Xia P: “*Computer-Assisted, Atlas-Based Segmentation for Target Volume Delineation in Whole Pelvic IMRT for Prostate Cancer*”, Technol Cancer Res Treat, Vol. 12, 199 (2013).
2. Shang QY, Sheplan LJ, Stephans KL, Xia P: “*Prostate rotation detected from implanted markers can affect dose coverage and cannot be simply dismissed*”, J. App. Clin. Med. Phys. Vol. 14(3), 4262 (2013).
3. Curtis W, Khan M, Magnelli A, Stephans K, Tendulkar R, Xia P: “*Relationship of Imaging Frequency and Planning Margin to Account for Intrafraction Prostate Motion: Analysis Based on Real-Time Monitoring Data.*” Int J Radiat Oncol Biol Phys, 85(3),700-6 (2013).
4. Xia P, Qi P, Hwang A, Kinsey E, Pouliot J, Roach III M: “*Comparison of Three Strategies in Management of Independent Movement of the Prostate and Pelvic Lymph Nodes*”, Med Phys. 37(9), 5006-13. (2010).
5. Ferjami S, Huang G, Shang QY, Stephans KL, Zhong Y, Qi P, Tendulkar R, and Xia P: “*Alignment focus of Daily Image Guidance for Concurrent Treatment Of Prostate and Pelvic Lymph Nodes*”, Int J Radiat Oncol Biol Phys (2013, in press)
6. Shang QY, Qi P, Ferjami S, and Xia P: “*Effect of MLC leaf width on treatment adaptation and accuracy for concurrent irradiation of prostate and pelvic lymph nodes*”, Med. Phys. Vol. 6, 061701 (2103).

Personnel supported by this award

Ping Xia, PI, Cleveland Clinic

Jean Pouliot, Co-PI, University of California San Francisco

Raul Tendulkar, Co-PI, Cleveland Clinic

Peng Qi, post-doctoral fellow, University of California San Francisco

Guangshun Huang, post-doctoral fellow, Cleveland Clinic

Qingya Shang, post-doctoral fellow, Cleveland Clinic

Samah Ferjami, Post-doctoral fellow, Cleveland Clinic

Appendices

Appendix A-L

Computer-Assisted, Atlas-Based Segmentation for Target Volume Delineation in Whole Pelvic IMRT for Prostate Cancer

www.tcr.org

DOI: 10.7785/tcr.2012.500313

The purpose of this study is to evaluate whether computer-assisted segmentation is clinically feasible in target volume delineation for prostate cancer patients treated with whole pelvic IMRT. An atlas was created, comprised of 44 clinically node-negative prostate cancer patients. Three regions of interest (ROIs) were chosen for analysis: prostate, pelvic lymph nodes, and rectum. For a separate tester set of 15 patients with previously contoured ROIs by three experienced physicians, atlas-assisted contours were compared to manual contours by calculating a volumetric overlap index. In the tester set patients, the average overlap between the manually drawn and atlas-based contours for the prostate, pelvic lymph nodes, and rectum was 60%, 51%, and 64%, respectively. The volume differences were significant in the rectum and pelvic lymph nodes ($p = 0.049$ and $p = 0.016$, respectively); this was not true for the prostate. A subset analysis based on physician-specific atlases showed that the average overlap index for the pelvic lymph nodal volume increased from 51% to 60%, while the other ROIs had no significant changes. Despite significant inter-physician differences, atlas-based segmentation for pelvic lymph node delineation serves as an initial guideline for physicians, potentially improving both consistency and efficiency in contouring.

Key words: Prostate cancer; Target volume delineation; Pelvic lymph nodes; Automatic segmentation; Computer-assisted.

Introduction

Intensity-modulated radiation therapy (IMRT) has become a standard practice in the treatment of localized prostate cancer. The dosimetric superiority of IMRT over conventional external beam techniques has allowed for better dose conformity to target volumes and improved sparing of critical normal tissues. Enhanced dose distributions have made it possible to escalate the delivered radiotherapy dose, resulting in both improved tumor control and reduced treatment toxicity.

Conformal radiotherapy techniques such as IMRT are based on the accurate delineation of target volumes using computed tomography (CT) planning systems. In the case of advanced prostate cancer, whole pelvic IMRT typically requires contouring the prostate, lymph nodes, and seminal vesicles as well as selected

Sunanda Pejavar, M.D.¹
Sue S. Yom, M.D., Ph.D.¹
Andrew Hwang, Ph.D.¹
Joycelyn Speight, M.D., Ph.D.¹
Alexander Gottschalk, M.D.,
Ph.D.¹
I-Chow Hsu, M.D.¹
Mack Roach III, M.D.,
F.A.C.R.
Ping Xia, Ph.D.^{1,2*}

¹Department of Radiation Oncology,
University of California, San Francisco,
San Francisco, CA, USA

²Department of Radiation Oncology,
Cleveland Clinic, Cleveland, OH, USA

Abbreviations: ABS: Atlas-Based Segmentation; CT: Computed Tomography, CTV: Clinical Tumor Volume; DSC: Dice Similarity Coefficient, HN: Head and Neck; IMRT: Intensity Modulated Radiotherapy; ROI: Region of Interest; RTOG: Radiation Therapy Oncology Group.

*Corresponding author:
Ping Xia, Ph.D.
E-mail: xiap@ccf.org

normal structures in proximity. Physicians in high-volume centers allocate a significant amount of time and resources for this laborious job. Several studies (1, 2) have highlighted the time-consuming nature of manual contouring for IMRT in the treatment of both prostate and head and neck (HN) cancer. Miles *et al.* (2) reported an average time spend on target delineation per patient was 1.4 hours prostate alone treatment and 2.3 hours for HN treatment, respectively. Hong *et al.* (1) showed that physicians spent an average of 100 minutes contouring HN tumor volumes and critical structures.

Substantial variations have also been observed among physicians in the contouring of target volumes and critical structures. Hong *et al.* (1) observed significant differences in the determination (what to include) and delineation (where to contour) of HN targets among 20 physicians from various well-known institutions. A recent study reported by Lawton *et al.* (3) also showed significant disagreements in the definitions of iliac and presacral clinical target volumes (CTVs) for pelvic nodal radiation between different genitourinary radiation oncologists.

An increasing literature documents the use of computer-assisted target volume delineation (CAT) systems for

contouring. Several studies (4-6) have shown promising results in decreasing the amount of time spent on this task as well as reducing variation amongst physicians contouring the same structures. The purpose of this study was to evaluate whether computer-assisted segmentation using a pre-defined atlas is feasible clinically in target volume delineation in prostate cancer patients treated with whole pelvic IMRT.

Materials and Methods

Computer-Assisted Target Volume Delineation (CAT) System

A commercially available program was used for atlas creation and subsequent segmentation (automatic contour generation). An overview of the steps involved in this process is shown in Figure 1. Assuming that pelvic lymph node distributions do not vary drastically from patient to patient, patients with similar pelvic anatomy presumably also have similar pelvic node distributions, excluding enlarged lymph nodes. Based on this assumption, an uncountoured CT scan of a subject can be automatically

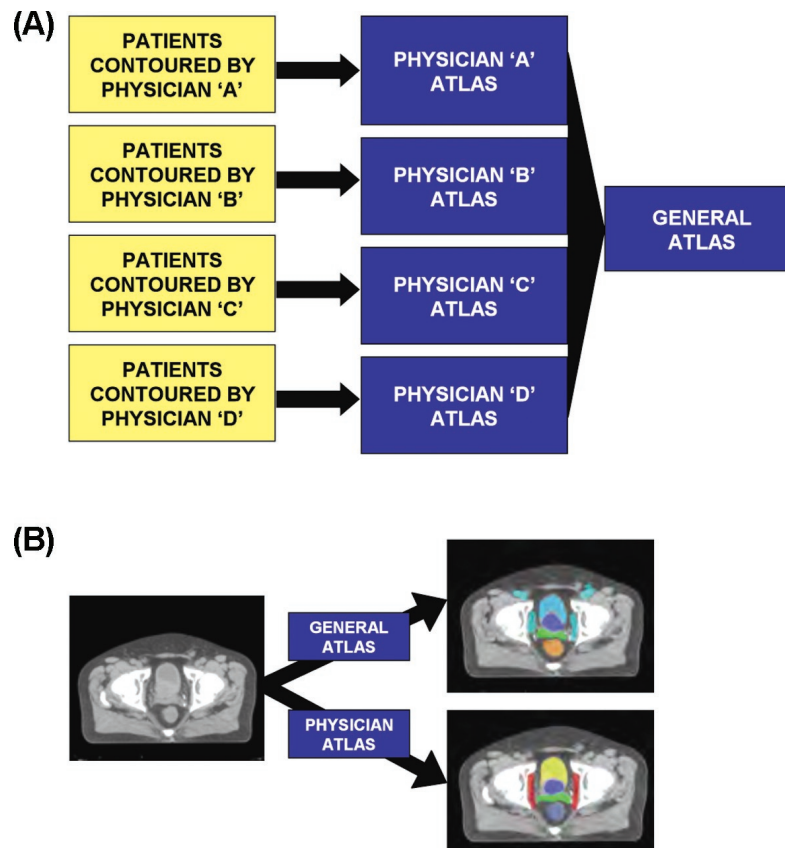


Figure 1: Overview of atlas-based segmentation (A) Shows atlas construction; (B) Shows Segmentation.

segmented based on previously contoured CT scans of patients with similar pelvic anatomy. A library (or “atlas”) can be constructed that is composed of selected CT scans with previously contoured target volumes and critical structures, and used for computer assisted target volume delineation (CAT). In the CAT system used for this study (MIM, MIMvista, Cleveland, OH), the best-matching atlas patient is chosen by the system based on user-defined structures such as bladder or pelvic bones as selection criteria, and deformable image registration is then performed to match the atlas patient’s CT scan to the subject patient’s scan to correct for anatomical differences. In this study, we chose the bladder and pelvic bony structure as the matching criteria because these two structures had most distinctive characteristics. Contours are then deformably transformed from the atlas patient to the subject patient’s CT scan. Because the CAT system we used for this study is a commercially available product, the detail algorithm of how the atlas based contouring is protected property. The only information we obtained from the manufactory is that this system is based on an intensity-based free-form deformable registration algorithm utilizes regularization to minimize the likelihood of folds or tears in the deformation fields to fit one CT to another. The automated portion of the procedure by the CAT system takes approximately one to two minutes.

Atlas Construction

Our atlases consisted of clinically node-negative patients with intermediate- to high-risk prostate cancer treated with whole pelvic IMRT by one of four board-certified radiation oncologists at our institution specializing in prostate cancer. All four physicians had an annual prostate IMRT experience of 30 cases or more, and had been practicing radiation oncology for an average of 11 years (range, 8 to 19 years) at our institution. The regions of interest (ROIs) had been previously contoured on these patients’ planning CT scans by the treating physician, and included the prostate, seminal vesicles (depending on the disease extension), lymph nodes, bladder, and rectum. Contouring on all patients was done on the Pinnacle treatment planning system (Philips Healthcare, Andover, MA).

Patient Characteristics

Table I shows characteristics of the patients included in the atlases. Of a total of 44 patients, all but one had adenocarcinoma histology, and all were clinically node-negative (cN0). The majority of patients (50%) had a Gleason grade of 7. Most of the patients had stage T2 cancers, although there was a fairly even distribution between the various stages. More than half of the patients (55%) had prostate specific antigen

Table I
Atlas characteristics.

Total # patients	44
Physician	
A	13
B	12
C	10
D	9
Nodal status	
cN0	44
cN+	0
TNM stage	
T1c	14
T2	18
T2a	10
T2b	3
T2c	3
Unknown	2
T3	12
T3a	5
T3b	4
T3c	1
Unknown	2
Gleason	
6	2
7	22
8	11
9	8
10	1
PSA	
<10	24
10-20	8
>20	7
Unknown	4

(PSA) values of 10 or less. Table II summarizes the characteristics of the 15 test subject patients.

Segmentation

A second, independent set of patients was chosen for segmentation by the CAT system and designated as “test subjects.” These patients were also clinically node-negative patients with intermediate- to high-risk prostate cancer who had been treated with whole pelvic IMRT by the same radiation oncologists. Although these patients had previously contoured ROIs, their blank planning CT scans were used for atlas-based segmentation; the manual contours were used for analysis only.

Analysis

Three ROIs were chosen for analysis: prostate, lymph nodes, and rectum. The bladder was not chosen for analysis because this organ was selected as one of the matching organs (bladder and pelvic bony structure) as mentioned above. Segmented contours were compared to the previously drawn

Table II
Subject characteristics.

Total # patients	15
Physician	
A	5
B	5
C	5
D	0
Nodal status	
cN0	15
cN+	0
TNM stage	
T1c	5
T2	7
T2a	5
T2b	0
T2c	2
T3	3
T3a	1
T3b	1
T3c	0
Unknown	1
Gleason	
6	2
7	9
8	2
9	2
PSA	
<10	9
10-20	2
>20	1
Unknown	3

manual contours by calculating volume overlap and volume difference between the two contours. The dice similarity coefficient (DSC) was used to quantify volume overlap as defined in Eq. [1].

$$DSC = \frac{2(V_m \cap V_a)}{V_m + V_a} \quad [1]$$

Where V_m and V_a are manually and automatically contoured structures. The paired t -test was used to test the significance of differences in volumetric overlap and volume difference between the manually drawn contours and the atlas-based contours for each ROI.

Results

Volume Overlap

A side-by-side comparison of a patient with manually drawn contours and atlas-based contours is shown in Figure 2. The average overlap between the manually drawn and atlas-based contours for the prostate, pelvic lymph nodes, and rectum

was $60\% \pm 20\%$, $51\% \pm 11\%$, and $64\% \pm 12\%$, respectively. The average volume difference for these ROIs was $34\% \pm 27\%$, $29\% \pm 27\%$, and $27\% \pm 18\%$, respectively. Comparing the atlas contours with the manual contours, there was a statistically significant difference in the volumes of the rectum and pelvic lymph nodes ($p = 0.049$ and $p = 0.016$, respectively), but not the prostate.

Moreover, among three radiation oncologists, each contributed more than 9 subjects in the atlas and at least 5 patients in the test group. We thus further analyzed the data with three physician-specific atlases, attempting to determine whether the differences in volume were due to variations of individual physicians' manual contours. When segmented from the physician-specific atlas, the average overlap between the physician's manual contour and the physician-specific atlas based contour was $56\% \pm 22\%$, $60\% \pm 8\%$, and $60\% \pm 13\%$ for the prostate, pelvic lymph nodes, and rectum, respectively. The average volume difference was $38\% \pm 58\%$, $20\% \pm 22\%$, and $33\% \pm 28\%$. Results are summarized in Table III.

In this subset analysis, the sample size was decreased from 44 in the general atlas to 10-13 in physician specific atlases and the sample size in the testing group was decreased from 15 to 5. However, the average overlap in the pelvic lymph nodal volume increased from 51% to 60%. Figure 3 shows axial, coronal, and sagittal images of a patient segmented by a physician-specific atlas and the general atlas.

As less controversial structures, the contours of the prostate and rectum were more consistent among the participating physicians. The volume overlap index and volume differences were decreased in physician-specific atlases due to the sample size reduction in both the atlas and test group.

Time Savings

Atlas-based segmentation took approximately two minutes per patient, compared to an estimated manual contouring time of 1.5 hours based on clinical observation of our participating physicians. Even accounting for the additional time needed for review and manual editing of the automatically generated contours, the atlas-based segmentation process would result in time saving over manual contouring.

Discussion

In summary, atlas-based segmentation (ABS) for delineation of regions of interest in whole pelvic was clinically feasible, potentially improving both efficiency and potential consistency for the same radiation oncologist treating different patients, particularly for the pelvic lymph nodes. As we

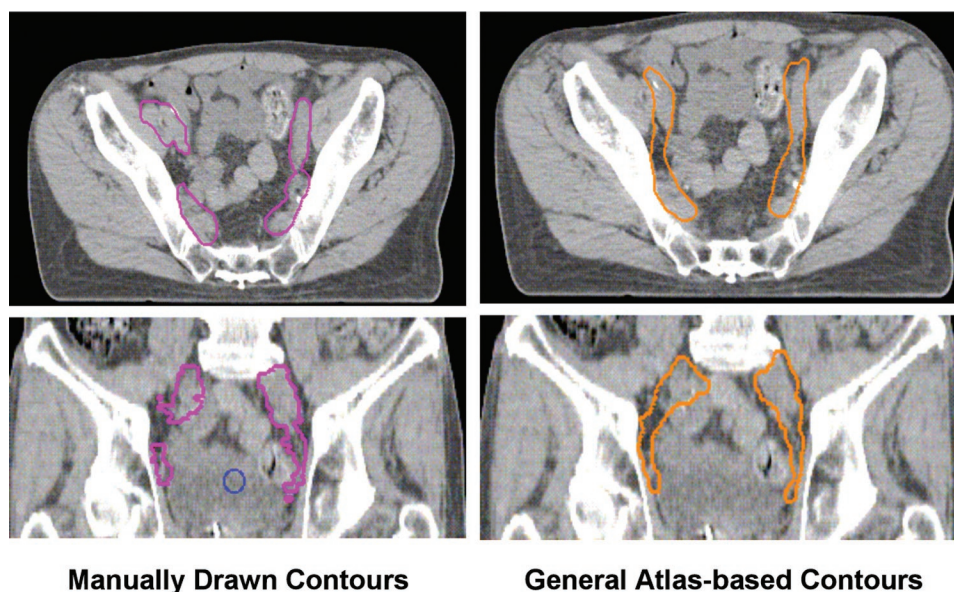


Figure 2: Comparison between manual contours, and the general Atlas-based contours for a selected patient.

reported in this study, even for radiation oncologists practicing in the same institution, the variation in pelvic lymph nodal contours were great among physicians. One can speculate that this variation would be even greater for physicians practicing at different institutions. Of note, our study was based on contours drawn before the publication of Radiation Therapy Oncology Group (RTOG) consensus (7). This publication is important and timely and will lead to better concordance in the pelvic lymph nodal delineation if the guideline is carefully followed. Compute assisted contouring will further facilitate implementation of the guideline when the contours drawn following the guideline are included in the atlas. Therefore, we believe that concordance of delineation of the pelvic lymph nodal volumes will improve.

The results of this study have important implications in clinical radiation oncology practice because of the rapidly growing acceptance and use of IMRT. The widespread use of IMRT in the treatment of prostate cancer has resulted in an increased clinical workload and allocation of additional

resources due to the complexity of IMRT compared with conventional techniques. In a report by Miles *et al.* (2), IMRT was found to increase overall planning times and had particular impact on clinician and physicist workflow. Other studies (8, 9) have reported times of between 3 and 10 hours for whole pelvic IMRT planning, although little information was provided regarding the time spent on individual stages of the planning process.

Variability in target volume delineation has become an increasing concern and creates difficulties in studying and comparing treatment outcomes in the era of IMRT. Possible reasons for inconsistencies between physicians include differences in training and experience, discrepancies in the understanding of microscopic extension of disease and patterns of nodal spread, and variable interpretation of anatomical differences on CT scans. Several reports have been published showing variability in the determination and delineation of target volumes for several different tumor sites, including bladder, breast, HN, and prostate. A recent report by Li *et al.* (10) showed substantial

Table III
Volumetric overlap between manually drawn and Atlas-based contours.

	General atlas			Physician-specific atlas		
	Average overlap	Average volume difference	<i>p</i> -value	Average overlap	Average volume difference	<i>p</i> -value
Prostate	60% ± 20%	34% ± 27%	0.821	56% ± 22%	38% ± 58%	0.990
Lymph nodes	51% ± 11%	29% ± 27%	0.016*	60% ± 8%	20% ± 22%	0.203
Rectum	64% ± 12%	27% ± 18%	0.049*	60% ± 13%	33% ± 28%	0.239

*Statistically significant by paired *t*-test at $p < 0.05$.

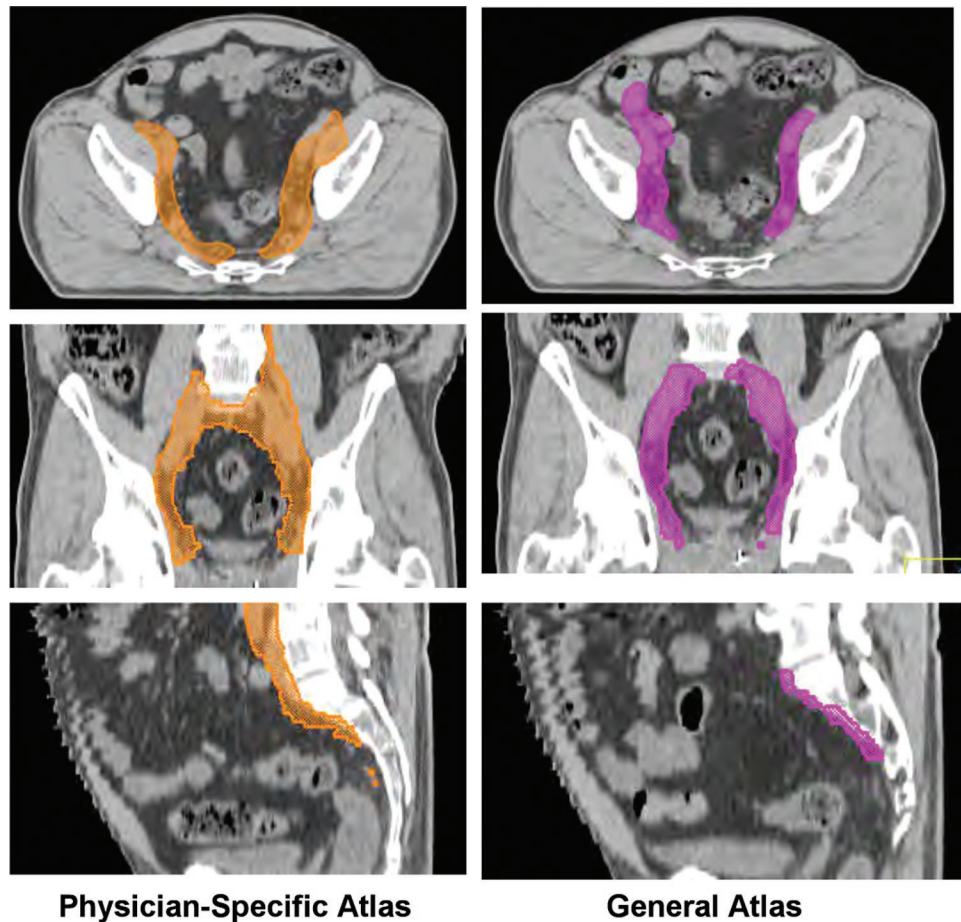


Figure 3: Comparison of Segmentation by the Physician-Specific atlases and the general atlas.

variability in breast cancer target volumes and normal structure contours between multiple institutions and observers, with structure overlap as low as 10% and volume variations with standard deviations of up to 60%. In a study by Fiorino *et al.* (11), significant inter-physician variability was shown amongst five radiation oncologists contouring the prostate and seminal vesicles of patients previously treated with conformal techniques. Similarly, Cazzaniga *et al.* (12) showed variability in the manual delineation of the PTV in three different prostate cancer patients, both in the cranio-caudal direction and extension of tumor on separate axial CT slices.

Maintaining consistency in the contouring of pelvic lymph nodes is particularly important in whole pelvic IMRT. Several studies (13-15) have shown that pelvic nodal irradiation may impact outcome in high-risk prostate cancer patients who have a significant risk of nodal involvement. Treatment of pelvic nodes was included in two radiation therapy oncology group (RTOG) trials (protocols 0521 and 05-34). A consensus guideline for the delineation of lymph node volumes for whole pelvic IMRT does exist (7), and the use of computer assisted, atlas based segmentation can facilitate

the implementation of the guideline thus reducing individual variability in the delineation of these volumes. In a comparative study of clinical target volume (CTV) definition of pelvic lymph nodes by Lawton *et al.* (3), significant variations in the delineation of iliac and presacral CTVs were seen amongst multiple radiation oncologists. Perhaps, atlas based contouring tool may provide a means to disseminate RTOG consensus guideline effectively if contours for all subjects included in the atlas meet the guideline. The fact that there was a significant difference in the volume overlap and volume difference between the master and physician-specific atlases, as well as between manually drawn nodal contours and nodal contours segmented from the master atlas, suggests that a level of variability exists even within our single institution with long-standing experience in pelvic lymph node delineation. There has been recent interest in the use of new imaging techniques such as magnetic resonance lymphography to develop an accurate, objective description of the nodal locations for radiation treatment planning (16, 17). With these newer techniques, it will likely become even more important to define and implement consistency in the contouring of pelvic lymph nodes.

Several different groups have evaluated the applicability and feasibility of semiautomatic CAT systems for target volume delineation. Reed *et al.* (18) described a deformable image registration-based breast segmentation method to generate a clinical target volume from a template case with a consensus contour definition to a new patient. This method improved both consistency and efficiency compared with manual contouring. Another study by Lu *et al.* (19) looked at a recontouring method based on deformable image registration that was validated in the setting of four-dimensional CT planning for lung cancer. Chao *et al.* (6) developed a deformable image registration using a CAT system that mapped HN contours from a template case to a patient with similar clinical characteristics. This study found that there was significant variability between manual contours drawn by different physicians and this variability was reduced by generating contours using the deformable image registration. The average timesaving was 26% to 29% for more experienced physicians and 38% to 47% for less experienced physicians.

In an abstract reported by Hu *et al.* (20), the same commercially available software used in this study was employed for atlas creation and segmentation of head and neck IMRT patients. Patients treated at two different institutions were randomly chosen, and the times required for ABS and manual contouring by an attending physician were recorded. At institution 1, ABS proved to be almost as helpful to the attending physician as resident contours, and resulted in an overall time savings of 87% for normal structures, nodal targets, and primary targets. At institution 2, there was a 68% decrease in contouring time for nodal targets and normal structures, but only a 25% reduction in time for primary targets. The authors noted that the patients chosen at institution 2 had uncharacteristically early stage cancers and therefore required less complex contouring than those at institution 2.

In another recent abstract by Lin *et al.* (21), ABS was applied to prostate IMRT patients. There was a significant reduction in the time required to contour and edit a patient, with a 47.4% decrease in contour generation time by the resident physician and a 36% reduction in editing time by the attending physician. The most time saving was experienced in generating contours for the femurs (54.1%), followed by the prostate (46.2%) and bladder (45%), and finally the rectum (34.9%). Unlike our study, pelvic lymph nodes were not included as an ROI in this abstract.

Similar to the reports above, the present study did show that atlas-based segmentation could provide an efficient means of contouring regions of interest in whole pelvic IMRT. However, the main focus of our study was to demonstrate the feasibility of atlas-based segmentation in generating clinical useful contours, particularly for pelvic lymph nodes. The overlap between segmented and manual contours, or the degree of

similarity between the contours generated by the CAT system and those drawn by the physician, was between 50% and 64%. It is important to recall that auto-segmented contours are meant to represent a starting point for editing, not a substitute for manual contours. Consensus guidelines are constantly changed and updated, and furthermore each patient must be assessed on a case-by-case basis. Clinical judgment is still of utmost importance in treating patients. We believe that editing of segmented contours is still a necessary step in the atlas-based segmentation process, but that atlas-based segmentation provides a useful guideline for physicians.

Although a reasonable degree of overlap was achieved between manual and segmented contours in our study, areas of future research remain for the improvement of the segmentation process. For example, by increasing the number of patients in an atlas and improving consensus among radiation oncologists, improvement in consistency and efficiency would be expected. In addition, additional atlas matching parameters, such as waist size of the patient, or diameter of the pelvic inlet, could also be set during segmentation to fine-tune the process of matching patients to the atlas. Furthermore, newer version of the program can produce a synthetic atlas from a pool of patients in the library. We believe that atlas-based segmentation procedures are robust enough to refine and move into the clinical use.

Conclusions

Atlas-based segmentation for ROI delineation is clinically feasible, and can potentially improve both consistency and efficiency in contouring. A reasonable overlap between atlas based segmentation and manually drawn regions of interest was achieved. Inconsistency in pelvic lymph nodal delineation was observed among experienced radiation oncologists in our institution, but not in the delineation of the prostate and rectum. Modification of atlas-based contours is an acceptable means for delineating pelvic lymph node volumes.

Conflict of Interest

We certify that regarding this paper, no actual or potential conflicts of interests exist; the work is original, has not been accepted for publication nor is concurrently under consideration elsewhere, and will not be published elsewhere without the permission of the Editor and that all the authors have contributed directly to the planning, execution or analysis of the work reported or to the writing of the paper.

Acknowledgement

This research is supported in part by the United States Army Medical Research and Materiel Command (USAMRMC, PC073349).

References

- Hong, T. S., Tome, W. A., Harari, P. M. Heterogeneity in head and neck IMRT target design and clinical practice. *Radiother Oncol* 103, 92-98 (2012). DOI: 10.1016/j.radonc.2012.02.010
- Miles, E. A., Clark, C. H., Urbano, M. T., Bidmead, M., Dearnaley, D. P., Harrington, K. J., A'Hern, R., Nutting, C. M. The impact of introducing intensity modulated radiotherapy into routine clinical practice. *Radiother Oncol* 77, 241-246 (2005). DOI: 10.1016/j.radonc.2005.10.011
- Lawton, C. A., Michalski, J., El-Naqa, I., Kuban, D., Lee, W. R., Rosenthal, S. A., Zietman, A., Sandler, H., Shipley, W., Ritter, M., Valicenti, R., Catton, C., Roach, M., 3rd, Pisansky, T. M., Seider, M. Variation in the definition of clinical target volumes for pelvic nodal conformal radiation therapy for prostate cancer. *Int J Radiat Oncol Biol Phys* 74, 377-382 (2009). DOI: 10.1016/j.ijrobp.2008.08.003
- Pasquier, D., Lacornerie, T., Vermandel, M., Rousseau, J., Lartigau, E., Betrouni, N. Automatic segmentation of pelvic structures from magnetic resonance images for prostate cancer radiotherapy. *Int J Radiat Oncol Biol Phys* 68, 592-600 (2007). DOI: 10.1016/j.ijrobp.2007.02.005
- Zhang, T., Chi, Y., Meldolesi, E., Yan, D. Automatic delineation of on-line head-and-neck computed tomography images: toward on-line adaptive radiotherapy. *Int J Radiat Oncol Biol Phys* 68, 522-530 (2007). DOI: 10.1016/j.ijrobp.2007.01.038
- Chao, K. S., Bhide, S., Chen, H., Asper, J., Bush, S., Franklin, G., Kavadi, V., Liengswangwong, V., Gordon, W., Raben, A., Strasser, J., Koprowski, C., Frank, S., Chronowski, G., Ahamad, A., Malyapa, R., Zhang, L., Dong, L. Reduce in variation and improve efficiency of target volume delineation by a computer-assisted system using a deformable image registration approach. *Int J Radiat Oncol Biol Phys* 68, 1512-1521 (2007). DOI: 10.1016/j.ijrobp.2007.04.037
- Lawton, C. A., Michalski, J., El-Naqa, I., Buyyounouski, M. K., Lee, W. R., Menard, C., O'Meara, E., Rosenthal, S. A., Ritter, M., Seider, M. RTOG GU Radiation oncology specialists reach consensus on pelvic lymph node volumes for high-risk prostate cancer. *Int J Radiat Oncol Biol Phys* 74, 383-387 (2009). DOI: 10.1016/j.ijrobp.2008.08.002
- Adams, E. J., Convery, D. J., Cosgrove, V. P., McNair, H. A., Staffurth, J. N., Vaarkamp, J., Nutting, C. M., Warrington, A. P., Webb, S., Balycky, J., Dearnaley, D. P. Clinical implementation of dynamic and step-and-shoot IMRT to treat prostate cancer with high risk of pelvic lymph node involvement. *Radiother Oncol* 70, 1-10 (2004). DOI: 10.1016/j.radonc.2003.09.004
- Clark, C. H., Mubata, C. D., Meehan, C. A., Bidmead, A. M., Staffurth, J., Humphreys, M. E., Dearnaley, D. P. IMRT clinical implementation: prostate and pelvic node irradiation using Helios and a 120-leaf multileaf collimator. *J Appl Clin Med Phys* 3, 273-284 (2002). DOI: 10.1120/1.1499095
- Li, X. A., Tai, A., Arthur, D. W., Buchholz, T. A., Macdonald, S., Marks, L. B., Moran, J. M., Pierce, L. J., Rabinovitch, R., Taghian, A., Vicini, F., Woodward, W., White, J. R. Variability of target and normal structure delineation for breast cancer radiotherapy: an RTOG multi-institutional and multiobserver study. *Int J Radiat Oncol Biol Phys* 73, 944-951 (2009). DOI: 10.1016/j.ijrobp.2008.10.034
- Fiorino, C., Reni, M., Bolognesi, A., Cattaneo, G. M., Calandrino, R. Intra- and inter-observer variability in contouring prostate and seminal vesicles: implications for conformal treatment planning. *Radiother Oncol* 47, 285-292 (1998). DOI: 10.1016/S0167-8140(98)00021-8
- Cazzaniga, L. F., Marinoni, M. A., Bossi, A., Bianchi, E., Cagna, E., Cosentino, D., Scandolaro, L., Valli, M., Frigerio, M. Interphysician variability in defining the planning target volume in the irradiation of prostate and seminal vesicles. *Radiother Oncol* 47, 293-296 (1998). DOI: 10.1016/S0167-8140(98)00028-0
- Lawton, C. A., DeSilvio, M., Roach, M., 3rd, Uhl, V., Kirsch, R., Seider, M., Rotman, M., Jones, C., Asbell, S., Valicenti, R., Hahn, S., Thomas, C. R., Jr. An update of the phase III trial comparing whole pelvic to prostate only radiotherapy and neoadjuvant to adjuvant total androgen suppression: updated analysis of RTOG 94-13, with emphasis on unexpected hormone/radiation interactions. *Int J Radiat Oncol Biol Phys* 69, 646-655 (2007). DOI: 10.1016/j.ijrobp.2007.04.003
- Roach, M., 3rd, DeSilvio, M., Valicenti, R., Grignon, D., Asbell, S. O., Lawton, C., Thomas, C. R., Jr., Shipley, W. U. Whole-pelvis, "mini-pelvis," or prostate-only external beam radiotherapy after neoadjuvant and concurrent hormonal therapy in patients treated in the Radiation Therapy Oncology Group 9413 trial. *Int J Radiat Oncol Biol Phys* 66, 647-653 (2006). DOI: 10.1016/j.ijrobp.2006.05.074
- Seaward, S. A., Weinberg, V., Lewis, P., Leigh, B., Phillips, T. L., Roach, M., 3rd. Improved freedom from PSA failure with whole pelvic irradiation for high-risk prostate cancer. *Int J Radiat Oncol Biol Phys* 42, 1055-1062 (1998). DOI: 10.1016/S0360-3016(98)00282-X
- Dinniwell, R., Chan, P., Czarnota, G., Haider, M. A., Jhaveri, K., Jewett, M., Fyles, A., Jaffray, D., Milosevic, M. Pelvic lymph node topography for radiotherapy treatment planning from ferumoxtran-10 contrast-enhanced magnetic resonance imaging. *Int J Radiat Oncol Biol Phys* 74, 844-851 (2009). DOI: 10.1016/j.ijrobp.2008.09.026
- Taylor, A., Rockall, A. G., Reznick, R. H., Powell, M. E. Mapping pelvic lymph nodes: guidelines for delineation in intensity-modulated radiotherapy. *Int J Radiat Oncol Biol Phys* 63, 1604-1612 (2005). DOI: 10.1016/j.ijrobp.2005.05.062
- Reed, V. K., Woodward, W. A., Zhang, L., Strom, E. A., Perkins, G. H., Tereffe, W., Oh, J. L., Yu, T. K., Bedrosian, I., Whitman, G. J., Buchholz, T. A., Dong, L. Automatic segmentation of whole breast using atlas approach and deformable image registration. *Int J Radiat Oncol Biol Phys* 73, 1493-1500 (2009). DOI: 10.1016/j.ijrobp.2008.07.001
- Lu, W., Olivera, G. H., Chen, Q., Chen, M. L., Ruchala, K. J. Automatic re-contouring in 4D radiotherapy. *Phys Med Biol* 51, 1077-1099 (2006). DOI: 10.1088/0031-9155/51/5/002
- Hu, K., Lin, A., Young, A., Kubicek, G., Piper, J. W., Nelson, A. S., Dolan, J., Masino, R., Machtay, M. Timesavings for contour generation in head and neck IMRT: Multi-institutional experience with an atlas-based segmentation method. *International Journal of Radiation Oncology Biology Physics* 72, S391-S391 (2008). DOI: 10.1016/j.ijrobp.2008.06.1261
- Lin, A., Kubicek, G., Piper, J. W., Nelson, A. S., Dicker, A. P., Valicenti, R. K. Atlas-based segmentation in prostate IMRT: Time-savings in the clinical workflow. *International Journal of Radiation Oncology Biology Physics* 72, S328-S329 (2008). DOI: 10.1016/j.ijrobp.2008.06.1120

Received: May 14, 2012; Revised: August 21, 2012;

Accepted: September 3, 2012

Appendix B

Daily Dose Monitoring with Atlas-Based Auto-Segmentation on Diagnostic Quality CT for Prostate Cancer

Wen Li, Ph.D.¹, Andrew Vassil, M.D.¹, Yahua Zhong, M.D.², Ping Xia, Ph.D.¹

¹Department of Radiation Oncology, Cleveland Clinic Foundation, Cleveland, OH

²Department of Radiation Oncology, Zhongnan Hospital, Wuhan, China

Short Title: Daily dose monitoring with ABAS

Word count: 3584

Number of Figures: 4

Number of Tables: 1

Conflict of Interest: This study is supported in part by United States Army Medical Research and Material Command (USAMRMC, PC073349) and in part by a research grant from Siemens Medical Solutions.

Address correspondence to: Ping Xia, Ph.D.
T2-028A
Cleveland Clinic Foundation

9500 Euclid Avenue

Cleveland, OH 44106

Tel: 216-444-1938

Fax: 216-444-8934

Email: xiap@ccf.org

Introduction

Daily anatomical variations may affect the dose delivered to patients for prostate cancer treatment (1). A common approach to compensate for the inter-fractional anatomic change is to re-position patients based on the verification images acquired prior to daily treatment (2, 3). Dosimetric data of the target and avoidance structures are usually not obtained to verify the effectiveness of this approach (4). A recent study showed that the residual inter-fractional variations after daily re-positioning resulted in compromised dose coverage to prostate in approximately one third of the treatment fractions (5). This inter-fractional dose deviation may significantly affect the treatment outcomes, particularly for hypo-fractionated treatments such as stereotactic body radiation therapy (SBRT) (6, 7).

With CT based image-guidance techniques routinely utilized in conventional radiotherapy and SBRT, the daily “delivered dose” (not planned dose) can now be calculated for prospective and retrospective correlation with the treatment outcomes. For conventional radiotherapy, if a significant dose deviation occurs, dose deficiency may be compensated with offline adaptive replanning approaches (3, 8). For SBRT, online daily dose monitoring may become paramount to prevent the “delivered dose” deviating from the planned dose. A bottleneck of daily dose monitoring lies in the time-consuming task of delineating the prostate and the organs at risk (OARs) such as the rectum and bladder. The average time to manually contour these regions of interests (ROIs) was reported to be longer than 30 minutes even with the advanced auxiliary tools (9). Such long contouring time makes daily dose monitoring impractical for routine clinical uses.

Recently, an atlas-based auto-segmentation (ABAS) method has been proposed to generate new contours by deforming priori atlas contour sets (10). The improvement in the contouring efficiency with ABAS has been demonstrated on both planning CT (11-13) and daily cone beam CT (CBCT) images for prostate cancer (14). However, a manual adjustment was generally recommended (11-14), which may hamper the practice of daily dose monitoring. To minimize the manual adjustment time, the performance of ABAS needs further improvement. Previous studies have shown that the inclusion of more datasets in the atlas could increase the accuracy of ABAS-generated auto-contours (15-17). According to the algorithm of ABAS, the use of patient specific atlas may also improve the performance of ABAS (10).

In the present study, the feasibility of daily dose monitoring was explored with the aid of ABAS. Daily diagnostic quality verification images, provided by a CT-on-rails system, were used to form patient specific atlases and test datasets. The performance of ABAS was evaluated by the geometrical comparison of the auto- and manual-contours of the test image sets. The feasibility of daily dose monitoring was assessed by the comparison of dose distributions on the auto- and manual-contours of the test image sets. The necessity of daily dose monitoring was also characterized by the daily dose deviations from the planned dose.

Materials and Methods

Seven patients treated with definitive external beam radiotherapy for prostate cancer were included in the current study. The original intensity modulated radiotherapy plans were created using 5 or 7 beam angles ranging from 200° to 160°. The prescription doses of all original plans were set to 78 Gy for the dosimetric comparison of different patients. The planning target volume (PTV) was an expansion of 8 mm in all directions except for 5 mm posteriorly from the prostate (CTV). The prescription isodose line was chosen to ensure that at least 95% of the PTV received the prescription dose. Prior to daily treatments, patients were instructed to have a full bladder and empty rectum, the same condition applied at simulation. After patients were positioned to align the skin markers with the room lasers, daily verification CT images were acquired using an in-room CT-on-rails system (Siemens Medical Solution, Concord, CA). Patients were then re-positioned to align the CTV in the daily verification CT and the planning CT with a manual rigid registration.

Geometrical Evaluation of ABAS

The prostate, rectum and bladder were manually delineated according to Radiation Therapy Oncology Group 0126 (18) for the verification CT sets of the first six and last seven treatment days. For each patient, three patient specific atlases were constructed using manual contours from planning CT alone (1-image atlas), planning CT plus first three verification CTs (4-image atlas), and planning CT plus first six verification CTs (7-image atlas). These atlases were subsequently applied to the last seven verification image sets of the same patient to generate the auto-contours. Manual delineation and ABAS processes were both performed using a commercial software program, MIM version 5.4 (MIMVista, Cleveland, OH).

The algorithm of ABAS in MIM has been described in the previous reports (10, 15, 19). For the current MIM version, multiple atlas image sets can be selected and undergo a rigid and a deformable registration with the new image set. The contours of the selected atlas image sets are then deformed according to the composite matrix from the above two registrations (10). The new contour set is determined from these deformed contour sets using a major vote method (19). In the current study, every atlas contour set was selected and deformed. The new contours were then determined as the areas overlapped by at least half of the deformed contour sets (1 out of 1-, 3 out of 4-, and 4 out of 7-image atlases). The current ABAS process took less than 2 minutes for each image set.

The volumes of the manual-contours (V_m), the auto-contours (V_a), and their intersectional areas, were recorded on a pixel-by-pixel basis. The performance of ABAS was evaluated by a geometrical comparison of the manual- and the auto-contours using the dice similarity coefficient (DSC) (15) and overlap index (OI) (17) defined as below:

$$\text{DSC} = 2(V_m \cap V_a) / (V_m + V_a)$$
$$\text{OI} = (V_m \cap V_a) / V_m$$

The performance of ABAS was also evaluated with a non-patient specific atlas. This 4-image atlas consisted of the planning CT and associated manual contours of four patients. With this atlas, ABAS was applied to the last seven daily image sets of another three patients. The DSC and OI were calculated as described above and were compared to those obtained with 4-image patient specific atlases.

Dosimetric Evaluation of ABAS for Daily Dose Monitoring

Following the geometric evaluation, the forty-nine test image sets and their associated manual- and auto-contours were transferred to Pinnacle 9.0 (Philips, Fitchburg, WI) for dosimetric analysis. For each daily image set, the radiation dose was calculated using the beam configurations from the original plan. The isocenter of the beams was shifted according to the clinically performed patient re-positioning. The dose received by 99% (D99) of the prostate (CTV) volume was compared with the prescription dose to evaluate the target coverage. The daily D5 of the bladder and rectum were compared with those in the corresponding original plans to evaluate the sparing of OARs. Using the manual contours as the reference, the above dosimetric endpoints were compared with those of the auto-contours obtained using 1-, 4- and 7-image patient specific atlases.

Statistical Analysis

All results were expressed as mean \pm standard deviation. Two-tailed paired student *t* tests were used for the geometrical and dosimetric comparisons. Statistical significance was assigned at $p < 0.05$.

Results

Geometrical Evaluation of ABAS

Figure 1 shows an example of the geometrical agreement between the manual contours and the auto-contours obtained with 1-, 4- and 7-image patient specific atlases. With the increase of atlas size from one to four, the DSC and OI of the prostate increased from $82.5\% \pm 6.4\%$ and $84.6\% \pm 5.5\%$ to $86.9\% \pm 4.9\%$ ($p < 0.01$) and $87.8\% \pm 5.4\%$ ($p < 0.01$), respectively. Similarly, the DSC and OI of the rectum increased from $81.0\% \pm 8.7\%$ and $81.1\% \pm 12.9\%$ to $84.7\% \pm 8.6\%$ ($p < 0.01$) and $82.9\% \pm 14.3\%$ ($p = 0.34$), respectively. For the bladder, the DSC improved from $91.4\% \pm 5.0\%$ to $93.6\% \pm 4.3\%$ ($p < 0.05$) while the OI dropped from $96.5\% \pm 3.1\%$ to $95.5\% \pm 2.7\%$ ($p < 0.05$). A further increase of atlas size from four to seven did not result in any significant changes in the DSC and OI of the prostate ($p = 0.51$ and 0.26), rectum ($p = 0.15$ and 0.08) or bladder ($p = 0.05$ and 0.08).

Figure 2 shows the impact of patient specificity for atlas. Compared with the results obtained using the 4-image patient specific atlases, the DSC and OI from the non-patient specific 4-image atlas decreased by 12.4% ($p < 0.01$) and 13.7% ($p < 0.01$) for the prostate, respectively. For the rectum, the reduction in the DSC and OI values were 13.9% ($p < 0.01$) and 10.2% ($p = 0.02$), respectively. For the bladder, the decreases in the DSC and OI values were 15.1% ($p < 0.05$) and 1.1% ($p = 0.45$), respectively.

Dosimetric Evaluation of ABAS for Daily Dose Monitoring

Figure 3 shows the daily dose variations based on the manual contours of the forty-nine test image sets. Daily prostate D99 was $>95\%$ and $>98\%$ of the prescription dose in 93.4% and 78.3% of the tested image sets, respectively. The maximum daily deviation was 9.4% below the prescription dose (Fig. 3a). Daily rectum D5 was $>105\%$ and $>102\%$ of the planned D5 in 2.1% and 43.5% of the tested image sets, respectively (Fig. 3b). Daily bladder D5 was $>105\%$ and $>102\%$ of the planned D5 in 11.2% and 19.6% of the tested fractions, respectively (Fig. 3c). The maximum daily rectum and bladder D5 were 4.9% and 12.4% higher than the planned D5, respectively. Based on the auto-contours obtained with 1-, 4- and 7-image atlases, daily prostate D99 was $>95\%$ of the prescription dose in 97.8% , 93.5% and 93.5% of the tested image sets, respectively. Daily rectum D5 was $>105\%$ of the planned D5 in 2.6% , 2.6% and 2.6% of the tested image sets, respectively. Daily bladder D5 was $>105\%$ of the planned D5 in 2.2% , 8.7% and 13.6% of the tested fractions, respectively.

Figure 4 shows the feasibility evaluation of daily dose monitoring for all three sizes of patient specific atlases. The differences in the prostate (CTV) D99 between the manual contours and the auto-contours obtained with 1-, 4- and 7-image set atlases were less than 2% for 80.4%, 82.6% and 84.8% of the tested image sets, and less than 5% for 89.2%, 91.3% and 95.7% of the tested image sets, respectively (Fig. 4a). Similarly, the differences in the rectum D5 were less than 2% in 89.8%, 92.3% and 100.0% of the tested image sets, and less than 5% in 94.9%, 97.4% and 100.0% of the tested image sets, respectively (Fig. 4b). For the bladder D5, the differences were less than 2% in 56.5%, 67.4% and 76.1% of the tested fractions, and less than 5% in 76.1%, 87.0% and 87.0% of the tested fractions, respectively (Fig. 4c).

Discussion & Conclusion

In the present study, the potential of using ABAS-generated contours for daily dose monitoring was explored. With patient specific atlases, ABAS rendered contours with reasonable geometrical similarity to the manual counterparts. As a result, the daily dose distributions of the manual- and auto-contours were in a good agreement. These results, together with the speed of ABAS (<2 min), demonstrate the feasibility of daily dose monitoring, which may have important clinical implications for patients receiving hypo-fractionated treatment.

Compared with the planned dose, the monitoring of the actual ‘delivered’ daily dose would provide more accurate correlation between the treatment outcomes and the toxicity profiles. Because of the deformation and volume changes in the rectum and bladder, patient re-positioning inevitably leaves some inter-fractional variations and therefore deviates the daily dose from the planned dose. As shown in the current study, approximately 10% of the tested fractions had D99 of the prostate less than 95% of the planned D99. In addition, D5 of the rectum and D5 of the bladder were 5% higher than the corresponding planned D5 in 10% of the tested fractions, respectively.

For hypo-fractionated treatment such as SBRT, daily dose monitoring may have a significant clinical impact. With the planning margin smaller than that for the conventional fractionated radiotherapy, SBRT is subject to greater dose deviations from the same inter-fractional variations (6). In addition, SBRT has large dose delivered in each treatment fraction, which increases the impact of the daily dose deviations. Online daily dose monitoring would serve as a quality assurance to ensure an adequate dose to the treatment target while prevent significant overdose to the OARs. Offline daily dose monitoring would identify the dose deficiencies and offer the opportunity for compensation in the following treatment fractions. The auto-contours generated for daily dose monitoring can also be used to expedite the adaptive replanning process, if needed.

The performance of ABAS in the current study was improved compared with previous studies using the same commercial software for ABAS (12, 14, 20). Specifically, with the diagnostic quality test image sets, the current DSC of all three ROIs were 10% greater than those obtained on daily CBCT (12). With atlases consisted of patient specific datasets, the current OI of the prostate and the rectum were 29% and 19% greater than those obtained with non-patient specific atlases, respectively (15). These comparison results are in agreement with the ABAS algorithm that the accuracy of ABAS is positively related to the geometrical difference between the atlas and the test dataset, as well as the image quality of them (10, 15). Recently, incorporating a prior knowledge, Godley et al. showed DSC values similar to those in the current study (21), in concordance with our results that patient specific atlases can improve auto-segmentation.

The improved geometrical similarity from the current ABAS method led to a reasonable agreement in dose distributions between the auto- and manual-contours, which demonstrated the feasibility of daily dose monitoring. If 5% difference from the manual-contours is considered clinically acceptable, the auto-contours obtained from 4-image patient specific atlases could be directly used for the daily monitoring of the rectum (Fig. 4b). For the prostate and bladder, a manual editing may be necessary in 4% and 14% of the tested fractions, respectively (Fig. 4a&c). However, the time for a manual editing is significantly shorter than that for manual contouring de novo (14). Simmat et. al. showed that a manual editing of six ABAS-generated contours took less than 20 min (14). With more accurate auto-contours and fewer ROI for editing, our preliminary experience showed a manual editing time of ~6 min. This, together with the rapid ABAS process (<2 min), suggests that the addition of daily dose monitoring to the current clinical workflow is logistically practical.

It should be noted that the feasibility of daily dose monitoring is based on the availability of daily diagnostic quality images. If daily images are acquired with CBCT, dose calculation is subject to uncertainties caused by the instable HU numbers. The CT density table may need to be calibrated for each patient and for each acquisition protocol (22). Another limitation of the study is that the test dataset may not represent patients with drastic physiological changes on different treatment days. Validation on more patients may alter the application range of the current conclusion.

In conclusion, with patient specific atlases consisting of contours from the planning CT plus the first three daily verification CTs, atlas-based auto-segmentation can facilitate daily dose monitoring for prostate cancer to provide image- and dose-guided radiotherapy. This practice may be more valuable to patients receiving hypo-fractionated treatment.

References

1. Sterzing F, Engenhardt-Cabillic R, Flentje M, Debus J. Image-guided radiotherapy: a new dimension in radiation oncology. *Dtsch Arztebl Int* 2011;108(16):274-280.
2. Ruan D, Kupelian P, Low DA. Image-guided positioning and tracking. *Cancer J* 2011;17(3):155-158.
3. Ghilezan M, Yan D, Martinez A. Adaptive radiation therapy for prostate cancer. *Semin Radiat Oncol* 2010;20(2):130-137.
4. Li AX. *Adaptive Radiation Therapy*. 1 ed. CRC Press; 2011.
5. Peng C, Ahunbay E, Chen G, Anderson S, Lawton C, Li XA. Characterizing interfraction variations and their dosimetric effects in prostate cancer radiotherapy. *Int J Radiat Oncol Biol Phys* 2011;79(3):909-914.
6. Freeman DE, King CR. Stereotactic body radiotherapy for low-risk prostate cancer: five-year outcomes. *Radiat Oncol* 2011;6:3.
7. Friedland JL, Freeman DE, Masterson-McGary ME, Spellberg DM. Stereotactic body radiotherapy: an emerging treatment approach for localized prostate cancer. *Technol Cancer Res Treat* 2009;8(5):387-392.
8. Mohan R, Zhang X, Wang H, Kang Y, Wang X, Liu H, Ang KK, Kuban D, Dong L. Use of deformed intensity distributions for on-line modification of image-guided IMRT to account for interfractional anatomic changes. *Int J Radiat Oncol Biol Phys* 2005;61(4):1258-1266.
9. Das IJ, Moskvina V, Johnstone PA. Analysis of treatment planning time among systems and planners for intensity-modulated radiation therapy. *J Am Coll Radiol* 2009;6(7):514-517.
10. Piper, J. Evaluation of an intensity-based free-form deformable registration algorithm [abstract]. In: Anonymous. 2007. 2353-2354.
11. Acosta, O, Simon, A, Monge, F, Commandeur, F, Bassirou, C, Cazoulat, G, de Crevoisier, R, and Haigron, P. Evaluation of multi-atlas-based segmentation of CT scans in prostate cancer radiotherapy [abstract]. In: Anonymous. 2011. 1966-1969.
12. Simmat I, Georg P, Georg D, Birkfellner W, Goldner G, Stock M. Assessment of accuracy and efficiency of atlas-based autosegmentation for prostate radiotherapy in a variety of clinical conditions. *Strahlenther Onkol* 2012;188(9):807-815.
13. Granberg C. Clinical evaluation of atlas based segmentation for radiotherapy of prostate tumors [dissertation]. UMEA University; 2011.
14. La MM, Fellin F, Amichetti M, Cianchetti M, Gianolini S, Paola V, Lomax AJ, Widesott L. Systematic evaluation of three different commercial software solutions for automatic segmentation for adaptive therapy in head-and-neck, prostate and pleural cancer. *Radiat Oncol* 2012;7:160.
15. Hwee J, Louie AV, Gaede S, Bauman G, D'Souza D, Sexton T, Lock M, Ahmad B, Rodrigues G. Technology assessment of automated atlas based segmentation in prostate bed contouring. *Radiat Oncol* 2011;6:110.
16. Tsuji SY, Hwang A, Weinberg V, Yom SS, Quivey JM, Xia P. Dosimetric evaluation of automatic segmentation for adaptive IMRT for head-and-neck cancer. *Int J Radiat Oncol Biol Phys* 2010;77(3):707-714.
17. Young AV, Wortham A, Wernick I, Evans A, Ennis RD. Atlas-based segmentation improves consistency and decreases time required for contouring postoperative endometrial cancer nodal volumes. *Int J Radiat Oncol Biol Phys* 2011;79(3):943-947.
18. Michalski J. RTOG 0126. Available at <http://www.rtog.org/ClinicalTrials/ProtocolTable/StudyDetails.aspx?study=0126> 2010.

19. Pirozzi, S, Horvat, M, Piper, J, and Nelson, AS. Atlas-based segmentation: Evaluation of a multi-atlas approach for lung cancer [abstract]. In: Anonymous. 2012. 3677.
20. Pejavar S, Yom SS, Hwang A, Speight J, Gottschalk A, Hsu IC, Roach M, Xia P. Computer-Assisted, Atlas-Based Segmentation for Target Volume Delineation in Whole Pelvic IMRT for Prostate Cancer. Technol Cancer Res Treat 2012.
21. Godley A, Sheplan Olsen LJ, Stephans K, Zhao A. Combining prior day contours to improve automated prostate segmentation. Med Phys 2013;40(2):021722.
22. Bissonnette JP, Balter PA, Dong L, Langen KM, Lovelock DM, Miften M, Moseley DJ, Pouliot J, Sonke JJ, Yoo S. Quality assurance for image-guided radiation therapy utilizing CT-based technologies: a report of the AAPM TG-179. Med Phys 2012;39(4):1946-1963.

Figure Legends

Figure 1. Manually and automatically generated contours on a representative mid-level slice. ABAS was performed using patient specific atlases with various sizes.

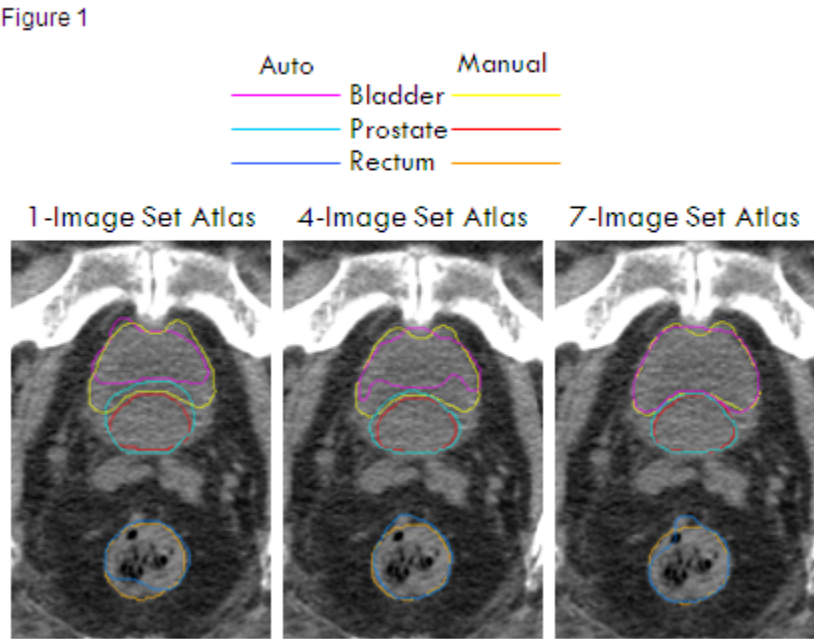


Figure 2. Effect of the patient specificity of atlas on the performance of ABAS. *P<0.05 compared to the results obtained using an atlas with four non-patient specific image sets.

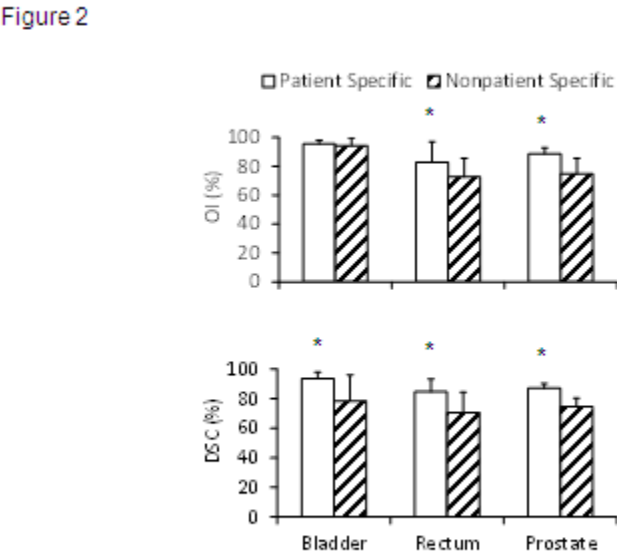


Figure 3. (a) Histogram of the difference in D99 between daily treatments and prescription dose for prostate (CTV). (b)&(c) Histogram of the difference in D5 between daily treatments and original plans for rectum (b) and bladder (c).

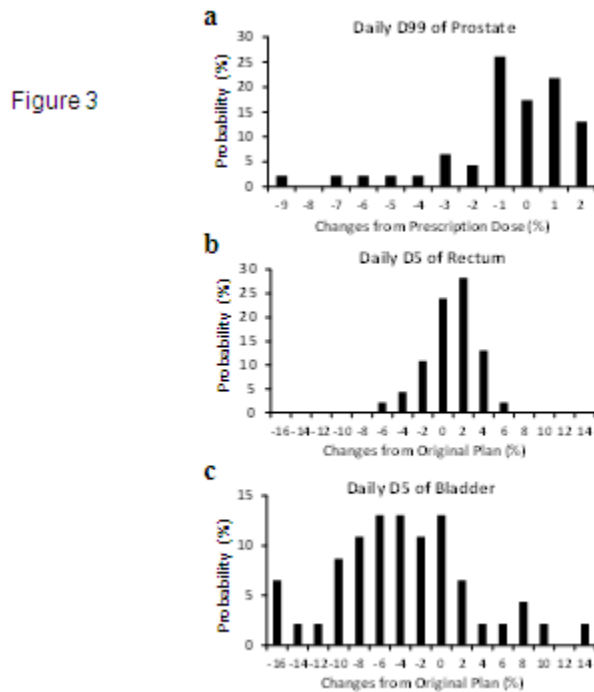
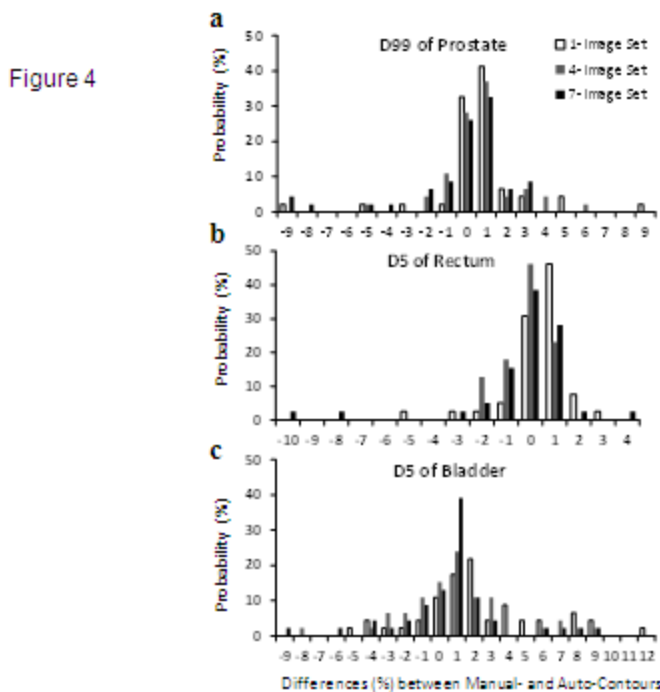


Figure 4. Probability histogram of the differences in dose parameters between the auto- and manual contours. The differences were normalized by the dose parameters for the manual contours.



Prostate rotation detected from implanted markers can affect dose coverage and cannot be simply dismissed

Qingyang Shang, Lawrence J Sheplan Olsen, Kevin Stephans, Rahul Tendulkar, Ping Xia^a

*Department of Radiation Oncology, Cleveland Clinic, Cleveland, OH, USA
xiap@ccf.org*

Received 17 October, 2012; accepted 25 January, 2013

With implanted markers, daily prostate displacements can be automatically detected with six degrees of freedom. The reported magnitudes of the rotations, however, are often greater than the typical range of a six-degree treatment couch. The purpose of this study is to quantify geometric and dosimetric effects if the prostate rotations are not corrected (ROT_NC) and if they can be compensated with translational shifts (ROT_C). Forty-three kilovoltage cone-beam CTs (KV-CBCT) with implanted markers from five patients were available for this retrospective study. On each KV-CBCT, the prostate, bladder, and rectum were manually contoured by a physician. The prostate contours from the planning CT and CBCT were aligned manually to achieve the best overlaps. This contour registration served as the benchmark method for comparison with two marker registration methods: (a) using six degrees of freedom, but rotations were not corrected (ROT_NC); and (b) using three degrees of freedom while compensating rotations into the translational shifts (ROT_C). The center of mass distance (CMD) and overlap index (OI) were used to evaluate these two methods. The dosimetric effects were also analyzed by comparing the dose coverage of the prostate clinical target volume (CTV) in relation to the planning margins. According to our analysis, the detected rotations dominated in the left–right axis with systematic and random components of 4.6° and 4.1° , respectively. When the rotation angles were greater than 10° , the differences in CMD between the two registrations were greater than 5 mm in 85.7% of these fractions; when the rotation angles were greater than 6° , the differences of CMD were greater than 4 mm in 61.1% of these fractions. With 6 mm/4 mm posterior planning margins, the average difference between the dose to 99% (D99) of the prostate in CBCTs and the planning D99 of the prostate was $-8.0 \pm 12.3\%$ for the ROT_NC registration, and $-3.6 \pm 9.0\%$ for the ROT_C registration ($p = 0.01$). When the planning margin decreased to 4 mm/2 mm posterior, the average difference in D99 of the prostate was $-22.0 \pm 16.2\%$ and $-15.1 \pm 15.2\%$ for the ROT_NC and ROT_C methods, respectively ($p < 0.05$). In conclusion, prostate rotation cannot be simply dismissed, and the impact of the rotational errors depends on the distance between the isocenter and the centroid of implanted markers and the rotation angle.

PACS number: 87.55

Key words: prostate rotation, implanted markers, image-guided radiotherapy, IMRT, image registration

I. INTRODUCTION

During radiotherapy of patients with prostate cancer, the prostate position may vary due to the changes in the filling of the bladder and rectum.⁽¹⁻²⁾ Such variations pose a great challenge to

^a Corresponding author: Ping Xia, Department of Radiation Oncology, Cleveland Clinic, T28, 9500 Euclid Ave., Cleveland, OH 44195, USA; phone: (216) 444-1938; fax: (216) 444-8934; email: xiap@ccf.org

the precision of treatment delivery. The use of image-guided radiotherapy (IGRT) improves treatment precision considerably by correcting daily patient setup error and internal organ motion. Most target localization corrections from IGRT, however, are limited in translation only. Rotational setup error and rotational organ motion have been reported, but often dismissed clinically.

For patient positional setup errors, which are often detected by registering bony structures from the verification images with those from the planning images, most studies reported that rotational setup errors were relatively small with a standard deviation of about 1° around each axis.⁽³⁻⁶⁾ Because of the small magnitude, some have suggested that the rotational errors can be ignored,⁽⁷⁻⁸⁾ while others have suggested use of a robotic treatment couch to correct for this magnitude of rotation.⁽⁹⁾

For intertreatment organ motion of the prostate, several studies showed that the prostate organ rotation could be greater than setup error and might have an important dosimetric impact.^(3,10-19) Large prostate rotations are often reported by registering the implanted markers between the verification and planning images. Rotations around left-right (LR) axis were found to be dominant because of influence of the filling of the rectum. Deutschmann et al.⁽¹⁸⁾ found the average LR rotation was $5.3^\circ \pm 4.9^\circ$, with maximum at 30.7° for 31 patients. Lips et al.⁽¹⁹⁾ reported rotational errors with systematic error of 6.3° and random error of 4.9° , ranging from -12.1° to 9.1° for a cohort of 19 patients.

Although using implanted markers as a surrogate to localize the prostate is a well-adopted method for daily IGRT,⁽²⁰⁻²¹⁾ large rotations reported from the implanted marker registration are beyond the maximum correction ranges for most commercially available six-degree couches. Others may even question the accuracy of such large rotations, and how the stability of the markers and their implanted locations affect the accuracy of these detected rotations. The purpose of this study is to quantify geometric and dosimetric effects with and without compensation for rotations detected based on marker registration, rather than to determine accuracy of the rotations detected from the marker registration.

II. MATERIALS AND METHODS

A. Patient selection and treatment planning

Five patients, who underwent definitive external beam radiotherapy for prostate cancer, had three electromagnetic transponders implanted in the prostate for daily IGRT, using the Calypso 4D localization system (Calypso Medical, Seattle, WA). In addition, weekly or daily kilovoltage cone-beam CTs (KV-CBCT) were also acquired to cross-check the Calypso system, as needed, upon the request of radiation oncologists. A total of 43 KV-CBCTs were available for this retrospective study.

The patients were treated with two different dose schemes: 2 Gy per fraction to a total dose of 78 Gy, and 2.5 Gy per fraction to a total dose of 70 Gy. For the purpose of this study, the prescription dose for all plans was renormalized to 2 Gy per fraction to a total dose of 78 Gy without altering IMRT optimization. The CTV was the prostate and the organs at risk (OAR) were the bladder and rectum. The clinical planning margins for these patients were 6 mm/4 mm posterior. The IMRT plans were created with the Pinnacle treatment planning system (Pinnacle³, 8.0m-9.0, Philips Radiation Oncology System, Madison, WI), using a typical five beam arrangement with 10 MV photon beams.

B. Quantification of the prostate displacement

On each KV-CBCT, the prostate, rectum, and bladder were manually contoured by a physician. Subsequently, each CBCT was registered with the corresponding planning CT using four different alignment methods (a total of 172 imaging registrations) including (i) manually align the bones using three degrees of freedom (three translations only) (Bone_T); (ii) automatically

align the three markers using six degrees of freedom (three translations and three rotations), but rotations are not corrected (ROT_NC); (iii) manually align the three markers using three degrees of freedom, which partially compensates rotations with translational shifts (ROT_C); and (iv) manually align the prostate contour using three degrees of freedom (Contour_T), which also partially compensates rotations with translational shifts. After subtracting translational shifts from the bony alignment (Bone_T), patient setup error was removed from the other three alignment methods. All the reported shifts in this paper were the prostate displacements relative to the pelvic bones.

To quantify rotations of the prostate, overall mean and standard deviation of the rotational errors were determined from the measurements of all patients. Systematic and random errors were calculated according to the method published by Remeijer et al.⁽⁵⁾ The systematic error of the entire group is the standard deviation of the individual patient means corrected for the limited and different number of measurements for each patient. The random error of the entire group is the root mean square of the individual patient standard deviation, also weighted by the number of measurements for each patient.

To investigate whether the rotations of the prostate can be compensated with translational shifts, we used the contour registration method (Contour_T) as a benchmark to evaluate the two marker registration methods (ROT_NC and ROT_C) by comparing their geometric and dosimetric indices.

C. Marker migration and false identification

Marker migration is critical for detection of the daily prostate rotation. It can be quantified by measuring the intermarker distance variation of the implanted markers between the planning CT and the daily CBCT. Besides marker migration, other causes that might produce intermarker distance variation include organ shrinkage, organ deformation, and position localization errors of the markers. These factors can affect the accuracy of the detected rotations. To examine the stability and localization error of the implanted markers, we measured the intermarker distances of the treatment day with detected rotations greater than 10° and compared them with the intermarker distances in the planning CT. We also simulated marker migration/false identification by manually adjusting the position of one of the three markers to investigate how it affects the detected rotations. For 7 fractions with rotations greater than 10°, we moved the selected marker by 1 mm and 2 mm from its original position in axial plane and moved one slice thickness (1.5 mm) superiorly and inferiorly.

D. Geometric analysis

To minimize potential prostate contour variations in daily CBCT, manually contoured prostate on each CBCT, denoted as Prostate_CBCT, was used only for contour-based alignment, not for geometric analysis. After each image registration, we used the transferred contours from the planning CT for geometric analysis. The transferred contours, denoted as Prostate_ROT_NC, Prostate_ROT_C, and Prostate_Contour_T, corresponded to the ROT_NC, ROT_C, and Contour_T registrations, respectively. All these contours were the CTV contours. For the ROT_NC registration, rotations were ignored for contour transferring, reflecting a certain clinical scenario in which a registration with six degrees of freedom was performed, but only translational shifts were corrected. Figure 1 is an example illustrating these prostate contours obtained from different registration methods.

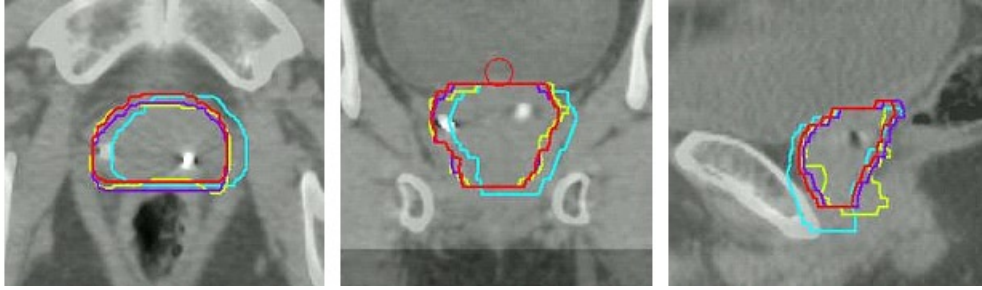


FIG. 1. Prostate contours from different registration methods in (a) transverse, (b) coronal, and (c) sagittal views. Prostate_ROT_NC is shown in blue, Prostate_ROT_C in red, Prostate_Contour_T in purple, and Prostate_CBCT in yellow.

D.1 Center of mass distance

For each of these prostate contours, a center of mass (COM) was calculated in the same CBCT frame. As a global measure of daily prostate displacement, the center-of-mass distance (CMD) of the prostate contours between the bony registration and each of the other three registration methods was calculated using the following equation:

$$d = \sqrt{(x - x_0)^2 + (y - y_0)^2 + (z - z_0)^2} \quad (1)$$

where d is the CMD, and x , y , and z are the coordinates of the COM of the transferred prostate contour after each registration method, and x_0 , y_0 , and z_0 are the coordinates of the COM of the transferred prostate contour after bony registration. Using this equation, we verified the result of the contour-based registration by calculating the relative CMD between the Prostate_CBCT and the Prostate_Contour_T.

Using the contour registration (Contour_T) as a benchmark, we compared the accuracy of the two marker registration methods (ROT_NC and ROT_C) by calculating the relative CMDs between the Prostate_Contour_T and Prostate_ROT_NC, and between the Prostate_Contour_T and Prostate_ROT_C.

D.2 Overlap index

To quantitatively evaluate the geometric properties of the two marker registration methods, we defined the volume overlap index (OI) as:

$$OI = \frac{Prostate_Contour_T \cap T[Prostate_CT]}{Prostate_Contour_T} \quad (2)$$

where T is the transformation applied to the prostate contour from the planning CT (Prostate_CT) by the two marker registration methods, and the operator \cap defines the common area between the two regions of interest. Thus we have:

$$OI_{NC} = \frac{Prostate_Contour_T \cap Prostate_ROT_NC}{Prostate_Contour_T} \quad (3)$$

and

$$OI_C = \frac{Prostate_Contour_T \cap Prostate_ROT_C}{Prostate_Contour_T} \quad (4)$$

where subscript *NC* and *C* represent the ROT_NC and ROT_C methods, respectively. OI is a volumetric measure for registration accuracy, describing the geometric overlap between the “prostate of the day” and the “prostate at planning”. Since all the contours (Prostate_Contour_T, Prostate_ROT_NC, and Prostate_ROT_C) presented in Eqs. (3) and (4) are contours transferred from the planning CT based on different registration methods, OI is a value ranging between 0 and 1. The higher the value, the more the overlap between the actual target volume and the planned target volume, and thus the better the registration outcome.

E. Dosimetric analysis

For each CBCT, three verification plans were created to calculate the radiation dose of the treatment day using the same beam configuration as the original treatment plan. The treatment isocenters for these three verification plans were placed according to the three registration methods, ROT_NC, ROT_C, and Contour_T, respectively. A total of 129 verification plans were created and analyzed. Since the Hounsfield Units (HU) in CBCT is inaccurate and unreliable for dose calculation, the electron density of the CBCT was overridden with 1 g/cm³ for voxels inside the patient external body contour, and 0 (air) for voxels outside the external contour.

The clinical planning margins for the prostate were 6 mm, except 4 mm posterior. To investigate the effect of prostate rotation with reduced planning margins, we chose not to conduct replanning for each patient using progressively reduced planning margins, which may introduce variations in initial plan quality. Instead, we created three expanded prostates (namely Prostate-CTVs) to simulate replanning with reduced margins. These Prostate-CTVs were created by three-dimensionally expanding the Prostate_CBCT contour with 2 mm, 4 mm, and 6 mm /4 mm posterior. We calculated the doses to 99% (\bar{D}_{99}) of these Prostate-CTVs. For verification plans with 6 mm and 4 mm posterior planning margins, we also evaluated the dose to 5% and 50% (\bar{D}_5 and \bar{D}_{50}) of the bladder and rectum.

III. RESULTS

A. Prostate rotations

The prostate rotations detected from the ROT_NC registration were recorded and are shown in Fig. 2 for all 43 fractions. The rotations around the anterior–posterior (AP) and superior–inferior (SI) axes were relatively small and primarily within the range of -5° and $+5^\circ$, while the rotations around the left–right (LR) axis were larger, at times exceeding 10° . The overall mean and standard deviation (SD) of the rotations were $3.3^\circ \pm 5.8^\circ$, $-1.4^\circ \pm 2.9^\circ$, and $-0.8^\circ \pm 2.8^\circ$, for the LR, AP, and SI axes, respectively. The systematic SDs were 4.6° , 2.3° , and 2.1° , and the random SDs were 4.1° , 2.0° , and 2.0° for the three axes, respectively (Table 1).

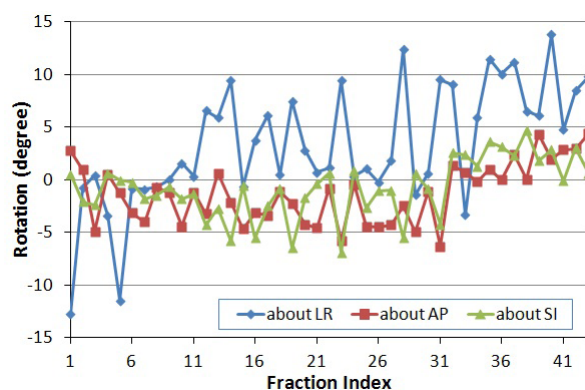


FIG. 2. Prostate rotations about the left–right (LR), anterior–posterior (AP), and superior–inferior (SI) axes for 43 fractions.

TABLE 1. Prostate rotation variations (in degrees) about the left–right (LR), anterior–posterior (AP), and superior–inferior (SI) axes.

	<i>LR</i>	<i>AP</i>	<i>SI</i>
Overall Mean	3.3	-1.4	-0.8
Overall SD	5.8	2.9	2.8
Systematic SD	4.6	2.3	2.1
Random SD	4.1	2.0	2.0

B. Marker migration and false identification

Among 43 fractions, 7 fractions from three patients had rotations greater than 10° . The average intermarker distance for these fractions was 23.3 ± 7.0 mm. The average absolute variation of intermarker distance was 0.8 ± 0.6 mm. Four fractions exhibited marker migrations greater than 1 mm, with a maximum of 2.4 mm. Simulation results of marker migration/false identification showed that with 1 mm variation of the marker position, variation in rotations was less than 2° ; with 2 mm variation of the marker position, the maximum variation in the rotations was 6° . Changing the marker position to its adjacent image slice (slice thickness 1.5 mm) resulted in 3° variation of the rotations.

C. Geometric analysis

The CMD between the transferred prostate contour based on contour registration and the physician drawn contour on the CBCT is shown in Fig. 3(a). This distance is a global measure of the potential prostate deformation and contouring uncertainty, which was detected to be less than 1.9 mm (1.3 ± 0.5 mm) for 95.3% of the fractions. Thus, it is reasonable to use contour-based registration as our benchmark for comparison of the two marker-based registration methods.

Figure 3(b) demonstrates the CMDs between the prostates from the contour-based registration (Contour_T) and from the marker-based registration with rotations zero out (ROT_NC), and the CMD between the prostates from the contour-based registration and from the marker-based translation only registration (ROT_C). Figure 3(b) also shows the CMD differences between the two marker-based registrations. It is observed that when compared with the prostate contour from the ROT_NC registration, the prostate contour from the ROT_C registration is closer to the prostate contour from the Contour_T registration, especially when the rotation is large. The mean CMDs were 6.6 mm and 3.9 mm, respectively. The difference between the two CMDs ranged from -0.9 mm to 8.3 mm when the maximum rotation (absolute value) from all three axes varied from 0.9° to 13.8° . When the rotation was greater than 10° , the difference in CMD between the prostates from the two marker-based registrations was greater than 5 mm in 6 of 7 (85.7%) fractions. When the rotation was greater than 6° , the difference in CMD was greater than 4 mm in 11 of 18 fractions (61.1%). The statistics of the two CMDs and their differences are summarized in Table 2.

The average OI between the transferred prostate contour based on contour registration and the physician drawn contour on the CBCT is 0.79 ± 0.06 , as shown in Fig. 4(a). This index includes the potential prostate deformation, as well as prostate contour uncertainties in the CBCTs. We were not able to separate these two factors. However, the contouring uncertainties had a smaller impact on the CMDs. As shown in Fig. 3(a), the average CMD between the Prostate_Contour_T and the Prostate_CBCT of 1.3 ± 0.5 mm indicated that the prostate deformation might be minimal.

Figure 4(b) compares the OI averaged over each patient for the two marker registration methods. In general, OI_C exhibits greater value than OI_{NC} , indicating that better geometric overlap between the “prostate of the day” and the “prostate at planning” can result from the marker registration with translational correction. In three of five patients, OI_C shows over 10% improvement of overlap when compared with OI_{NC} .

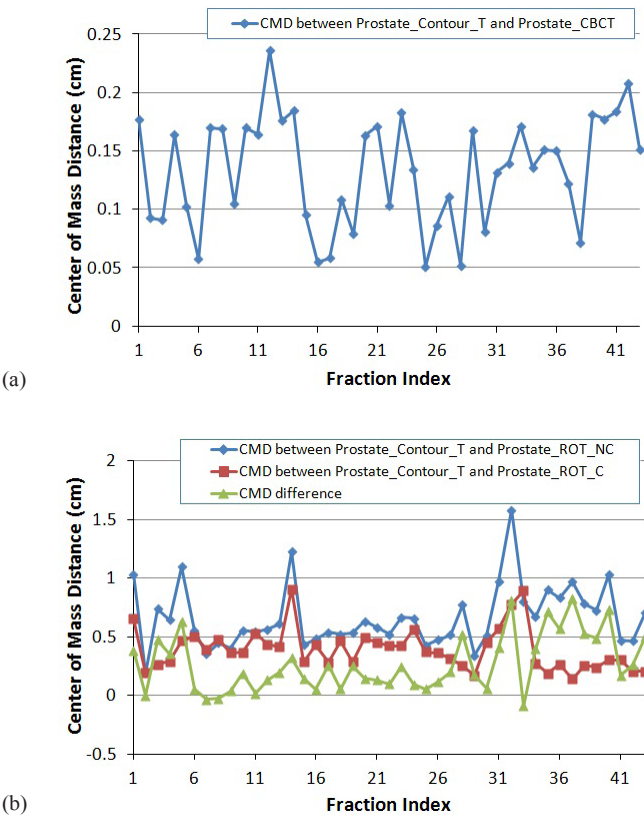


FIG. 3. Center of mass distance (CMD): (a) between the Prostate_Contour_T and Prostate_CBCT; (b) between the Prostate_Contour_T and Prostate_ROT_NC, between the Prostate_Contour_T and Prostate_ROT_C, and the difference.

TABLE 2. Center of mass distance (CMD) of prostate shifts between the contour-based and two marker-based registrations.

	<i>CMD Between ROT_{NC} and Contour_T⁽³⁹⁾</i>	<i>CMD Between ROT_C and Contour_T⁽³⁹⁾</i>	<i>Difference⁽³⁹⁾</i>
Max.	15.8	9.1	8.3
Min.	1.9	1.4	-0.9
Mean	6.6	3.9	2.7
SD	2.6	1.8	2.4

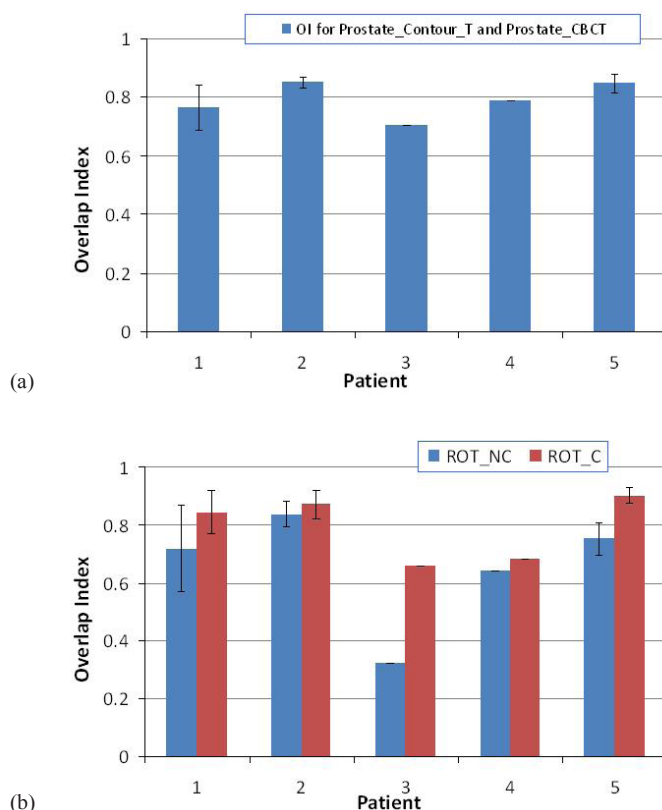


FIG. 4. Overlap index (OI): (a) the average OI for Prostate_Contour_T and Prostate_CBCT for each patient; (b) the average OI for each patient compared between the two marker-based registration methods. Error bar shows one standard deviation.

D. Dosimetric analysis

Figure 5 shows the ratios of D99 of the Prostate-CTVs from three types of verification plans to the planned D99 of the prostate with three equivalent planning margins. With 6 mm/4 mm posterior planning margins, D99 of the prostate was significantly different between the two marker registrations ($p = 0.01$) — $-3.6 \pm 9.0\%$ difference from the planned dose for the ROT_C method, compared to $-8.0 \pm 12.3\%$ for the ROT_NC method. The dose differences ($p < 0.05$) between the two methods increased as the planning margins decreased, as shown in Table 3. For example, with a 2 mm margin reduction (equivalent to a 2 mm expansion of the prostate in this study), the ROT_C method could improve dose coverage to the Prostate-CTV D99 by 6.9%. From Fig. 5, the contour-based registration achieved the best dose coverage, followed by the ROT_C method as the planning margin progressively reduced.

The dosimetric improvement of translational correction is greater when the magnitude of the rotation is large. For example, for a patient with detected rotations of $8.8^\circ \pm 2.9^\circ$ around the LR axis, the average daily D99 of the prostate was 1.99 Gy (99.7% of the planned dose, with a daily prescription dose of 2.0 Gy) with the ROT_C method, compared to 1.68 Gy (84.4% of the planned dose) with the ROT_NC method. As the planning margin decreased to 4 mm/2 mm posterior, the average daily D99 of the Prostate-CTV improved from 1.39 Gy from the ROT_NC method to 1.82 Gy from the ROT_C method, a 21.4% improvement by compensating rotations with translational shifts.

Figure 6 shows doses to 5% (D5) and 50% (D50) of the bladder and rectum for the two marker registration methods. D5 of the bladder and D50 of the rectum did not reach statistically

significant differences (p-values were 0.09 and 0.44, respectively) by the ROT_NC and ROT_C methods. D5 of the rectum was lower than the planned dose for both methods, and D50 of the bladder was significantly lower for the ROT_C method ($p = 0.004$). We also noticed that the dose variation in D50 of the bladder was largely due to the large volume variation of the bladder during the treatment course. The average dose differences for OAR from all fractions between the dose of the day and the dose of the plan are listed in Table 4.

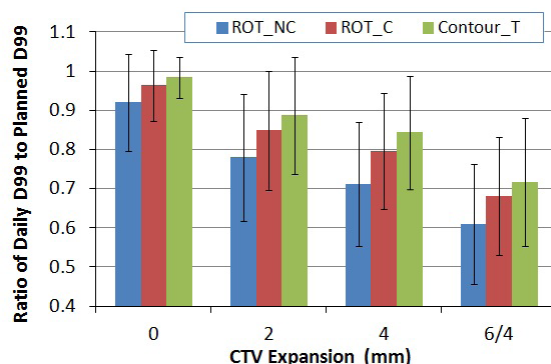


FIG. 5. Average D99 of the Prostate-CTV as a function of CTV expansion margins for the three registration methods. D99 is expressed as a ratio of the daily dose to the planned daily D99 of the prostate. Error bar represents one standard deviation.

TABLE 3. Average difference in D99 of the Prostate-CTV between the daily and planned dose.

Registration Methods	CTV Expansion ⁽³⁹⁾			
	0	2	4	6/4
ROT_NC	-8.0±12.3%	-22.0±16.2%	-28.7±15.8%	-39.0±15.3%
ROT_C	-3.6±9.0%	-15.1±15.2%	-20.4±14.7%	-31.9±15.1%
Contour_T	-1.6±5.2%	-11.3±15.0%	-15.6±14.4%	-28.3±16.3%
Improvement by correction	4.4%	6.9%	8.3%	7.1%

Note: The differences are expressed in percentage (%) of the planned D99 of the prostate as a function of CTV expansion margins. Negative mean value indicates less dose in daily D99 of the Prostate-CTV when compared to the planned dose.

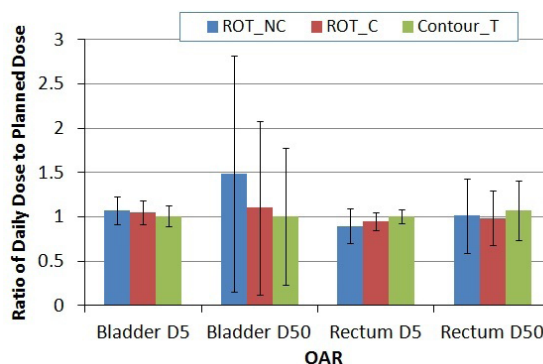


FIG. 6. Average D5 and D50 of the bladder and rectum. Column represents mean value (normalized to the planned dose) and error bar corresponds to one standard deviation.

TABLE 4. Average dose difference for OAR between the daily and planned dose.

Registration Methods	OAR Dose			
	Bladder D5	Bladder D50	Rectum D5	Rectum D50
ROT_NC	7.2±15.9%	48.5±133.4%	-10.5±19.5%	1.2±41.7%
ROT_C	4.8±13.2%	10.1±98.4%	-4.7±10.2%	-1.3±30.5%
Contour_T	0.8±11.8%	0.9±77.2%	0.2±7.9%	7.2±40.0%

Note: The differences are expressed in percentage (%) of the planned dose as the mean ± standard deviation. Negative mean value indicates better organ sparing compared with the original plan.

IV. DISCUSSION

We investigated the magnitude and distribution of the prostate interfractional rotations and evaluated the geometric and dosimetric effects of the rotations. Precisely correcting the prostate organ rotation is clinically important but challenging, especially when rotation angles are large. Recent development of six-degree treatment couches has enabled correction of the rotations,^(9,17,22-23) but such treatment couches are not widely available or able to correct large magnitude of rotations. For the purpose of patient safety, the correction range for a typical six-degree couch is about 4°–5°. Other correction strategies have been proposed, such as gantry and collimator angle adjustments to partially correct for left–right rotations,⁽²⁴⁾ offline adaptive planning,⁽²⁵⁻²⁷⁾ and dynamic MLC tracking.⁽²⁸⁾ However, most of these strategies are in the investigation stages and are not yet clinically practical.

During treatment for most patients with prostate cancer, patient positioning errors and prostate displacement are often not separated. In this study, we used a dual imaging registration method to separate the positioning errors and prostate displacement. Because reported rotation errors in patient positioning were small, we used the bony registration with translational shifts to determine the positional setup errors. Subtracting the translational shifts from the bone registration, the translational shifts and rotations from the marker registration were primarily from the displacement of the prostate, or artifact of the registration method.

Nevertheless, Table 5 compares our data with other reported data in the literature for both systematic and random components of prostate rotations detected with three imaging registration methods. The systematic component describes the variation of the mean displacement of the prostate, while the random component delineates the day-to-day position variation of the prostate. Compared to the results from marker registration, our data agree well with previous

TABLE 5. Systematic and random components (in degrees) of prostate rotations in the literature.

Authors		Systematic Components			Random Components		
		LR	AP	SI	LR	AP	SI
Contour-based Registration	Van Herk et al. ⁽²⁹⁾	N/A	N/A	N/A	4.0	1.3	2.1
	Stroom et al. ⁽¹⁰⁾	3.6	0.8	1.7	3.3	0.9	1.5
	Hoogeman et al. ⁽¹³⁾	5.1	1.3	2.2	3.6	1.6	2.0
Image-based Registration	Nijkamp et al. ⁽²⁵⁾	2.9	0.9	1.0	3.0	1.0	1.1
Marker-based Registration	Dehnad et al. ⁽¹¹⁾	4.7	2.0	2.7	3.6	1.7	1.9
	Aubry et al. ⁽¹²⁾	5.6	2.2	2.4	6.1	2	2.8
	Graf et al. ⁽¹⁷⁾	4.1	2.3	1.6	3.1	1.8	2.0
	Van der Heide et al. ⁽²⁰⁾	6.8	2.8	2.8	3.1	1.7	2.0
	Lips et al. ⁽¹⁹⁾	6.3	2.0	2.8	4.9	1.0	1.4
	Owen et al. ⁽¹⁶⁾	7.6	5.0	7.7	10.2	6.5	15.8
	Our study	4.6	2.3	2.1	4.1	2.0	2.0

results from Dehnad et al.⁽¹¹⁾ and Graf et al.⁽¹⁷⁾ Except for the study conducted by Owen et al.,⁽¹⁶⁾ prostate rotation around the LR axis was found to be the largest of the three axes. Lips et al.⁽¹⁹⁾ and van der Heide et al.⁽²⁰⁾ found larger systematic error (6.3° and 6.8°, respectively) than others around the LR axis, and Aubry et al.⁽¹²⁾ also reported greater random error (6.1°) around the LR axis.

The variation of the reported prostate rotations (Table 5) may stem from differences in treatment protocols, image registration approaches, and mathematical methods for error computation at each institute. Some studies matched the prostate contours in the planning CT with those in the repeated CT scans to get the rotations of the prostate relative to the pelvic bones,^(3,10,13) while others performed the registration based on the implanted markers.^(11-12,16-17,19-20) In addition, the mathematical equations used to compute the systematic and random errors might be slightly different from one study to another. For example, Owen et al.⁽¹⁶⁾ computed the errors using the method described by van Herk,⁽²⁹⁾ and Stroom et al.,⁽¹⁰⁾ and Hoogeman et al.⁽¹³⁾ utilized a similar method but corrected the systematic error for the finite number of measurements. Aubry et al.⁽¹²⁾ employed an approach by Remeijer et al.,⁽⁵⁾ not only considering the limited size of samples, but also accounting for the different number of measurements for each patient. In this study, we used the same method as that in the Remeijer study. Furthermore, the selection of rotation center has a strong effect on the resultant rotations. Owen and colleagues used the marker placed near the apex of the prostate as the pivot point for rotation computation, while for most of the other studies, rotations were measured at the centroid of the prostate contours or the centroid of the markers, depending on whether the contour-based or marker-based registration method is used. The Owen study reported much greater rotations (7.6°, 5.0°, and 7.7° for systematic and 10.2°, 6.5°, and 15.8° for random) than others.

In this study, the registration was performed in the treatment planning system instead of the on-board imaging system of the linear accelerator. Daily CBCT and the planning CT are served as the primary and secondary image for fusion, respectively. The secondary image is translated and rotated to match the primary image. The resultant rotations were measured around the image volume center of the secondary image (planning CT). Rotations could also be measured at the treatment isocenter.⁽³⁰⁾ However, the centroid of the markers, which in general represents the center of mass of the prostate organ, could be different from the treatment isocenter or the image center. For example, for concurrent treatment of the prostate and pelvic lymph nodes, the isocenter is usually placed outside of the prostate. Isocenter may also be adjusted away from the center of the prostate because of practical reasons. In these cases, if rotations are measured around the isocenter, or any point other than the centroid of the markers (e.g., image volume center), ignoring such rotation will introduce a translational error at the centroid of the markers, indicating prostate displacement from its supposed position. For instance, Linthout et al.⁽²³⁾ reported that a tilt rotation of 2.5° at the foot end of the couch could lead to a vertical shift of 4.5 cm at the isocenter for a standard prostate cancer patient positioning (where the isocenter is close to the center of the prostate).

The ROT_NC method obtains a six-degree-of-freedom solution, but only applies the translational components of the solution for correction. In the scenario where the rotation center is different from the centroid of the markers, only the rotation center is corrected precisely with the ROT_NC method (under the assumption of no prostate deformation and other uncertainties such as marker migration). For all the other points in the image, especially for points inside the prostate which we are interested in, there will be a translational error produced by the uncorrected rotation. The magnitude of the error depends on the distance to the rotation center and the detected rotation at that point. Mathematically, the translational error at the centroid of the markers due to uncorrected rotations can be estimated roughly by Eq. (5) according to the law of cosines in Euclidean geometry:

$$error = D\sqrt{2(1 - \cos\theta)} \quad (5)$$

where D is the distance between the centroid of the markers and the rotation center, and θ is the rotation angle about the LR axis (assuming rotations about the AP and SI axes are small enough to be neglected). Figure 7 shows the magnitude of the measured and estimated error of the ROT_NC method at the centroid of the markers from its true position where rotations are corrected precisely. Except for a few fractions where the assumption of small rotations about the other two axes was not satisfied, the measured errors agreed well with the estimated ones for the majority of fractions. A greater distance D and/or larger rotation angle θ creates larger error. For example, for a patient with $D = 7.3$ cm and $\theta = 4.9^\circ$, the measured translational error associated with the ROT_NC method was 6.8 mm; for another patient with $D = 3.5$ cm and $\theta = 4.5^\circ$, the error was 2.2 mm. For the same patient with $D = 3.5$ cm, the error was 4.0 mm when the detected rotation was 9.4° , compared to 0.5 mm error when the rotation was less than 1° .

On the other hand, the ROT_C method uses only three degrees of freedom for correction. The resultant translational solution contains two separable components. The first component corrects the initial translational error (three translations from the six-degree-of-freedom solution) to the rotation center; and the second component compensates for translations caused by the rotation for points in the prostate by matching the three markers. Therefore, the centroid of the three implanted markers is precisely corrected (theoretically, with the same assumption as above). For other points inside the prostate, the second translational component only partially corrects for rotations. Thus, the residual translational errors of the prostate from the ROT_C method are smaller than those from the ROT_NC method. Using contour-based registration as our benchmark, the displacement of the prostate from its supposed position after correction by the two marker-based registration methods was quantified by the center of mass distance and overlap index (Figs. 3 and 4). In the scenario where the rotation center is the centroid of the prostate, the ROT_NC method will produce the same results as that of the ROT_C method. To avoid substantial shifts of the prostate centroid caused by the ROT_NC method, placing the isocenter close to the centroid of the implanted markers is recommended. Otherwise, using the ROT_C method is recommended.

The detected rotations from marker registration may depend on spatial relationship of the implanted markers, marker stability within the prostate, and the accuracy of the marker identification. It is speculated that when markers are implanted close to each other, large organ rotations may be falsely rendered. Migration or localization errors of implanted markers could also lead to falsely rendered rotations. Although several studies reported that the average marker movement was very small, on the order of 1 mm,^(11,31-34) there was evidence of relatively large intermarker distance variations for individual patients. McNair et al.⁽³⁵⁾ found marker migration of more than 2 mm in 10% (3 of 30) patients; Deutschmann et al.⁽¹⁸⁾ observed 24 of 342 patients had intraprostatic migrations of one of four markers greater than 3 mm, and 10 greater

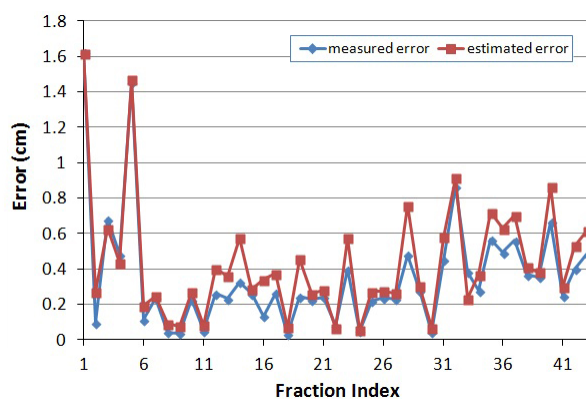


FIG. 7. The magnitude of measured and estimated errors associated with the ROT_NC method.

than 4 mm; while Kupelian et al.⁽³⁴⁾ reported that in 47 of 56 patients (84%), the maximum intermarker distance variation was at least 2 mm, and the percentage for 3, 4, 5 mm variation were 41%, 18%, and 9%, respectively. They also reported that the maximum standard deviation of the intermarker distance was 4.2 mm and the maximum observed variation was 10.2 mm. The infrequent yet potential marker migrations may have more profound effect on the resulted rotations than translations.⁽¹⁸⁾

By examining the intermarker distance variation of fractions with detected rotations greater than 10° , we observed the maximum variation of the Calypso transponders exceeded 2 mm in two patients. Studies have shown that the migration of Calypso transponders is within the similar range of gold markers routinely implanted for prostate treatment.⁽³⁶⁾ When large intermarker distance variations (up to a few millimeters) occurred, either substantial marker migration or significant organ deformation was indicated.^(31,34) In these cases, the rotations detected by marker registration may not truly represent the actual organ displacement. Our simulation experiment reported up to 6° of rotation variation resulted from 2 mm marker migration/false identification, indicating that a small migration of the implanted markers or a small localization error in marker positions may result in a large degree of rotation. Such uncertainties in rotation detection will further hamper the accuracy of rotation correction. On the other hand, marker migrations and false identification will have less influence on the accuracy of the translational shifts. Using translational shifts to compensate for rotational error of the prostate is a safe strategy which will not be affected substantially by the potential marker migration or localization errors of the marker positions.

Mutunga et al.⁽³⁷⁾ found the benefit of rotation corrections was insignificant for systematic error around the LR axis of 4.3° and random error of 4.5° for patients receiving treatment to the prostate only. With 3 mm uniform planning margin, they reported the average increase in population D_{\min} with rotation corrections was only 0.3 ± 0.8 Gy. However, Lips et al.⁽¹⁹⁾ observed patients with large rotations had considerable dose reduction in the CTV in a study with planning margins of 2, 4, 6, and 8 mm. It was concluded that without correcting the rotation errors, online translational correction produced little improvement compared with off-line verification for complex prostate IMRT plans. A study by Li et al.⁽³⁰⁾ also shown that the dosimetric impact of prostate rotation was more significant than the impact of translational shifts in intrafractional motion. They concluded that the treatment margin can be reduced substantially if the residual rotational errors can be managed within 1° in any direction. In our study, we found that correcting rotation errors becomes more important when a smaller planning margin is used to reduce normal tissue toxicity, as well as for patients with greater distances between the centroid of the markers and the rotation center, and patients with large rotation angles. For example, for patients with distances 7.3 cm and 3.5 cm, the daily D99 of the prostate was 1.82 Gy (90.9% of the planned dose) and 1.91 Gy (95.3% of the planned dose), respectively, for the ROT_NC method when the rotation was about 4° for both cases. As the planning margin decreased from 6 mm/4 mm to 4 mm/2 mm, and further to 2 mm/0 mm posterior, the improvement of D99 of the prostate with translational correction increased from 4.4% to 6.9%, and further to 8.3% (Table 3). Such improvement in D99 is even greater for patients exhibiting large rotations. For example, for a selected patient with rotations of $8.8^\circ \pm 2.9^\circ$, $2.0^\circ \pm 1.7^\circ$, and $2.3^\circ \pm 1.5^\circ$ around the LR, AP, and SI axes, for planning margins of 6 mm/4 mm, 4 mm/2 mm, and 2 mm/0 mm posterior, the translational correction method improved D99 of the prostate by 15.3%, 21.4%, and 25.9%, respectively.

It should be noted that, in this study, we only investigated the rotations from the prostate motion alone. We did not specifically examine the movement of the seminal vesicles because fiducial markers were not routinely implanted in the seminal vesicles to monitor the organ motion. However, the dosimetric impact of rotation errors on seminal vesicles is worthy of further investigation, since it is known that the seminal vesicles move even more than the prostate.⁽³⁸⁾

V. CONCLUSIONS

This study indicates that the rotation of the prostate resulting from marker registration may be substantial. Without correcting the rotation error, inadequate dosimetric coverage to the prostate may result, especially when the rotations are large. Purposely placing the isocenter, which is presumed to be the rotation center of the image registration method, close to the centroid of the implanted markers can minimize the potential rotation error when an automatic marker registration method is applied without a six-degree couch. Otherwise, manually registering the implanted markers with translational shifts, which partially compensates rotations, is recommended, especially when the magnitude of the rotation is large.

ACKNOWLEDGMENTS

This research is supported in part by the United States Army Medical Research and Material Command (USAMRMC, PC073349).

REFERENCES

1. Langen KM and Jones DT. Organ motion and its management. *Int J Radiat Oncol Biol Phys.* 2001;50(1):265–78.
2. Byrne TE. A review of prostate motion with considerations for the treatment of prostate cancer. *Med Dosim.* 2005;30(3):155–61.
3. van Herk M, Bruce A, Kroes AP, Shouman T, Touw A, Lebesque JV. Quantification of organ motion during conformal radiotherapy of the prostate by three dimensional image registration. *Int J Radiat Oncol Biol Phys.* 1995;33(5):1311–20.
4. Hanley J, Lumley MA, Mageras GS, et al. Measurement of patient positioning errors in three-dimensional conformal radiotherapy of the prostate. *Int J Radiat Oncol Biol Phys.* 1997;37(2):435–44.
5. Remeijer P, Geerlof E, Ploeger L, Gilhuijs K, van Herk M, Lebesque JV. 3-D portal image analysis in clinical practice: an evaluation of 2-D and 3-D analysis techniques as applied to 30 prostate cancer patients. *Int J Radiat Oncol Biol Phys.* 2000;46(5):1281–90.
6. Guckenberger M, Meyer J, Vordermark D, Baier K, Wilbert J, Flentje M. Magnitude and clinical relevance of translational and rotational patient setup errors: a cone-beam CT study. *Int J Radiat Oncol Biol Phys.* 2006;65(3):934–42.
7. Fu W, Yang Y, Li X, Heron DE, Huq MS, Yue NJ. Dosimetric effects of patient rotational setup errors on prostate IMRT treatments. *Phys Med Biol.* 2006;51(20):5321–31.
8. Cranmer-Sargison G. A treatment planning investigation into the dosimetric effects of systematic prostate patient rotational set-up errors. *Med Dosim.* 2008;33(3):199–205.
9. Soete G, Verellen D, Tournel K, Storme G. Setup accuracy of stereoscopic X-ray positioning with automated correction for rotational errors in patients treated with conformal arc radiotherapy for prostate cancer. *Radiother Oncol.* 2006;80(3):371–73.
10. Stroom JC, Koper PC, Korevaar GA, et al. Internal organ motion in prostate cancer patients treated in prone and supine treatment position. *Radiother Oncol.* 1999;51(3):237–48.
11. Dehnad H, Nederveen AJ, van der Heide UA, van Moerselaar RJA, Hofman P, Lagendijk JJW. Clinical feasibility study for the use of implanted gold seeds in the prostate as reliable positioning markers during megavoltage irradiation. *Radiother Oncol.* 2003;67(3):295–302.
12. Aubry JF, Beaulieu L, Girouard LM, et al. Measurements of intrafraction motion and interfraction and intrafraction rotation of prostate by three-dimensional analysis of daily portal imaging with radiopaque markers. *Int J Radiat Oncol Biol Phys.* 2004;60(1):30–39.
13. Hoogeman MS, van Herk M, de Bois J, Lebesque JV. Strategies to reduce the systematic error due to tumor and rectum motion in radiotherapy of prostate cancer. *Radiother Oncol.* 2005;74(2):177–85.
14. Wu QW, Ivaldi G, Liang J, Lockman D, Yan D, Martinez A. Geometric and dosimetric evaluations of an online image-guidance strategy for 3D-CRT of prostate cancer. *Int J Radiat Oncol Biol Phys.* 2006;64(5):1596–609.
15. Boda-Heggemann J, Kohler F, Wertz H, et al. Fiducial-based quantification of prostate tilt using cone beam computer tomography (CBCT). *Radiother Oncol.* 2007;85(2):247–50.
16. Owen R, Kron T, Foroudi F, Milner A, Cox J, Duchesne G. Interfraction prostate rotation determined from in-room computerized tomography images. *Med Dosim.* 2011;36(2):188–94.
17. Graf R, Boehmer D, Budach V, Wust P. Interfraction rotation of the prostate as evaluated by kilovoltage X-ray fiducial marker imaging in intensity-modulated radiotherapy of localized prostate cancer. *Med Dosim.* 2012;37(4):396–400.

18. Deutschmann H, Kametraser G, Steininger P, et al. First clinical release of an online, adaptive, aperture-based image-guided radiotherapy strategy in intensity-modulated radiotherapy to correct for inter- and intrafractional rotations of the prostate. *Int J Radiat Oncol Biol Phys*. 2012;83(5):1624–32.
19. Lips IM, van der Heide UA, Kotte AN, van Vulpen M, Bel A. Effect of translational and rotational errors on complex dose distributions with off-line and on-line position verification. *Int J Radiat Oncol Biol Phys*. 2009;74(5):1600–08.
20. van der Heide UA, Kotte AN, Dehnad H, Hofman P, Lagenijk JJ, van Vulpen M. Analysis of fiducial marker-based position verification in the external beam radiotherapy of patients with prostate cancer. *Radiother Oncol*. 2007;82(1):38–45.
21. Khosa R, Nangia S, Chufal KS, Ghosh D, Kaul R, Sharma L. Daily online localization using implanted fiducial markers and its impact on planning target volume for carcinoma prostate. *J Cancer Res Ther*. 2010;6(2):172–78.
22. van Herten YR, van de Kamer JB, van Wieringen N, Pieters BR, Bel A. Dosimetric evaluation of prostate rotations and their correction by couch rotations. *Radiother Oncol*. 2008;88(1):156–62.
23. Linthout N, Verellen D, Tournel K, Reynders T, Duchateau M, Storme G. Assessment of secondary patient motion induced by automated couch movement during on-line 6 dimensional repositioning in prostate cancer treatment. *Radiother Oncol*. 2007;83(2):168–74.
24. Rijkhorst EJ, Van Herk M, Lebesque JV, Sonke JJ. Strategy for online correction of rotational organ motion for intensity-modulated radiotherapy of prostate cancer. *Int J Radiat Oncol Biol Phys*. 2007;69(5):1608–17.
25. Nijkamp J, Pos FJ, Nuver TT, et al. Adaptive radiotherapy for prostate cancer using kilovoltage cone-beam computed tomography: first clinical results. *Int J Radiat Oncol Biol Phys*. 2008;70(1):75–82.
26. Lei Y and Wu QW. A hybrid strategy of offline adaptive planning and online image guidance for prostate cancer radiotherapy. *Phys Med Biol*. 2010;55(8):2221–34.
27. Liu H and Wu QW. Dosimetric and geometric evaluation of a hybrid strategy of offline adaptive planning and online image guidance for prostate cancer radiotherapy. *Phys Med Biol*. 2011;56(15):5045–62.
28. Wu J, Ruan D, Cho B, et al. Electromagnetic detection and real-time DMLC adaptation to target rotation during radiotherapy. *Int J Radiat Oncol Biol Phys*. 2012;82(3):e545–53.
29. van Herk M. Errors and margins in radiotherapy. *Semin Radiat Oncol*. 2004;14(1):52–64.
30. Li JS, Jin L, Pollack A, et al. Gains from real-time tracking of prostate motion during external beam radiation therapy. *Int J Radiat Oncol Biol Phys*. 2009;75(5):1613–20.
31. Poggi MM, Gant DA, Sewchand W, Warlick WB. Marker seed migration in prostate localization. *Int J Radiat Oncol Biol Phys*. 2003;56(5):1248–51.
32. Litzenberg D, Dawson LA, Sandler H, et al. Daily prostate targeting using implanted radiopaque markers. *Int J Radiat Oncol Biol Phys*. 2002;52(3):699–703.
33. Pouliot J, Aubin M, Langen KM, et al. (Non)-migration of radiopaque markers used for on-line localization of the prostate with an electronic portal imaging device. *Int J Radiat Oncol Biol Phys*. 2003;56(3):862–66.
34. Kupelian PA, Willoughby TR, Meeks SL, et al. Intraprostatic fiducials for localization of the prostate gland: monitoring intermarker distances during radiation therapy to test for marker stability. *Int J Radiat Oncol Biol Phys*. 2005;62(5):1291–96.
35. McNair HA, Hansen VN, Parker CC, et al. A comparison of the use of bony anatomy and internal markers for offline verification and an evaluation of the potential benefit of online and offline verification protocols for prostate radiotherapy. *Int J Radiat Oncol Biol Phys*. 2008;71(1):41–50.
36. Willoughby TR, Kupelian PA, Pouliot J, et al. Target localization and real-time tracking using the Calypso 4D localization system in patients with localized prostate cancer. *Int J Radiat Oncol Biol Phys*. 2006;65(2):528–34.
37. Mutanga TF, de Boer HC, van der Wielen GJ, Hoogeman MS, Incrocci L, Heijmen BJ. Margin evaluation in the presence of deformation, rotation, and translation in prostate and entire seminal vesicle irradiation with daily marker-based setup corrections. *Int J Radiat Oncol Biol Phys*. 2011;81(4):1160–67.
38. Beard CJ, Kijewski P, Bussiere M, et al. Analysis of prostate and seminal vesicle motion: implications for treatment planning. *Int J Radiat Oncol Biol Phys*. 1996;34(2):451–58.

Clinical Investigation: Genitourinary Cancer

Relationship of Imaging Frequency and Planning Margin to Account for Intrafraction Prostate Motion: Analysis Based on Real-Time Monitoring Data

William Curtis, MD, MSEE,* Mohammad Khan, MD, PhD,[†] Anthony Magnelli, MS,[†] Kevin Stephans, MD,[†] Rahul Tendulkar, MD,[†] and Ping Xia, PhD[†]

**School of Medicine, Case Western Reserve University, and [†]Department of Radiation Oncology, Cleveland Clinic, Cleveland, Ohio*

Received Sep 6, 2011, and in revised form May 9, 2012. Accepted for publication May 30, 2012

Summary

One thousand forty-five fractions of real-time prostate tracking data from 31 patients were used to assess the relationship of repositioning frequency and planning margins on geometric coverage of the prostate. Results showed comparable magnitude of intrafraction prostate motion between the superior-inferior and anterior-posterior directions. Under ideal circumstances, 1-, 2-, and 3-mm vector planning margins require an imaging frequency of every 15, 60, and 240 seconds to account for intrafraction prostate motion, respectively.

Purpose: Correction for intrafraction prostate motion becomes important for hypofraction treatment of prostate cancer. The purpose of this study was to estimate an ideal planning margin to account for intrafraction prostate motion as a function of imaging and repositioning frequency in the absence of continuous prostate motion monitoring.

Methods and Materials: For 31 patients receiving intensity modulated radiation therapy treatment, prostate positions sampled at 10 Hz during treatment using the Calypso system were analyzed. Using these data, we simulated multiple, less frequent imaging protocols, including intervals of every 10, 15, 20, 30, 45, 60, 90, 120, 180, and 240 seconds. For each imaging protocol, the prostate displacement at the imaging time was corrected by subtracting prostate shifts from the subsequent displacements in that fraction. Furthermore, we conducted a principal component analysis to quantify the direction of prostate motion.

Results: Averaging histograms of every 240 and 60 seconds for all patients, vector displacements of the prostate were, respectively, within 3 and 2 mm for 95% of the treatment time. A vector margin of 1 mm achieved 91.2% coverage of the prostate with 30 second imaging. The principal component analysis for all fractions showed the largest variance in prostate position in the midsagittal plane at 54° from the anterior direction, indicating that anterosuperior to inferoposterior is the direction of greatest motion. The smallest prostate motion is in the left-right direction.

Conclusions: The magnitudes of intrafraction prostate motion along the superior-inferior and anterior-posterior directions are comparable, and the smallest motion is in the left-right direction. In the absence of continuous prostate motion monitoring, and under ideal circumstances, 1-, 2-, and 3-mm vector planning margins require a respective imaging frequency of every 15, 60, and 240 to account for intrafraction prostate motion while achieving adequate geometric target coverage for 95% of the time. © 2013 Elsevier Inc.

Reprint requests to: Ping Xia, PhD, 9500 Euclid Ave, Department of Radiation Oncology, Cleveland Clinic, Cleveland, OH 44195. Tel: (216) 444-1938; Fax: (216) 444-8934; E-mail: xiap@ccf.org

This research is supported in part by the United States Army Medical Research and Materiel Command (USAMRMC, W81XWH-080-0358). Conflict of interest: none.

Introduction

Modern radiation therapy for prostate cancer, imaging-guided radiotherapy in particular, has significantly improved our ability to localize the prostate prior to each treatment. With daily imaging guidance, the reduction of planning margins from 1.0-1.5 cm to 0.5-0.8 cm in intensity modulated treatment plans permits dose escalation with tolerable treatment toxicities in the rectum and bladder (1-5). Hypofractionated treatment regimens may further increase efficacy of radiation therapy according to the increasing evidence of a low alpha-beta ratio in prostate cancer (2). Further reduction of the planning margins in hypofractionated stereotactic body radiation therapy (SBRT) demands more precise prostate localization before treatment and more frequent imaging guidance during treatment. Furthermore, because the higher dose per fraction may prolong the treatment time, the probability of intrafraction prostate motion is greater than in conventional treatments. Using an electromagnetic device (Calypso, Calypso Medical, Seattle WA), monitoring the prostate motion and intervention during treatment is possible at a frequency of 10 Hz. If real-time monitoring at such a high frequency is not available, the relationship between the frequency of intrafraction monitoring and planning margins is not clear. The purpose of this study was to determine the magnitude of intrafraction prostate motion using real-time positioning data and to assess the idealized relationship between the planning margins and frequency of imaging guidance during treatment in the absence of continuous monitoring of the prostate location during treatment.

Methods and Materials

Thirty-one patients with prostate cancer were treated using intensity modulated radiation therapy (IMRT). They underwent real-time monitoring using an electromagnetic tracking system (Calypso) at our institution, and data from these patients were retrospectively analyzed. All patients underwent implantation of 3 beacon transponders within the prostate before simulation. A typical IMRT course consisted of 38-39 fractions. In our clinical practice, we used a threshold action level of 3 mm in any direction lasting >30 seconds to interrupt the treatment for repositioning. Thus, some daily treatments were split into 2-3 fractions. These split fractions were considered independent fractions for this analysis but only fractions with a treatment time >120 seconds of data available were included. The mean fraction length was 7 minutes and 23 seconds (± 94.1 seconds), and 1045 fractions were analyzed with a mean of 34 fractions (range 2-41) per patient.

Clinical alignment protocol

Pinnacle 8.0m treatment planning software (Philips, Amsterdam, the Netherlands) was used to identify the transponders and treatment isocenter coordinates. The coordinates of the transponders were manually entered by the therapists to the Calypso System and checked by a physicist to prepare for daily patient setup and real-time tracking during treatment.

Before the CT simulation, patients were instructed to have a bowel movement and to drink 20 oz of fluid, 30-45 minutes before the simulation. Patients were advised to follow the same instructions before each daily treatment to attempt to maintain the same anatomic relationship between the prostate and organs at

risk. No other interventions, such as enemas or rectal balloons, were used. Before each daily treatment, the patient was initially aligned to skin marks and then aligned to the target as defined by the Calypso isocenter. During treatment, the Calypso system continuously tracked the positions of the prostate. When the center of the transponders moved outside of the predetermined tolerance (3 mm displacement in any direction >30 seconds), the radiation beam was paused to reposition the patient. The operation and accuracy of the Calypso has been described previously with evidence in patients showing a mean (SD) agreement between Calypso and kV X-ray localization within 1.5 mm (0.9) and 1.9 mm (0.9) (4, 6-8). Data in phantoms has shown a mean (SD) agreement between X-ray and Calypso of 0.5 mm (0.1 mm) (7). These numbers only represent the difference between the KV X-ray and Calypso system as the ground truth is unknown. Of the 1045 fractions analyzed, 9 fractions in 8 patients had treatment interrupted.

Data process and analysis

Daily prostate localization and tracking data for each patient was stored on the Calypso workstation and was exported from the workstation onto individual spread sheets within Microsoft Excel (Microsoft, Seattle, WA). A Matlab (Mathworks, Natick, MA) tool was written to process the data efficiently.

The Calypso tracking data of each fraction contained a series of points composed of x, y, and z coordinates as a function of treatment time. The x, y, z in centimeters represents the prostate displacement relative to the isocenter at time zero with a sampling frequency of 10 Hz. The magnitude of the prostate displacement at a given time was calculated as the Euclidean distance from the initial position as given by Eq. (1).

$$D(t) = \sqrt{x(t)^2 + y(t)^2 + z(t)^2} \quad (1)$$

$D(t)$ is the magnitude of displacement and $x(t)$, $y(t)$, and $z(t)$ are the displacements in each of 3 orthogonal directions.

To simulate an ideal imaging and position correction of the prostate back to the isocenter, the displacement of x_i , y_i , and z_i at the time of correction, i , was set to zero by subtracting x_i , y_i , and z_i from the subsequent displacements of the fraction. For all fractions, to simulate different imaging protocols, this correction procedure was repeated at different intervals during each fraction (once every 10, 15, 20, 30, 45, 60, 90, 120, 180, and 240 seconds). Thus, for each fraction, the data was analyzed 10 times with a different simulated imaging frequency at each time.

To determine planning margins to account for intrafraction prostate motion, we calculated the percent of time during each fraction that the prostate displacement was greater than the given magnitudes of 1, 2, 3, 5, and 10 mm. In addition, a principal component analysis (PCA) was performed on each of the uncorrected fractions to characterize the 3-dimensional directions of prostate motion. PCA breaks down the data into 3 orthonormal principal component vectors, with the first in the direction of greatest variance. The second is orthogonal to the first and in the direction of greatest remaining variance, and the third is orthogonal to the other two and in the direction of least variance. The PCA provided the direction and magnitude of prostate motion as described by the variance of the probability distribution of prostate position.

The percentage of the total variance in prostate position accounted for by variance along each component axis was calculated for each fraction. This quantifies the percent of total prostate motion along that direction and the relative magnitude of motion in that direction. Also, the angle of each component axis from the anterior, superior, and right axes was calculated to characterize the direction of motion in anatomical context. The mean percent variance for each of the 3 principal components was calculated, and histograms of the angles from the anterior, superior, and right axes were created for all 3 components.

Results

Figure 1 shows the distribution of fraction durations, with a mean value of 7 minutes 21 seconds. Of note, the fraction duration for most fractions started from the first beam on to the last beam off of the entire daily treatment, except for 9 of 1045 fractions. Each of these 9 fractions could be a part of daily treatment, having a shorter time than a typical IMRT treatment time. Table 1 lists the mean and standard deviation percentage of treatment time during which the prostate was covered by 1-, 2-, 3-, 5-, and 10-mm geometric margins when no positional correction was simulated. From Table 1, the prostate displacement exceeded 1 mm for 74% of treatment time. Without intrafraction intervention, the geometric margin of 5 mm is needed to ensure complete geometric coverage. From a selected fraction, Fig. 2a-d show that more frequent repositioning of the prostate reduces the probability of the prostate moving out of the margins, defined in the horizontal axes. With intrafraction imaging and repositioning, the amount of time the displacement of the prostate exceeded 1 mm decreased from 75% with no intervention, to 40% with intervention every 4 minutes, to 15% with intervention every 1 minute, and to less than 5% with intervention every 10 seconds.

For each fraction, we generated similar data as in Fig. 2a-d, at imaging frequencies of 10, 15, 20, 30, 45, 60, 90, 120, 180, and 240 seconds. For all 1045 fractions and under each of these imaging frequencies, Table 2 lists the mean percentage of treatment time for which the adequate geometric coverage is achieved with margins of 1, 2, and 3 mm along with the standard deviation in parenthesis. These data show that with ideal imaging and position correction every 4 minutes, a 3-mm margin will contain the prostate for 95% of the treatment duration. However, a 2-mm

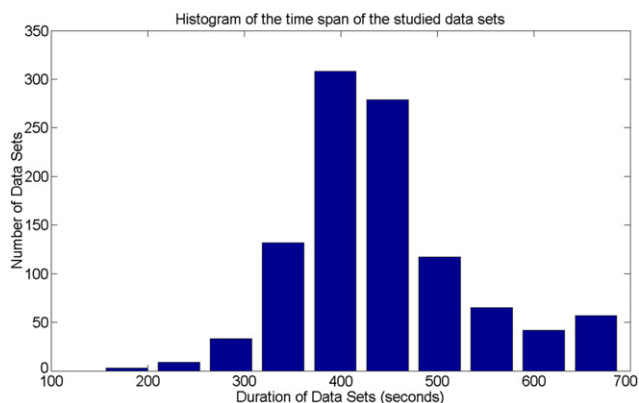


Fig. 1. Histogram showing the distribution of fraction lengths in the analyzed fractions of data.

Table 1 Geometric coverage without intrafraction motion correction

	Margin				
	1 mm	2 mm	3 mm	5 mm	10 mm
Mean geometric coverage	35.6%	76.5%	93.1%	99.4%	99.9%
Population SD	28.8%	24.6%	11.6%	2.2%	0.6%

Mean percent of each fraction the prostate was geometrically covered by 1-, 2-, 3-, 5-, and 10-mm margins with standard deviation for the fractions without simulated imaging correction.

motion margin requires imaging every 1 minute to ensure the geometric coverage for 95% of the treatment time. Furthermore, reducing the prostate motion margin to 1 mm may require imaging and repositioning every 15 seconds to achieve the same geometric coverage.

The PCA showed that the direction of the first component accounted for 81% of the total motion as described by the variance in prostate position, whereas the third principal component accounted for only 3%. Thus, most of the motion lies along the direction of the first principal component, and the third principal component has virtually no motion. The mean third principal component vector of all 2045 fractions lies at only 3.9° from the left-right axis. Therefore, prostate motion is almost completely contained to the sagittal plane. The angles of the first principal components from the anatomic axes were calculated for each fraction. Histograms of these angles can be seen in Fig. 3a-c and characterize the directions of the first principal components vectors. From Fig. 3, the direction with the greatest intrafraction prostate motion (81% as described by variance of position) lies in the anterior-superior quadrant of the sagittal plane with a median angle of 54° from the anterior axis. Because each principal component only describes a direction and is interchangeable with the 180-degree opposite of itself, the direction of greatest prostate motion lies in the superior-inferior, and slightly less along the anterior-posterior directions because of a median angle of 54° from the anterior axis.

Discussion

Intrafraction prostate motion has been estimated using various monitoring methods, including real-time tracking with the electromagnetic system (9), snap shooting of stereoscopic X-ray images (3), or using the combination of KV-MV X-ray images (10). The imaging frequencies used with these methods varied from 10 Hz to 0.01 Hz. Tanyi et al (11) showed that the appropriate planning margin to account for intrafraction prostate motion significantly depends on the imaging frequency. For systems using snap shooting X-rays, the imaging frequency, target position accuracy, extra X-ray exposure, and effect on treatment duration, must be carefully balanced, and trade-off decisions must be made. In the present study, using real-time, 3-dimensional tracking data from the Calypso system, we investigated the idealized relationship of positioning frequency and geometric coverage of theoretical planning margins.

Several studies (9, 12) have confirmed that the motion of the prostate is random, sporadic, and patient specific, which makes the prediction of the prostate motion difficult. Langen et al used 550

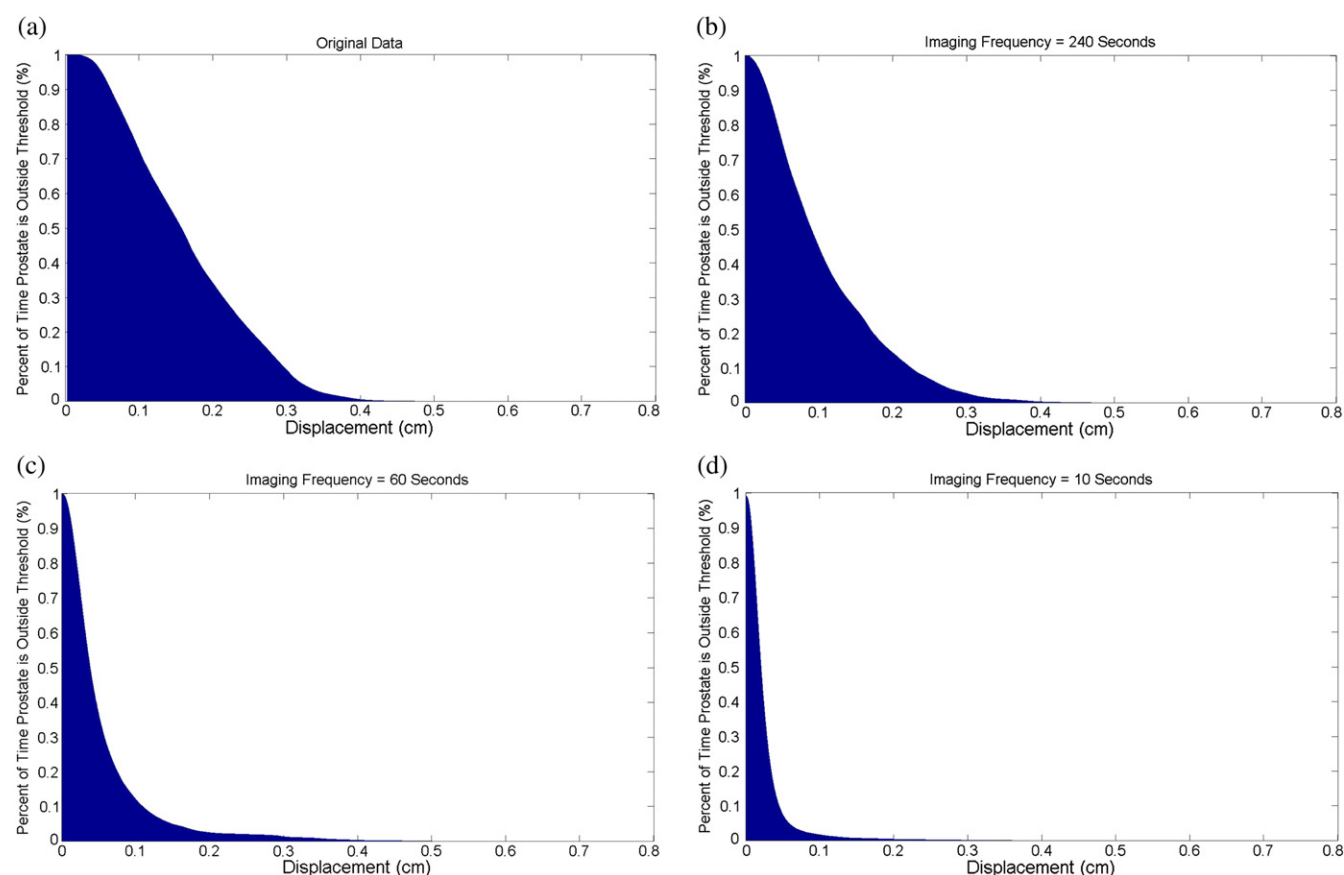


Fig. 2. Percentage of time (y axis) during the selected fraction the prostate spent displaced farther than a given distance (x axis) for no repositioning (a) and repositioning every 4 minutes (b), 1 minute (c), and 10 seconds (d).

fractions of Calypso data from 17 patients to characterize the intrafraction prostate movement without simulating any intervention or threshold. Their analysis showed average prostate displacement greater than 3 mm, 5 mm, and 10 mm of 13.6%, 3.3%, and 0.2% of the average treatment time of about 10 minutes, respectively. As seen in Table 1, our data showed that the prostate moved outside the respective planning margins only 7.1%, 0.7%, and 0.1% of treatment time. The smaller percentages of prostate displacements outside the corresponding planning margins from our data could be explained by shorter average treatment duration, approximately 7 minutes. Other clinical factors and specific patient populations may affect the pattern of intrafraction prostate motion.

In general, results obtained from Langen's study (9) and our study are in agreement, but our study has a different focus. We aimed to determine the idealized relationship of 3-dimensional positioning frequency and planning margin to assess practical limits of margin reduction when this technology is not available, instead of characterizing the pattern of the intrafraction prostate movements as in Langen's study (9). Therefore, we simulated an ideal correcting action by resetting the prostate displacement to zero at the rates of simulated imaging frequencies. Using low-frequency monitoring data from Cyberknife system, Xie et al (12) also investigated the optimal image sampling rate. They found that with a long sampling interval, it is difficult to guarantee not missing transient shifts of the prostate. By analyzing the discrete 427 data sets for 21 patients and allowing 5% of the data set to exceed the set motion limit, they found that the prostate

displacement >2 mm existed in 5%, 8%, 11%, and 14% of the data sets at 30, 60, 90, and 120-second imaging intervals, respectively. Using high-frequency monitoring data, our study showed that prostate displacement >2 mm occurred in 2.9%, 4.9%, 6.9%, and 8.9% of the data sets at 30, 60, 90, and 120 seconds, respectively.

Our results showed similar trends as observed by Xie et al (12). Because we reset the prostate displacement to an ideal position at the sampled imaging rate, the percentage of time the

Table 2 Geometric coverage with intrafraction motion correction

Seconds	1-mm margin	2-mm margin	3-mm margin
10	96.3% ($\pm 4.76\%$)	98.8% ($\pm 2.3\%$)	99.4% ($\pm 1.4\%$)
15	94.9% ($\pm 6.2\%$)	98.3% ($\pm 3.1\%$)	99.1% ($\pm 2.0\%$)
20	93.7% ($\pm 7.4\%$)	97.9% ($\pm 3.9\%$)	98.9% ($\pm 2.4\%$)
30	91.2% ($\pm 9.3\%$)	97.1% ($\pm 4.9\%$)	98.4% ($\pm 3.2\%$)
45	87.7% ($\pm 11.7\%$)	96.1% ($\pm 6.5\%$)	97.9% ($\pm 4.2\%$)
60	84.3% ($\pm 13.9\%$)	95.1% ($\pm 8.0\%$)	97.5% ($\pm 5.3\%$)
90	77.6% ($\pm 17.8\%$)	93.1% ($\pm 10.9\%$)	96.7% ($\pm 7.1\%$)
120	71.5% ($\pm 20.4\%$)	91.4% ($\pm 12.8\%$)	96.2% ($\pm 8.0\%$)
180	62.1% ($\pm 23.6\%$)	88.2% ($\pm 16.7\%$)	95.5% ($\pm 9.8\%$)
240	54.5% ($\pm 25.4\%$)	85.4% ($\pm 19.0\%$)	95.0% ($\pm 10.2\%$)

Mean (\pm SD) percent of each fraction the prostate was geometrically covered by a given margin with simulated correction at each imaging frequency.

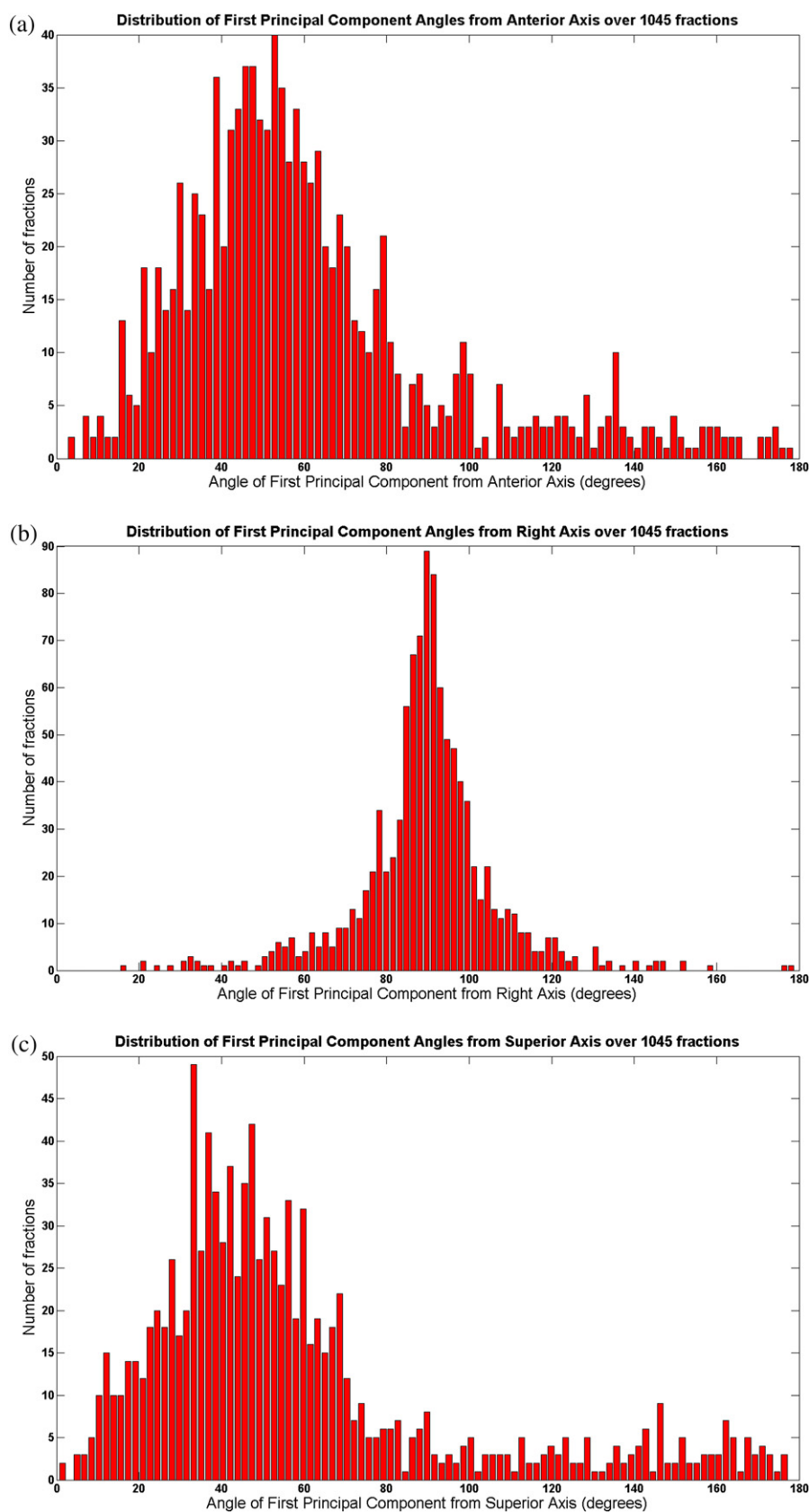


Fig. 3. Histogram of the angles of the first principal components from the (a) anterior, (b) right, and (c) superior axes.

prostate moved outside the margin was smaller than the corresponding data from Xie et al. Because of the idealized assumptions of a perfect correction immediately, our analysis estimates an upper bound of the gain possible from frequent repositioning. In their study, Xie et al (12) also showed that undersampling of the motion trajectory could lead to different motion pattern, potentially missing many transient shifts of the prostate. The high sampling rate of the Calypso system allows us to examine motion in high temporal resolution, which cannot be offered in other prostate motion monitoring systems because of practicality issues of treatment time and extra radiation exposure. Despite small differences, the results from this study and the study from Xie et al show a high degree of corroboration, indicating that an imaging frequency of 30 seconds does not contain a significant amount of transient deviations above the 1-mm margin.

The PCA shows that the direction of motion is mostly along the anterior-superior to inferior-posterior axis, with virtually no motion along the right-left axis. This is consistent with the theory that the organs at risk, the bladder and rectum, are driving the prostate motion and thus creating the direction of the prostate motion. These data show that intrafractional margins could be reduced along the right-left axis because there is little motion in this direction. On the basis of the PCA, the intrafraction prostate motion is slightly more likely along the superior-inferior direction than the anterior-posterior direction, and one can assume the an equal probability in both axes and zero possibility in the lateral directions. With this assumption, we can calculate the component planning margins from the vector margins. For example, 3-mm vector planning margin equals to 2.1-mm component planning margin in both superior-inferior and anterior-posterior directions.

One limitation that should be considered with this study is that simulated corrections were not actually performed during the treatment. This frequent intervention will, in practice, introduce other uncertainties and prolongation of treatment time. Action threshold strategies have been used as a trade-off to allow intrafraction monitoring, intervening only when necessary to stay within the prescribed margin. The result of the present study could provide guidance, combined with other uncertainty estimates, to choose the action (eg, imaging and repositioning) frequency when a continuous prostate motion surveillance is not available.

Another limitation of this study is that these data are collected from IMRT studies, which may have a shorter duration than a typical SBRT procedure using a conventional IMRT delivery. The protracted treatment time of SBRT could cause more frequent or larger prostate movement as the treatment time increases; however, one study of pre- and post-treatment displacement of prostate as a function of treatment length ranging from 2-27 minutes did not show any significant difference in prostate displacement (13). Furthermore, using a high dose rate (eg, 1000 MU/min) and intensity modulated volumetric arc delivery, SBRT treatment time may not be necessary longer than the conventional IMRT delivery.

In our study, we assumed the displacement of the prostate at the time of imaging was corrected perfectly and immediately. In clinical practice, the uncertainty of these corrections will be nonzero and will therefore increase the required margin above those estimated in this best-case analysis. Because of sporadic motion of the prostate, continuous monitoring of the prostate motion and intervening on a threshold will be more accurate than periodic, less frequent imaging. In the absence of a continuous

surveillance system, the data in Table 2 can offer guidance when making trade-off decisions between imaging frequency and margin size. Furthermore, we did not take into account potential prostate deformation or rotation, which was classified to be small and can be negligible (14). Our analysis is based on geometric coverage, not dosimetric coverage, which could depend on conformity of each individual plan.

Conclusions

Under ideal circumstances, to account for intrafraction prostate motion, a 3-mm vector planning margin is required for an imaging frequency of every 4 minutes. With 1-mm vector planning margin, prostate position correction every 15 seconds is required, which could be impractical without a precise automated real-time positioning system. Considering the innate uncertainty in repositioning and protracted treatment time due to frequent interventions, 2-mm vector planning margin to account for intrafraction prostate motion with an imaging frequency of every 2-3 minutes would be a practical approach. Two-millimeter vector planning margin is approximately 1.4 mm component margins along the superior-inferior and anterior-posterior direction with a zero component planning margin laterally.

References

1. Beltran C, Herman MG, Davis BJ. Planning target margin calculations for prostate radiotherapy based on intrafraction and interfraction motion using four localization methods. *Int J Radiat Oncol Biol Phys* 2008;70:289-295.
2. Rene N, Faria S, Cury F, et al. Hypofractionated radiotherapy for favorable risk prostate cancer. *Int J Radiat Oncol Biol Phys* 2010;77: 805-810.
3. Alonso-Arrizabalaga S, Brualla González L, Roselló Ferrando JV, et al. Prostate planning treatment volume margin calculation based on the ExacTrac X-Ray 6D image-guided system: margins for various clinical implementations. *Int J Radiat Oncol Biol Phys* 2007; 69:936-943.
4. Li HS, Chetty IJ, Enke CA, et al. Dosimetric consequences of intrafraction prostate motion. *Int J Radiat Oncol Biol Phys* 2008;71: 801-812.
5. Biagioli MC, Hoffe SE. Emerging technologies in prostate cancer radiation therapy: improving the therapeutic window. *Cancer Control* 2010;17:223-232.
6. Litzenberg DW, Balter JM, Hadley SW, et al. Influence of intrafraction motion on margins for prostate radiotherapy. *Int J Radiat Oncol Biol Phys* 2006;65:548-553.
7. Willoughby TR, Kupelian PA, Pouliot J, et al. Target localization and real-time tracking using the Calypso 4D localization system in patients with localized prostate cancer. *Int J Radiat Oncol Biol Phys* 2006;65: 528-534.
8. Kupelian P, Willoughby T, Mahadevan A, et al. Multi-institutional clinical experience with the Calypso System in localization and continuous, real-time monitoring of the prostate gland during external radiotherapy. *Int J Radiat Oncol Biol Phys* 2007;67: 1088-1098.
9. Langen KM, Willoughby TR, Meeks SL, et al. Observations on real-time prostate gland motion using electromagnetic tracking. *Int J Radiat Oncol Biol Phys* 2008;71:1084-1090.
10. Adamson J, Wu Q. Prostate intrafraction motion evaluation using kV fluoroscopy during treatment delivery: a feasibility and accuracy study. *Med Phys* 2008;35:1793-1806.

11. Tanyi JA, He T, Summers PA, et al. Assessment of planning target volume margins for intensity-modulated radiotherapy of the prostate gland: role of daily inter- and intrafraction motion. *Int J Radiat Oncol Biol Phys* 2010;78:1579-1585.
12. Xie Y, Djajaputra D, King CR, et al. Intrafractional motion of the prostate during hypofractionated radiotherapy. *Int J Radiat Oncol Biol Phys* 2008;72:236-246.
13. Enmark M, Korreman S, Nyström H. IGRT of prostate cancer; is the margin reduction gained from daily IG time-dependent? *Acta Oncol* 2006;45:907-914.
14. Deurloo KEI, Steenbakkers RJHM, Zijp LJ, et al. Quantification of shape variation of prostate and seminal vesicles during external beam radiotherapy. *Int J Radiat Oncol Biol Phys* 2005; 61:228-238.

Comparison of three strategies in management of independent movement of the prostate and pelvic lymph nodes

Ping Xia^{a)}

Department of Radiation Oncology, University of California-San Francisco, San Francisco, California 94143 and Department of Radiation Oncology, Cleveland Clinic, Cleveland, Ohio 44195

Peng Qi, Andrew Hwang, Erica Kinsey, Jean Pouliot, and Mack Roach III

Department of Radiation Oncology, University of California-San Francisco, San Francisco, California 94143

(Received 6 February 2010; revised 5 July 2010; accepted for publication 23 July 2010; published 27 August 2010)

Purpose: Concurrent irradiation of the prostate and pelvic lymph nodes is technically challenging due to treating one moving target and one immobile target. The purposes of this article are to propose a new management strategy and to compare this strategy to the conventional isocenter shift method and the previously proposed MLC-shifting method.

Methods: To cope with two target volumes (one moving and one immobile), the authors propose a new management strategy referred to as multiple adaptive plans (MAPs). This strategy involves the creation of a pool of plans for a number of potential prostate locations. Without requiring any additional hardware or software, the MAP strategy is to choose a plan from the pool that most closely matches the “prostate position of the day.” This position can be determined by dual image registrations: One aligned to the implant markers in the prostate and the other aligned to the pelvic bones. This strategy was clinically implemented for a special patient with high risk prostate cancer and pathologically confirmed positive pelvic lymph nodes, requiring concurrent IMRT treatment of the prostate and pelvic lymph nodes. Because this patient had an abdominal kidney, small planning margins around the both targets were desired. Using 17 daily acquired megavoltage cone beam CTs (CBCTs), three sets of validation plans were calculated to retrospectively evaluate the MAP strategy as well as the isoshifting and MLC-shifting strategies.

Results: According to the validation plans, MAP, isoshifting, and MLC-shifting strategies resulted in D_{95} of the prostate $>95\%$ of the daily dose on 65%, 100%, and 100% treatment days, respectively. Similarly, D_{95} of the pelvic lymph nodal was $>95\%$ of the daily dose on 100%, 75%, and 94% of treatment days, respectively.

Conclusions: None of the above strategies simultaneously achieved all treatment goals. Among the three strategies, the MLC shifting was most successful. Validation plans based on daily CBCTs are useful to evaluate the effectiveness of the motion management strategies and to provide additional dose guidance if further dose compensation is needed. © 2010 American Association of Physicists in Medicine. [DOI: [10.1118/1.3480505](https://doi.org/10.1118/1.3480505)]

Key words: movement management, adaptive strategy, prostate cancer, intensity-modulated radiotherapy, and image-guided radiotherapy

I. INTRODUCTION

Although the prophylactic irradiation of lymph nodes is a routine practice for many cancer sites, the role of pelvic lymph node irradiation in the treatment of localized prostate cancer is controversial. Since the initial reports in the 1980s,^{1,2} the typical four-field treatment technique for pelvic irradiation has largely remained unchanged. With this conventional technique, the benefits and risks of pelvic irradiation have been debated for more than two decades.^{1,3–5} Using a novel magnetic resonance lymphangiographic technique, Shih *et al.*⁶ showed that the conventional field borders, defined according to the bony anatomy, do not adequately include the pelvic lymph nodal regions, resulting in poor radiation dose coverage.⁷ Despite this inadequate dose

coverage, investigators from the Radiation Therapy Oncology Group (RTOG) still demonstrated progression free survival benefit with prophylactic pelvic nodal lymph irradiation.⁸

For the prostate only treatment,^{9,10} intensity-modulated radiotherapy (IMRT) has shown significant clinical advantages over conventional and three-dimensional conformal radiotherapy. There is also a growing body of data^{7,11} suggesting that IMRT provides even greater advantages when pelvic nodes are being irradiated. For the concurrent treatment of the prostate and pelvic lymph nodes, one⁷ of our previous studies reported that IMRT plans not only significantly improved the dose coverage to the pelvic lymph nodes but also greatly reduced the doses to the rectum, bladder, and the

small bowel. However, this concurrent treatment of the prostate and the pelvic lymph nodes poses the new technical challenge of simultaneously treating a moving organ and an immobile tumor volume.

Several previous studies suggest that movement of the prostate may vary from a few millimeters up to 1.5 cm relative to the pelvic bones.^{12–14} In contrast, the pelvic lymph nodes are relatively fixed in close proximity to vascular structures,⁶ which are presumably fixed with respect to the pelvic bony anatomy.¹⁵ This independent movement of two targeted volumes may require a large planning margin on one of the targets, depending on how the daily images are aligned. If the daily images are aligned to the pelvic bones, a large planning margin around the prostate would be needed. If the daily images are aligned to the prostate, a large planning margin would be needed for the pelvic lymph nodes. Both alignment methods would result in the inclusion of normal structures in the high dose area of the radiation fields, increasing the risk of normal tissue complications. Depending on the risk and benefit trade-off for a specific patient at the discretion of the treating physician, either alignment method could be clinically reasonable. The challenge is to satisfy the demand of achieving dose coverage while using a small planning margin for both targets.

The ideal approach to resolve this challenge is real time replanning on a daily basis, but because of extended planning time, real time replanning is not currently practical. Without requiring real time dose recalculation, we have proposed a MLC leaf-shifting algorithm to provide an alternative solution.¹⁶ The clinical implementation of this MLC-shifting approach requires a new feature in the record and verify system, which would allow users to adjust the MLC leaf positions at the treatment console in near real time. To circumvent this obstacle, in this paper, we proposed another strategy of creating a pool of IMRT plans to accommodate multiple presumed prostate positions. This strategy is referred to as multiple adaptive plan (MAP) IMRT. This strategy was implemented clinically for a special patient, for whom small planning margins around the prostate and the pelvic lymph nodes were demanded. Using the daily volumetric imaging acquired for the patient, we retrospectively evaluated and compared three strategies in the management of independent movement of the prostate and pelvic lymph nodes including MAP, isoshifting, and MLC-shifting strategies. In this paper, the isoshifting strategy consists of shifting the treatment isocenter based on the prostate movement relative to the pelvic bones. Because the pattern of prostate motion varies from patient to patient, the result of this comparison may not be directly generalized to other patients. The purpose of this paper is to explore the feasibility and limitations of each strategy.

II. MATERIALS AND METHODS

II.A. Multiple adaptive plan strategy

With the MAP strategy, a pool of IMRT plans was created based on a planning CT and each plan was individually optimized to accommodate a presumed prostate position. Be-

cause the number of possible prostate positions for each patient could be very large, for a special case (described below), we created a pool of five plans to compensate for prostate movements of 0.5 and 1.0 cm in the posterior and superior directions. To keep the number of plans in the pool and the workload reasonable, the prostate movement in the inferior and anterior directions was compensated by adding a 0.6 cm margin. It was assumed that lateral motion of the prostate is negligible^{12–14} and the enlarged inferior and anterior margins had a minimum impact on rectal sparing.¹⁷ An additional 0.2 cm planning margin in the posterior, superior, and lateral directions for the prostate accounted for uncertainties such as image registration uncertainty. The planning margin for the pelvic lymph nodes was 0.5 cm.

During treatment planning, five shifted prostate contours in the superior and posterior directions were created using an in-house program that read in the coordinates of the original prostate contours and shifted the coordinates of the contour to the presumed positions. These shifted prostate contours were input back into the treatment planning system (Pinnacle, version 7.6, Philips Medical Systems, Andover, MA) and appended in the set of planning contours for the patient. The initial IMRT plan for the patient was created based on our established planning protocol published elsewhere.^{7,18} Briefly, most patients were first treated with 54 Gy (2 Gy/fraction) to the prostate and seminal vesicles, with concurrent pelvic lymph node dose of 48.6 Gy (1.8 Gy/fraction). The prostate and seminal vesicles then received an additional cone-down dose of 18 Gy (2 Gy/fraction), bringing the total dose to 72 Gy. All of these doses were prescribed to cover 95% of the planning tumor volume (PTV). 18 MV photons were used throughout the treatment. All IMRT plans were delivered with a step and shoot method using Siemens Linear Accelerators (Oncor, Siemens Medical Solution, Concord, CA). The first portion of the treatment used 45 segments and seven beam angles (0°, 35°, 90°, 160°, 200°, 270°, and 315° in IEC convention). The second cone-down portion of the treatment used 25 segments and seven slightly different beam angles (0°, 55°, 90°, 135°, 225°, 270°, and 305° in IEC convention). A planning dose constraint template has been published elsewhere.¹⁸

For the MAP strategy, all plans were created with shifted prostate contours except for the initial plan, which was based on the anatomy of the planning CT. Since the rectum and bladder were not shifted with the prostate, the anatomic relationship of these two organs with the shifted prostate was invalidated, rendering the initial planning dose constraints to the rectum and bladder irrelevant. To circumvent this problem, we constructed an artificial ring structure¹⁹ around the shifted prostate to guide the planning system to produce highly conformal plans, thus effectively protecting the rectum and bladder. Figure 1 shows isodose distributions for five prostate positions, demonstrating that similarly conformal dose distributions can be achieved with this planning tactic.

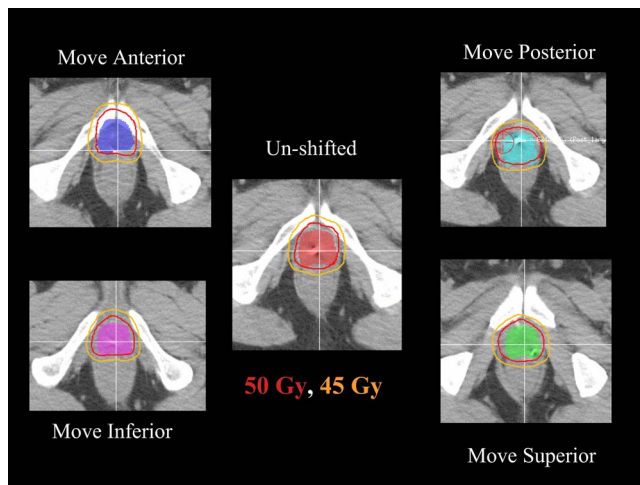


FIG. 1. Dose distributions of five MAP-IMRT plans displayed axial images, demonstrating similar conformal distributions in shifted plans can be achieved as the unshifted plan when using a rigid structure.

II.B. Isoshifting strategy

For prostate only treatment, shifting the treatment isocenter based on implanted markers inside the prostate is an effective strategy, which has been routinely used clinically. It should be noted that the isocenter shifts determined with this procedure often include two components: Prostate motion relative to the bony structure and patient setup error. For prostate only treatment, it was not necessary to separate the prostate motion from the patient setup error. As mentioned in Sec. I, this strategy may not be effective for concurrent treatment of the prostate (a moving target) and pelvic lymph nodes (an immobile target). Nevertheless, for a fair comparison among the three different strategies, the isoshifting strategy in this paper only corrected for the prostate motion, not including the setup error.

II.C. MLC-shifting strategy

The MLC-shifting strategy is based on our previously proposed leaf-shifting algorithm,¹⁶ which can follow the movement of the prostate while not significantly affecting dose distributions to the pelvic lymph nodes. Briefly, based on the magnitude and direction of the daily prostate movement, the algorithm was designed to adjust the positions of selected MLC leaf pairs to follow the translational motion of the prostate for each beam. The algorithm assumes that the prostate is a rigid body and the rotational motion is negligible. After shifting, the distance between the leaves in each shifted MLC pairs is kept the same as in the original plan. In

other words, the portion of each MLC aperture that encompasses the prostate is translated to match the prostate position as determined by daily imaging, while the MLC leaves that expose radiation to the lymph nodes are not moved. Because the field size is unchanged and the changes in the off-axis factors contribute only a negligible change to the dose distribution,¹⁶ a real time dose calculation is not required for this strategy. Currently, this strategy is not clinically feasible as it requires a new feature in the record and verify system to permit efficient adjustment of MLC leaf positions at the treatment console. Furthermore, logistic issues such as the pretreatment quality assurance have not been explored.

II.D. A special clinical case

A patient with high risk prostate cancer known to have nodal metastasis adjacent to a “horse-shoe” abdominal kidney was treated with the MAP strategy. The kidney was the major dose limiting organ for this patient. The kidney volume receiving more than 20 Gy (V20) was desired to be less than 15%. For this special case, an initial plan was designed to concurrently treat the prostate to 50 Gy and pelvic nodes to 45 Gy in 25 fractions, followed by a boost dose of 22 Gy to the prostate. For this patient, due to the special anatomy of abdominal kidney, the image guidance was initially altered to align to the pelvic bone to ensure the protection of the abdominal kidney while the planning margin to the prostate was enlarged to 1.0 cm (0.8 cm posteriorly). After eight treatments, the patient complained of rectal irritation; therefore, the subsequent treatment (17 fractions) was changed to MAP IMRT.

II.E. Dual image registration

To determine the prostate motion relative to the pelvic bone, two image registrations are needed using a single megavoltage cone beam CT (MV-CBCT) acquired prior to each treatment. The MV-CBCT was acquired with a total of 2 MU over 210° arc length using a commercial system (MVision™, Siemens Medical Solutions, Concord, CA). After MV-CBCT acquisition, two successive image registration procedures, one aligned to the pelvic bones and the other aligned to the implanted markers, were performed. The couch shifts from the bony alignment represent the setup error and were subsequently corrected by shifting the treatment couch. The prostate displacement relative to the pelvic bones was determined by the difference between the shifts of the two alignments. Based on the prostate position of the day, the IMRT plan in which the planned prostate position was best matched with the actual prostate position was chosen

TABLE I. MAP-IMRT plans and its clinical usage for 17 treatment days.

Plan type	Normal plan	Small posterior shifts	Large posterior shifts	Small superior shifts	Large superior shifts
Shifts	<0.3 cm ^a	0.4–0.7 cm	0.8–1.3 cm	0.4–0.7 cm	0.8–1.3 cm
Usage	6	1	0	7	3

^aShifts <0.3 cm in all directions or shifts dominantly in inferior or anterior directions.

according to the criteria shown in Table I. If the prostate moved in two different directions, the direction with the larger shift was compensated. If the shifts in superior and posterior directions were the same, the superior shift was compensated.

II.F. Relative treatment dose comparison and analysis

With daily MV-CBCT, we calculated the delivered dose to the patient anatomy of the day. While we are under development to calibrate the CT density and to correct for the cupping effect of the MV-CBCT, we assigned a CT density of 1 g/cm^3 to all tissue. We also used the external contour of the planning CT to supplement the missing tissue (assigned to a CT density of 1 g/cm^3) due to the limited field of view with the current MV-CBCT acquisition system. With these approximations, the dose distributions calculated on MV-CBCTs were used for relative dose comparison with intended plans for this study.

Because of limited soft tissue contrast of low dose (2 MU/scan) MV-CBCT, directly contouring all organs of interest is challenging. For this study, we focused on the validation of the dose coverage of the two tumor targets and the dose to the kidney. Because of daily organ deformation, in addition to limited soft tissue contrast in MV-CBCT, the rectum and bladder were not included in the validation plans.

After rigid image registration of the pelvic bones, we transferred contours of the pelvic lymph nodes and the kidney from the planning CT to each daily MV-CBCT. Each MV-CBCT was input into the Pinnacle planning system as the primary image set and an in-house program was written to allow the selected contoured planning structures to be input with the planning CT (as the secondary image) into the Pinnacle system. Assuming a stationary relationship between the pelvic lymph nodes and the pelvic bones, the pelvic lymph nodal volume and the kidney were transferred from the planning CT to the MV-CBCT after a rigid body image fusion by aligning the pelvic bony structures. It should be noted that the breathing motion associated with the kidney is ignored in this study. The great challenge was to transfer the prostate contour. Once again, one could register the implanted markers between the daily MV-CBCT and planning CT to transfer the contour of the prostate. The image registration tool provided by the Pinnacle system automatically utilized translation and rotation transformation, but during the treatment only translational shifts were available. To fairly represent the treatment position of the prostate, the prostate contour from the planning CT was shifted according to the daily detected motion using an in-house program. The shifted contour, which represented the “prostate position of the day,” was subsequently input into the corresponding MV-CBCT.

Three sets of validation plans were generated and compared. The first set of validation plans was created according to the MAP strategy; the second set was based on the isoshifting strategy; and the third set utilized the MLC-shifting method. For each MAP validation plan, the delivered plan of the day was directly applied to the corresponding MV-CBCT

of the day. For each isoshift plan, the treatment isocenter was shifted according to the detected prostate displacement of the day and the MLC segments from the original plan were again applied to the MV-CBCT of the day with the shifted isocenter. In each MLC-shift plan, the affected MLC pairs in all segments from the original IMRT plan (the plan for unshifted prostate position) were shifted to track the prostate position of the day. The resultant dose distribution of each MLC-shift plan was calculated on the corresponding MV-CBCT of the day.

III. RESULTS

III.A. MAP-IMRT plans

A set of five individually optimized IMRT plans, referred to as MAP plans, was prepared and approved for the treatment of this patient. Table I lists the clinical usage of each plan over 17 treatment days. Figures 2(a) and 2(b) show the resultant dose volume histograms (DVHs) of the PTV, pelvic lymph nodes, small bowel, and kidney. The DVHs of the MAP plans were slightly different from each other because the optimal solution found by the computer optimizer was slightly different for each scenario.

III.B. Image guidance

Based on the 17 MV-CBCT acquired for this patient, the prostate moved 0.4–0.7 cm in the superior direction in 38% of treatment days, ≥ 0.8 cm superiorly in 19%, 0.4–0.7 cm posteriorly in 12%, and ≤ 0.3 cm in all directions in 31%. Seven of 17 days had a setup error ≥ 0.5 cm in any direction, while the remaining days had a setup error ≤ 0.5 cm in any direction. Setup errors ≥ 0.1 cm in any direction were corrected. Figure 3 shows the detected daily setup errors and the prostate movements along the three major axes. For this specific patient, the prostate movement was not random, shifting in the superior direction in more than 50% of the treatment days.

III.C. Dose validation with MV-CBCT

Figure 4(a) shows the details of the dose to 95% of the prostate (D_{95}) calculated based on daily MV-CBCT. The D_{95} 's of the MAP strategy were the delivered daily dose calculated based on the chosen plan of the day, compared to the D_{95} of the isoshifting and MLC-shifting methods. Since the MAP method only accounted for prostate movement in one direction, $D_{95} \geq 95\%$ of the prescription dose was only achieved on 11 of 17 days (65%). As expected, the isoshifting method followed the prostate movement and achieved $D_{95} \geq 95\%$ of the prescription dose for all 17 treatment days. Similarly, the MLC-shifting method also achieved $D_{95} \geq 95\%$ of the prescription dose in each of the 17 days. As noticed in Fig. 4(a), on the 15th treatment day, the detected prostate movements were 1.2 cm superior and 1.2 cm posterior, but only the superior shift was compensated by choosing the large superiorly shifted MAP-IMRT plan for the treatment. A similar situation occurred on the fifth treatment day.

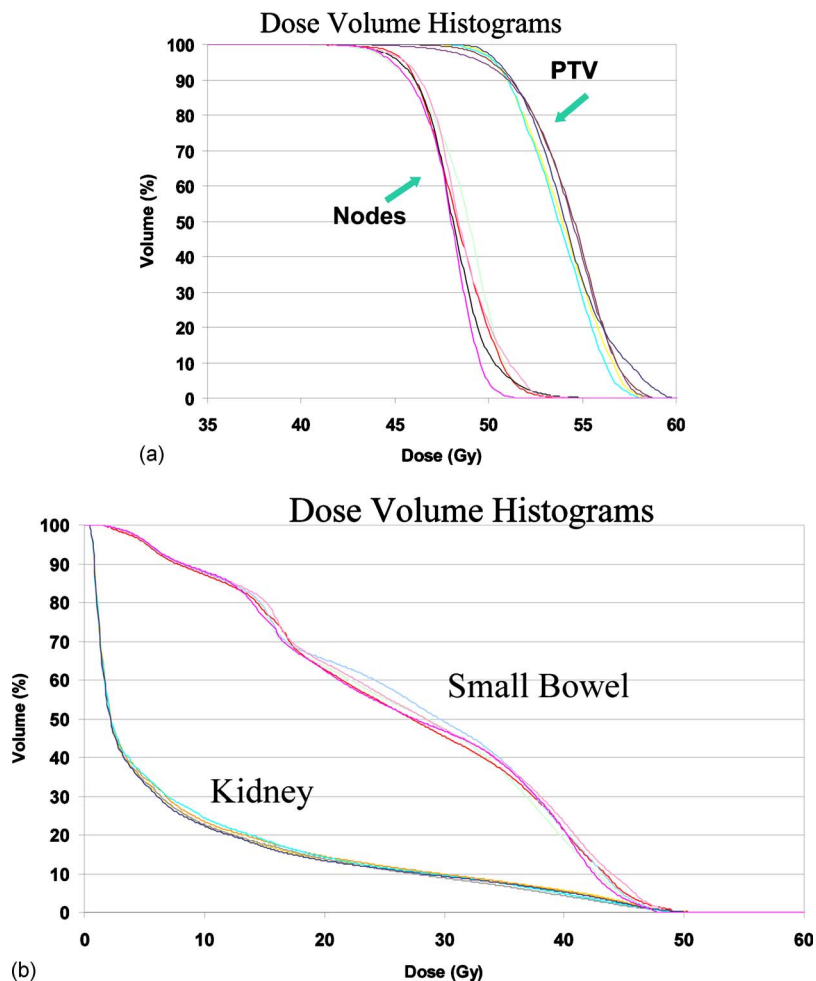


FIG. 2. (a) The dose volume histograms for the PTV and pelvic lymph nodes. (b) The DVHs for the small bowel and kidney.

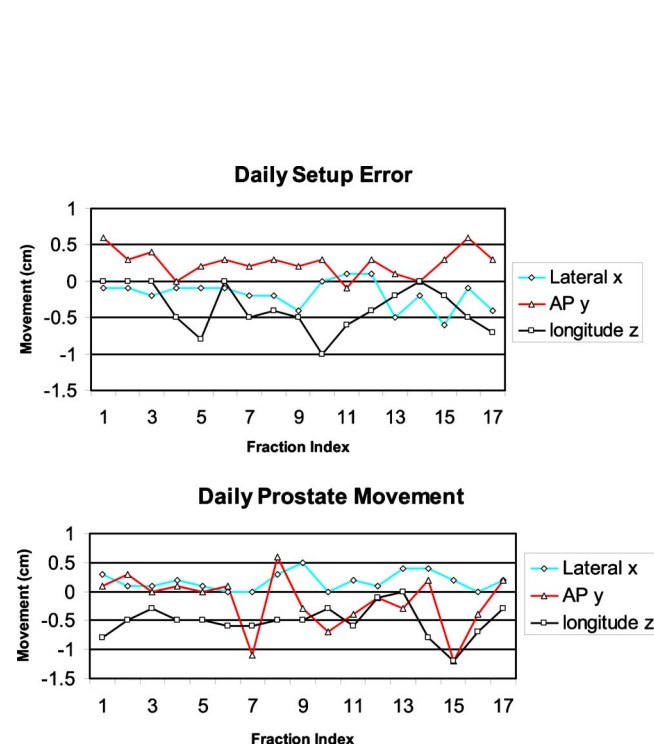


FIG. 3. The detected daily setup errors and the prostate movements along the three major axes for the 17 treatment days.

Figure 4(b) shows the dose to 95% of the pelvic lymph nodes (D_{95}). The MAP-IMRT method achieved $D_{95} \geq 95\%$ of the prescription dose for all 17 days. The isoshifting method would have delivered $D_{95} \geq 95\%$ of the prescription dose in 13 of 17 days (76% of the treatment time), compared to 16 days (94% of the treatment time) in MLC-shifting method.

For the kidney, we used the end point of V_{20} , the percentage volume receiving more than 20 Gy, to evaluate the three different strategies. With the MAP strategy, V_{20} of the kidney was $\leq 15\%$ for 13 of 17 days, as shown in Fig. 4(c). With the isoshifting method, V_{20} of the kidney was $\leq 15\%$ for only 2 of 17 days, compared to 14 of 17 days with MLC-shifting method. These results demonstrate that the MAP and MLC-shifting methods achieve better protection of the kidney than the isoshifting method.

IV. DISCUSSION

The current study describes our clinical experience in applying a new concept of multiple IMRT plans to accommodate independent movement of the prostate and pelvic lymph nodes under daily MV-CBCT image guidance. Although clinical implementation of this adaptive strategy at the current stage is still laborious and imperfect, this study provides a "proof of principle," describing a feasible planning, deliv-

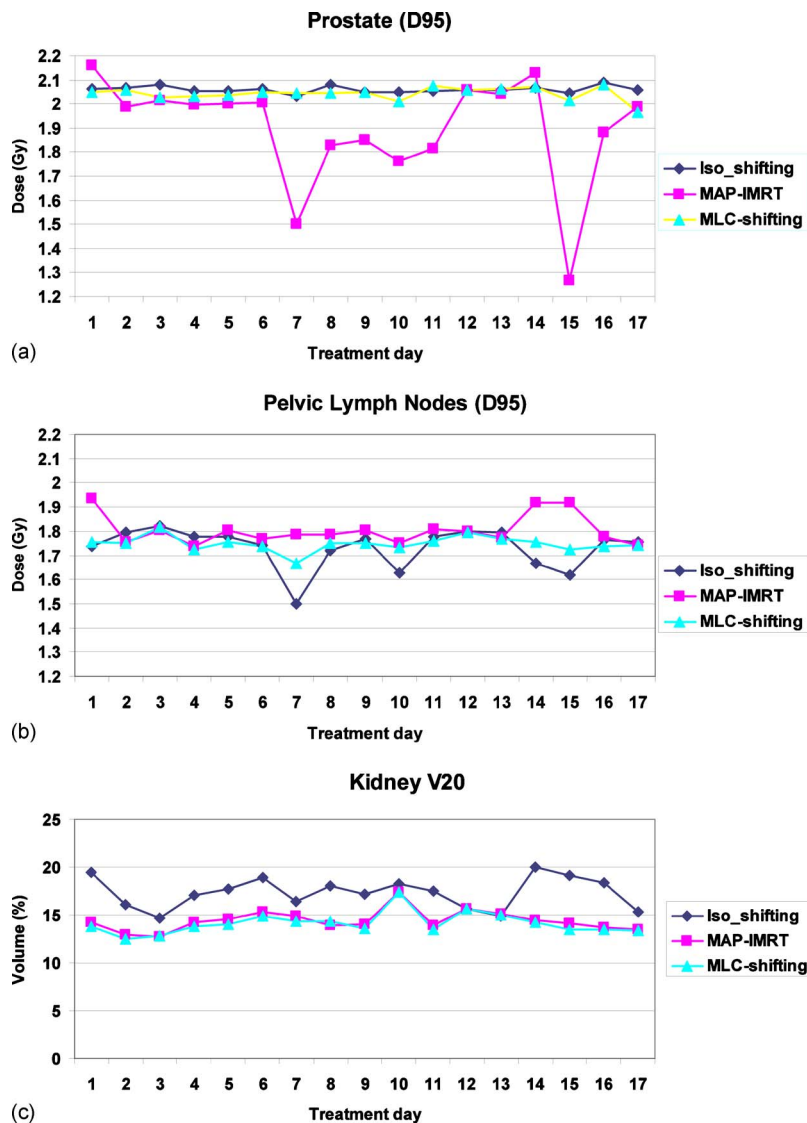


FIG. 4. (a) The dose to 95% of the prostate (D_{95}) calculated based on daily MV-CBCT for the isoshifting, MAP-IMRT, and MLC-shifting strategies. (b) The dose to 95% of the pelvic lymph nodes (D_{95}) calculated based on daily MV-CBCT for the three strategies. (c) The percentage volume receiving more than 20 Gy for the corresponding strategies.

ery, and verification process. For this particular patient, our primary goal of adequately treating the pelvic lymph nodes and prostate while protecting the kidney in the first phase of treatment was achieved. Because of the limited number of MAP IMRT plans in the pool for this early clinical implementation, only translational movement of the prostate in one direction was compensated. As shown in Fig. 4(a), this compensation was not sufficient when the prostate movement of the day was large in the superior and posterior directions, resulting in underdose of the prostate on these dates. Fortunately, the offline validation plans based on daily cone beam CT provided dose guidance for subsequent prostate boost treatments. This concept could be potentially extended to other pelvic, abdominal, and thoracic malignancies as well.

With advances in imaging technology and computer optimized treatment planning, we anticipated that it will be possible to acquire daily CT images and to develop an ideal strategy for real time replanning on a daily basis. Some researchers are already working to develop deformable image registration to improve the efficiency of structure

delineation,^{20–22} while others have sought to develop fast dose calculation engines and fast computer optimization algorithms.^{23–25} For prostate only treatment, our clinical experience and other published studies^{26,27} support that the iso-center shifting strategy is practical and effective. However, for concurrent treatment of the prostate and pelvic lymph nodes, this strategy may require a large planning margin for the pelvic lymph nodes, which may not be optimal if a small planning margin is desired, although a simulation study¹⁵ showed that the problem of independent movement of the prostate and pelvic lymph nodes was negligible. It should be noted that this study was based on an assumption of a random movement of the prostate from the position at the planning CT and the validity of this assumption may need to be further investigated. Other studies^{28–31} have demonstrated that prostate movement may not necessarily be random but depend on the shapes of the rectum and bladder during acquisition of the planning CT. The data from this study also show that the prostate position does not randomly displace from the position at CT simulation.

The MAP and MLC-shifting strategies investigated in this

study were not perfect and further improvement is necessary. Due to time and resource limitations, the MAP strategy can only anticipate a few presumed prostate positions. The planning process for five plans took about 1 day to complete. Quality assurance of these five plans took an additional 4 h to complete. In addition, a simple spread sheet (EXCEL and MICROSOFT OFFICE) was prepared to calculate the prostate movement relative to the pelvic bones. During each treatment, a physicist was present to help therapists to choose a proper plan. To create a relatively large number of MAP-IMRT plans without significantly increasing planning time, one could apply the MLC-shifting algorithm to create MAP plans for prostate motions in multiple directions provided that a fine MLC leaf width is available.

The clinical implementation of the MLC-shifting method requires a new feature in the record and verify system, which will allow users to adjust the MLC leaf positions at the treatment console in the near real time. As indicated in our study, this method can be considered as a simplified real time planning, without requiring contouring of each planning structures and fast dose calculation engines. With a finite MLC leaf width, the MLC-shifting strategy will have a limited resolution in the superior and inferior directions. Although a finer leaf width of 0.5 cm (rather than 1.0 cm used for this study) is commonly available, the impact of this limitation requires further investigations. Furthermore, other logistic issues, such as the pretreatment quality assurance process, decision of who should be responsible for shifting MLC leaf positions, etc., require further exploration.

One may consider other strategies to cope with the challenge of treating one moving target and one immobile target. One proposal is to prepare two plans: One for the pelvic lymph nodal volume and another for the prostate. If delivering the plans concurrently, overlap of the two plans when the prostate moved superiorly must be calculated on a day-to-day basis.¹⁵ Similar to real time replanning, this requirement is not clinically feasible. If delivering these two plans sequentially, the treatment course can be significantly prolonged and the problem of overdose in the overlap region may still exist, albeit with a lower daily dose compared to concurrent delivery.

There are some limitations in this study. First, only an atypical patient was analyzed, although this special clinical scenario inspired us to conduct this research. Except for the abdominal kidney that imposed a small planning margin on the pelvic lymph nodal volume, the prostate and pelvic lymph nodal volumes of the patient are similar to the volumes of a typical patient. For a typical patient, one may consider the use of a larger margin either around the prostate or around the lymph nodes, or large margins on both targets. Larger planning margins, in general, are a suboptimal strategy, irradiating more normal tissue as a part of the targeting volume and resulting in increased normal tissue complications. The methodology of this study can be applied to other typical patients, but since the prostate motion is patient dependent, a study with more patients' data may not reach a

different conclusion than the current study. For the same reason, the result of this study cannot be directly generalized to other patients.

Second, the MAP strategy only considers a few scenarios of possible prostate positions, not the actual prostate positions. By increasing the number of MAP plans in the pool, one can decrease the error associated with this strategy, but at the cost of significantly increased planning time, quality assurance, and decision making process during treatment. Third, due to the limitation of MV-CBCT, the validation plans could not include other organs of interest, such as the rectum and bladder. The validation plans can be applied to kilovoltage-CBCT, which may overcome the limitation of soft tissue contrast in MV-CBCT. In addition, the daily prostate contour was based on the implanted markers as a surrogate and rigidly transferred to the corresponding MV-CBCT, ignoring prostate rotation and deformation. Furthermore, the dose calculation in validation plans to verify the relative dose changes assumed a uniform tissue density. With a calibrated CT density table, it is possible to perform comparisons based on the absolute dose changes. However, because of the limited field of view (27 cm radius in an axial view) with our current MV-CBCT (Siemens Medical Solution), supplemental information from the planning CT for tissue outside the field of view³² would still be required, which may complicate the dose calculation process.³³ Our future study will consider the use of KV-CBCTs, with which, we can further analyze the daily dose to the prostate based on the direct soft tissue contouring as well as the daily doses to the rectum and bladder.³⁴

V. CONCLUSIONS

Although real time replanning may be the ideal strategy to accommodate independent movement of the prostate and pelvic lymph nodes during concurrent treatment, optimizing a set of IMRT plans with multiple prostate positions is an alternative strategy. The conventional isocenter shifting method is inadequate for selected cases where a small planning margin to both prostate and pelvic lymph nodal volumes is demanded. With an improved record and verification system, the MLC-shifting approach can further improve accommodation of prostate motion in the multiple directions, particularly with a fine MLC leaf width. Validation plans calculated with daily volumetric image guidance provide patient specific dosimetric monitoring and dose guidance, allowing us to adjust radiation dose in the boost phase of the treatment.

ACKNOWLEDGMENTS

This research was supported in part by the United States Army Medical Research and Materiel Command (USAM-RMC) (Grant No. W81XWH-080-0358) and in part by Siemens Medical OCS. The authors thank Dr. Guangwei Mu and Michele Aubin for helping in collecting data and Dr. Neil Woody for proof reading the manuscript.

- ^{a)} Author to whom correspondence should be addressed. Electronic mail: xiap@ccf.org; Telephone: 216-444-1938.
- ¹ D. G. McGowan, "The value of extended field radiation therapy in carcinoma of the prostate," *Int. J. Radiat. Oncol., Biol., Phys.* **7**(10), 1333–1339 (1981).
 - ² N. Rangala, J. D. Cox, R. W. Byhardt, J. F. Wilson, M. Greenberg, and A. Lopes da Conceicao, "Local control and survival after external irradiation for adenocarcinoma of the prostate," *Int. J. Radiat. Oncol., Biol., Phys.* **8**(11), 1909–1914 (1982).
 - ³ C. E. Vargas, R. Galalae, J. Demanes, A. Harsolia, E. Meldolesi, N. Nurnberg, L. Schour, and A. Martinez, "Lack of benefit of pelvic radiation in prostate cancer patients with a high risk of positive pelvic lymph nodes treated with high-dose radiation," *Int. J. Radiat. Oncol., Biol., Phys.* **63**(5), 1474–1482 (2005).
 - ⁴ S. A. Seaward, V. Weinberg, P. Lewis, B. Leigh, T. L. Phillips, and M. Roach III, "Identification of a high-risk clinically localized prostate cancer subgroup receiving maximum benefit from whole-pelvic irradiation," *Cancer J. Sci. Am.* **4**(6), 370–377 (1998).
 - ⁵ S. O. Asbell, J. M. Krall, M. V. Pilepich, H. Baerwald, W. T. Sause, G. E. Hanks, and C. A. Perez, "Elective pelvic irradiation in stage A2, B carcinoma of the prostate: Analysis of RTOG 77-06," *Int. J. Radiat. Oncol., Biol., Phys.* **15**(6), 1307–1316 (1988).
 - ⁶ H. A. Shih, M. Harisinghani, A. L. Zietman, J. A. Wolfgang, M. Saksena, and R. Weissleder, "Mapping of nodal disease in locally advanced prostate cancer: Rethinking the clinical target volume for pelvic nodal irradiation based on vascular rather than bony anatomy," *Int. J. Radiat. Oncol., Biol., Phys.* **63**(4), 1262–1269 (2005).
 - ⁷ A. Wang-Chesebro, P. Xia, J. Coleman, C. Akazawa, and M. Roach III, "Intensity-modulated radiotherapy improves lymph node coverage and dose to critical structures compared with three-dimensional conformal radiation therapy in clinically localized prostate cancer," *Int. J. Radiat. Oncol., Biol., Phys.* **66**(3), 654–662 (2006).
 - ⁸ M. Roach III, M. DeSilvio, C. Lawton, V. Uhl, M. Machtay, M. J. Seider, M. Rotman, C. Jones, S. O. Asbell, R. K. Valicenti, S. Han, C. R. Thomas, Jr., and W. S. Shipley, "Phase III trial comparing whole-pelvic versus prostate-only radiotherapy and neoadjuvant versus adjuvant combined androgen suppression: Radiation Therapy Oncology Group 9413," *J. Clin. Oncol.* **21**(10), 1904–1911 (2003).
 - ⁹ H. Lindsey, "Positive long-term outcomes for IMRT in prostate cancer," *Lancet Oncol.* **7**(11), 3:3 (2006).
 - ¹⁰ M. J. Zelefsky, H. Chan, M. Hunt, Y. Yamada, A. M. Shippy, and H. Amols, "Long-term outcome of high dose intensity modulated radiation therapy for patients with clinically localized prostate cancer," *J. Urol. (Paris)* **176**(4), 1415–1419 (2006).
 - ¹¹ M. Guckenberger, K. Baier, A. Richter, D. Vordermark, and M. Flentje, "Does intensity modulated radiation therapy (IMRT) prevent additional toxicity of treating the pelvic lymph nodes compared to treatment of the prostate only?," *Radiat. Oncol.* **3**, 3 (2008).
 - ¹² K. M. Langen and D. T. Jones, "Organ motion and its management," *Int. J. Radiat. Oncol., Biol., Phys.* **50**(1), 265–278 (2001).
 - ¹³ C. J. Beard, P. Kijewski, M. Bussiere, R. Gelman, D. Gladstone, K. Shaffer, M. Plunkett, P. Castello, and C. N. Coleman, "Analysis of prostate and seminal vesicle motion: Implications for treatment planning," *Int. J. Radiat. Oncol., Biol., Phys.* **34**(2), 451–458 (1996).
 - ¹⁴ J. C. Roeske, J. D. Forman, C. F. Mesina, T. He, C. A. Pelizzari, E. Fontenla, S. Vijayakumar, and G. T. Chen, "Evaluation of changes in the size and location of the prostate, seminal vesicles, bladder, and rectum during a course of external beam radiation therapy," *Int. J. Radiat. Oncol., Biol., Phys.* **33**(5), 1321–1329 (1995).
 - ¹⁵ A. Hsu, T. Pawlicki, G. Luxton, W. Hara, and C. R. King, "A study of image-guided intensity-modulated radiotherapy with fiducials for localized prostate cancer including pelvic lymph nodes," *Int. J. Radiat. Oncol., Biol., Phys.* **68**(3), 898–902 (2007).
 - ¹⁶ E. Ludlum, G. Mu, V. Weinberg, M. Roach III, L. J. Verhey, and P. Xia, "An algorithm for shifting MLC shapes to adjust for daily prostate movement during concurrent treatment with pelvic lymph nodes," *Med. Phys.* **34**(12), 4750–4756 (2007).
 - ¹⁷ B. Pickett, M. Roach III, L. Verhey, P. Horine, C. Malfatti, C. Akazawa, D. Dea, B. Varad, C. Rathbun, and T. L. Phillips, "The value of nonuniform margins for six-field conformal irradiation of localized prostate cancer," *Int. J. Radiat. Oncol., Biol., Phys.* **32**(1), 211–218 (1995).
 - ¹⁸ L. W. Chan, P. Xia, A. R. Gottschalk, M. Akazawa, M. Scala, B. Pickett, I. C. Hsu, J. Speight, and M. Roach III, "Proposed rectal dose constraints for patients undergoing definitive whole pelvic radiotherapy for clinically localized prostate cancer," *Int. J. Radiat. Oncol., Biol., Phys.* **72**(1), 69–77 (2008).
 - ¹⁹ R. A. Price, S. Murphy, S. W. McNeeley, C. M. Ma, E. Horwitz, B. Movsas, A. Raben, and A. Pollack, "A method for increased dose conformity and segment reduction for SMLC delivered IMRT treatment of the prostate," *Int. J. Radiat. Oncol., Biol., Phys.* **57**(3), 843–852 (2003).
 - ²⁰ L. E. Court, L. Dong, A. K. Lee, R. Cheung, M. D. Bonnen, J. O'Daniel, H. Wang, R. Mohan, and D. Kuban, "An automatic CT-guided adaptive radiation therapy technique by online modification of multileaf collimator leaf positions for prostate cancer," *Int. J. Radiat. Oncol., Biol., Phys.* **62**(1), 154–163 (2005).
 - ²¹ Y. Feng, C. Castro-Pareja, R. Shekhar, and C. Yu, "Direct aperture deformation: An interfraction image guidance strategy," *Med. Phys.* **33**(12), 4490–4498 (2006).
 - ²² R. Mohan, X. Zhang, H. Wang, Y. Kang, X. Wang, H. Liu, K. K. Ang, D. Kuban, and L. Dong, "Use of deformed intensity distributions for on-line modification of image-guided IMRT to account for interfractional anatomic changes," *Int. J. Radiat. Oncol., Biol., Phys.* **61**(4), 1258–1266 (2005).
 - ²³ P. J. Keall, J. V. Siebers, M. Armfield, J. O. Kim, and R. Mohan, "Monte Carlo dose calculations for dynamic IMRT treatments," *Phys. Med. Biol.* **46**(4), 929–941 (2001).
 - ²⁴ C. Scholz, C. Schulze, U. Oelfke, and T. Bortfeld, "Development and clinical application of a fast superposition algorithm in radiation therapy," *Radiation Oncol.* **69**(1), 79–90 (2003).
 - ²⁵ Q. Wu, D. Djajaputra, M. Lauterbach, Y. Wu, and R. Mohan, "A fast dose calculation method based on table lookup for IMRT optimization," *Phys. Med. Biol.* **48**(12), N159–N166 (2003).
 - ²⁶ P. W. Chung, T. Haycocks, T. Brown, Z. Cambridge, V. Kelly, H. Alasti, D. A. Jaffray, and C. N. Catton, "On-line aSi portal imaging of implanted fiducial markers for the reduction of interfraction error during conformal radiotherapy of prostate carcinoma," *Int. J. Radiat. Oncol., Biol., Phys.* **60**(1), 329–334 (2004).
 - ²⁷ K. E. Deurloo, R. J. Steenbakkers, L. J. Zijp, J. A. de Bois, P. J. Nowak, C. R. Rasch, and M. van Herk, "Quantification of shape variation of prostate and seminal vesicles during external beam radiotherapy," *Int. J. Radiat. Oncol., Biol., Phys.* **61**(1), 228–238 (2005).
 - ²⁸ V. Landoni, B. Saracino, S. Marzi, M. Gallucci, M. G. Petrongari, E. Chianese, M. Benassi, G. Iaccarino, A. Soriani, and G. Arcangeli, "A study of the effect of setup errors and organ motion on prostate cancer treatment with IMRT," *Int. J. Radiat. Oncol., Biol., Phys.* **65**(2), 587–594 (2006).
 - ²⁹ J. C. O'Daniel, L. Dong, L. Zhang, R. de Crevoisier, H. Wang, A. K. Lee, R. Cheung, S. L. Tucker, R. J. Kudchadker, M. D. Bonnen, J. D. Cox, R. Mohan, and D. A. Kuban, "Dosimetric comparison of four target alignment methods for prostate cancer radiotherapy," *Int. J. Radiat. Oncol., Biol., Phys.* **66**(3), 883–891 (2006).
 - ³⁰ C. F. Serago, S. J. Buskirk, T. C. Igel, A. A. Gale, N. E. Serago, and J. D. Earle, "Comparison of daily megavoltage electronic portal imaging or kilovoltage imaging with marker seeds to ultrasound imaging or skin marks for prostate localization and treatment positioning in patients with prostate cancer," *Int. J. Radiat. Oncol., Biol., Phys.* **65**(5), 1585–1592 (2006).
 - ³¹ X. Zhang, L. Dong, A. K. Lee, J. D. Cox, D. A. Kuban, R. X. Zhu, X. Wang, Y. Li, W. D. Newhauser, M. Gillin, and R. Mohan, "Effect of anatomic motion on proton therapy dose distributions in prostate cancer treatment," *Int. J. Radiat. Oncol., Biol., Phys.* **67**(2), 620–629 (2007).
 - ³² J. Cheung, J. F. Aubry, S. S. Yom, A. R. Gottschalk, J. C. Celi, and J. Pouliot, "Dose recalculation and the dose-guided radiation therapy (DGRT) process using megavoltage cone-beam CT," *Int. J. Radiat. Oncol., Biol., Phys.* **74**(2), 583–592 (2009).
 - ³³ J. F. Aubry, J. Pouliot, and L. Beaulieu, "Correction of megavoltage cone-beam CT images for dose calculation in the head and neck region," *Med. Phys.* **35**(3), 900–907 (2008).
 - ³⁴ Y. Yang, E. Schreibmann, T. Li, C. Wang, and L. Xing, "Evaluation of on-board kV cone beam CT (CBCT)-based dose calculation," *Phys. Med. Biol.* **52**(3), 685–705 (2007).

Appendix F

How many adaptive plans are sufficient for concurrent irradiation of the prostate and pelvic lymph nodes in Multiple Adaptive Planning (MAP) strategy?

Peng Qi¹, Jean Pouliot², Mack Roach III², and Ping Xia^{1,a)}

¹Department of Radiation Oncology, Cleveland Clinic, Cleveland, OH 44195

²Department of Radiation Oncology, University of California-San Francisco, San Francisco, CA 94143

^{a)} **Corresponding author:**

Ping Xia, Ph.D.

Department of Radiation Oncology

Cleveland Clinic

Cleveland, OH 44195

xiap@ccf.org

Abstract

Purpose: Concurrent irradiation of the prostate and pelvic lymph nodes (PLNs) can be challenging due to the independent motion of the two target volumes. To address this issue, a strategy referred to as Multiple Adaptive Planning (MAP) was proposed. With MAP, multiple IMRT plans are created with different presumed prostate locations with respect to PLNs prior to

treatment. During treatment, one of these IMRT plans is selected for treatment by closely matching location of the prostate the day with the presumed prostate location. In this work, we investigate the number of prepared IMRT plans are adequate to accommodate for independent motion of the prostate and PLNs.

Methods: Six patients, who received concurrent irradiation of the prostate and PLNs, were selected for this study. For each patient, nine IMRT plans were created with nine presumed prostate movements: 5 mm in either the anterior-posterior (A-P), or superior-inferior (S-I), or simultaneous 5 mm movements in these two directions. From treatment data of the six patients, thirty three fractions with useable megavoltage (MV) cone-beam CT (CBCT) images were identified. Through a process of dual image registrations between simulation CT and MV-CBCT: by aligning to the implanted markers inside the prostate and by aligning to the pelvic bones, large prostate displacements (> 3 mm in any directions) with respect to pelvic bones were found in 17 of these 33 fractions. For each of these 17 fractions, one MAP plan was selected and applied to the corresponding MV-CBCT images for fraction dose calculation. For comparison, an isocenter shifted plan and an adaptive plan based on the MV-CBCT were also created for each of these 17 fractions. The dose to 95% (D95) of the prostate and PLNs, and the dose to 5% (D5) of the rectum and bladder were calculated and analyzed.

Results: For the prostate, D95 $> 97\%$ of the prescription dose was achieved in 16, 16, and 17 of 17 fractions for the MAP, iso-shifting, and ART plans, respectively. For PLNs, D95 $> 97\%$ of the prescription doses was achieved in 10, 3, and 17 of 17 fractions for the MAP, iso-shifting, and rART plans, respectively. The average (± 1 SD) D5 of the rectum was 45.78 ± 5.75 Gy, 45.44 ± 4.64 Gy, and 44.64 ± 2.71 Gy, and the average (± 1 SD) D5 of the bladder was $45.18 \pm$

2.70 Gy, 46.91 ± 3.04 Gy, and 45.67 ± 3.61 Gy for the MAP, iso-shifting, and rART plans, respectively.

Conclusion: Although extra planning effort is required, the MAP strategy with nine IMRT plans achieved similar dose coverage to the prostate but improved dose coverage to PLNs compared to the conventional iso-shifting technique. The MAP approach can be immediately used in clinical practice without requiring extra hardware and software.

Keywords: prostate cancer, movement management, adaptive planning, intensity modulated radiotherapy, and image-guided radiotherapy

I. INTRODUCTION

Although the use of whole pelvic radiotherapy (WPRT) for patients with intermediate- and high-risk prostate cancer remains controversial, a growing body of data supports the role of this type of treatment.¹⁻⁹ For concurrent irradiation of the prostate and pelvic lymph nodes (PLNs) in WPRT, intensity-modulated radiotherapy (IMRT) has been shown to provide dosimetric advantages over 3D-conformal radiotherapy (3D-CRT).¹⁰⁻¹³ These advantages include more conformal dose distributions to lymph nodes and reduced doses to normal tissues such as the rectum, bladder, and bowel. Therefore, IMRT has become the standard treatment modality for external beam WPRT at many cancer centers.

One major challenge in IMRT-WPRT is the independent motion of two target volumes, the prostate and pelvic lymph nodes (PLNs). As the prostate is mobile with respect to the pelvic bones, PLNs are presumably fixed with respect to the pelvic bones.¹⁴ For example, the position of the prostate was found to vary daily up to 1.5 cm with respect to the pelvic bones (thus the PLNs) during a typical treatment course of 7-9 weeks.¹⁵ Therefore, the conventional method of shifting the isocenter to track and compensate the daily prostate position may result in reduced dose coverage to the PLNs, particularly in highly conformal IMRT treatment plans.^{16,17}

To address this challenge, , online re-optimization and adaptation approaches have been proposed by different investigators.¹⁷⁻²⁷ Using daily images sets and/or contours, a new treatment plan with plan quality comparable to the original plan is created through a process of re-optimization or MLC shape modification. Hwang et. al., showed the effectiveness of an adaptive morphing approach (with and without weight optimization) in compensation for the independent motion of the prostate and PLNs for five WPRT cases.¹⁷ Ludlum et. al., proposed a MLC adaptation method for WPRT without re-optimization or dose calculation.²² However, those proposed methods have not clinically implemented due to logistical issues such as quality

assurance, prolonged treatment time, or unavailable clinical tools. . Another intuitive approach is to increase the planning margins to the both target volumes. However, the use of enlarged planning margin increases doses to normal tissues and offsets the advantages of IMRT. For a special clinical case, we have proposed an off-line strategy, referred to as multiple adaptive planning (MAP)¹⁶, to compensate for independent motion of the prostate and PLNs. With MAP approach, multiple IMRT plans are prepared using the planning CT with different presumed prostate positions with respect to PLNs. Prior to each treatment, one of those IMRT plans is selected by closely matching the location of the prostate the day and a presumed prostate location. The workflow of the MAP approach for clinical use and this retrospective study is shown in Fig. 1.

In a feasibility study of the MAP strategy from our group, five IMRT plans was created to compensate for presumed prostate movements of 5 mm and 10 mm in a single superior or posterior direction for a specific patient.¹⁶ Because the prostate displacements could occur simultaneously in the both longitudinal and anterior-posterior (A-P) directions, the previous study did not accommodate this bi-directional movement, resulted in inadequate dose coverage to the prostate in 35% of treatment days. In this study, we aim to account for the prostate movements in the both longitudinal and anterior-posterior (A-P) directions and to determine a practical number of IMRT plans required for the clinical implementation of the MAP strategy for a larger pool of patients. Based on verification images from six patients, we retrospectively evaluated and compared this strategy with an online optimization and a conventional isocenter-shifting approach.

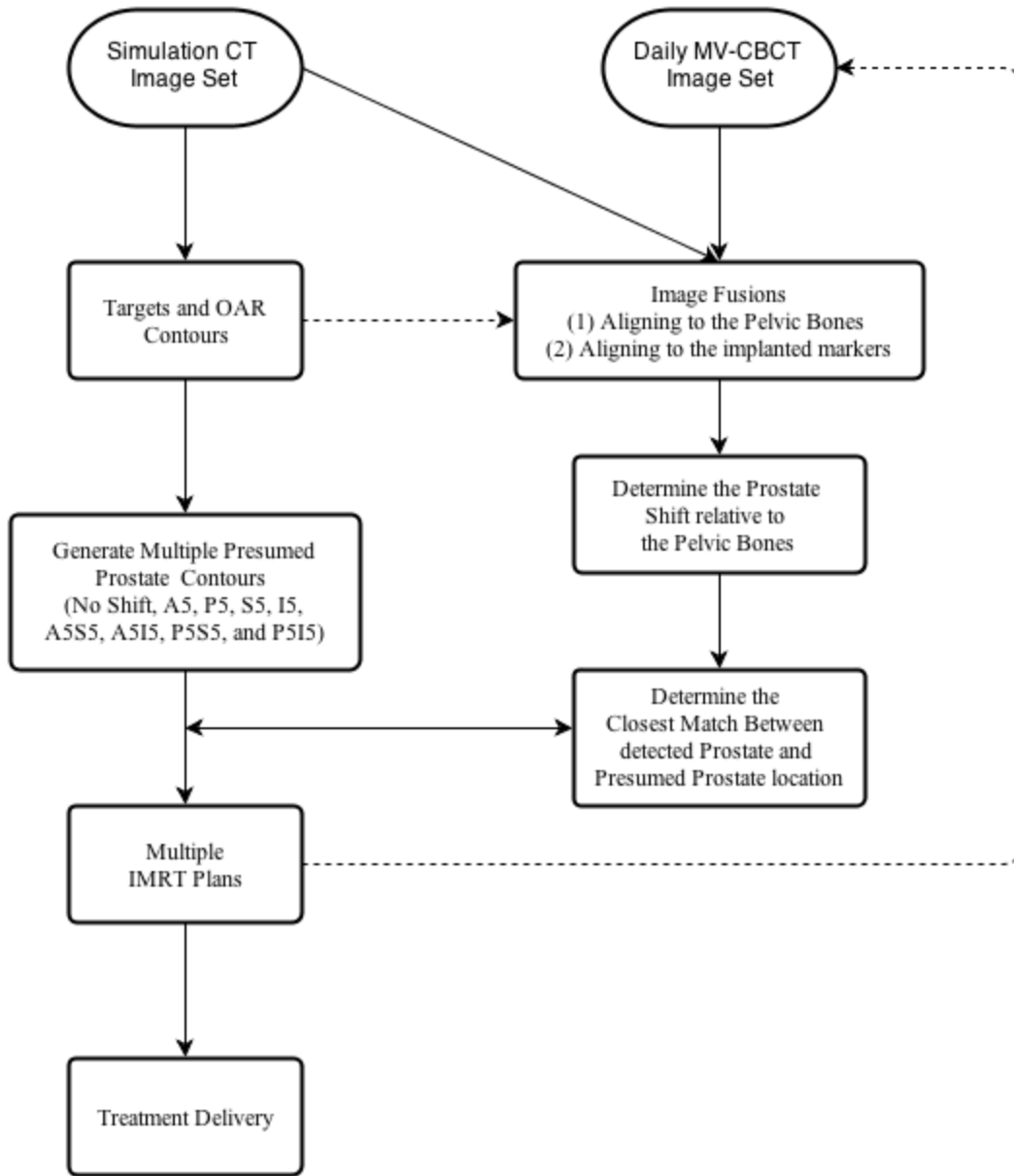


Fig. 1. Workflow of the MAP strategy (solid line). The dashed lines represent additional steps required for this retrospective study.

II. METHODS AND MATERIALS

II.A. Treatment planning

Planning and verification image data from six patients with advanced prostate cancer was retrospectively selected for this study, which was approved by the local Institutional Review Board (IRB). The WPRT consisted of two-phase sequential treatments: an initial IMRT

treatment for the pelvic lymph nodes and prostate; and a boost IMRT treatment for the prostate only. This study focused on the initial IMRT treatments, in which the prostate and seminal vesicles were treated with 45.0-54.0 Gy (1.8-2.0 Gy/fraction) and PLNs were simultaneously treated with 45.0-48.6 Gy (1.8 Gy/fraction). Seven coplanar beams (0°, 35°, 90°, 160°, 200°, 270°, and 315°) of 18 MV photon energy were used for IMRT planning. All IMRT plans were created using the Direct Machine Parameter Optimization (DMPO) within the Pinnacle treatment planning system (version 8.0, Philips Medical System, Fitchburg, WI). Each plan was designed to achieve adequate dose coverage to the targets while minimizing dose to normal tissues according to our local planning protocol¹⁰. In the clinical IMRT plans, the prescription doses were to be received by 95% of the PTV of the prostate and 95% of the PTV-PLNs. Because of daily image-guidance, the planning target volume (PTV) of the prostate (\pm seminal vesicles) was created by adding a uniform 2 mm margin to the prostate contour, and the PTV of PLNs was manually drawn by attending radiation oncologists, without clearly defined CTV of PLNs. Thus, the PTV of PLNs was the same as the CTV for the rest of this article. For the purpose of this study, the doses to “the prostate (CTV) of the day and PLNs (CTV) of the day” were evaluated. All IMRT plans were delivered on Siemens linear accelerators (Model: Oncor, Siemens Medical Solution, Concord, CA).

II.B. MV-CBCT Image Guidance and Dual image registrations

The volumetric image modality available on the ONCOR linac was megavoltage (MV) cone-beam CT (CBCT), using a 6 MV photon beam and an amorphous silicon (a-Si) flat panel detector (AG9-ES, PerkinElmer Optoelectronics, Fremont, CA). During acquisition of MV-

CBCT, a projection image was acquired for each degree during a 210° (from 270° to 100° , clockwise) gantry rotation. A typical reconstruction volume is $256 \times 256 \times 274$ ($1.1 \times 1.1 \times 1.0$ mm³ in voxel size).^{28,29}

To localize the prostate, the MV-CBCT and planning CT images were aligned to 3 implanted markers inside the prostate gland, using a commercial software system (MVision™, Siemens Medical Solutions, Concord, CA). The shifts from this alignment included the prostate inter-fraction motion and setup errors.

Another image registration aligned to the pelvic bones was performed to detect the setup errors, which can be corrected by repositioning the treatment couch. For this retrospective study, the process of dual image registration was performed within the Pinnacle TPS. The prostate location with respect to the pelvic bones were determined from the difference of two sets of translational shifts obtained from the process of dual image registrations.

II.D. Multiple Adaptive Planning (MAP) strategy

With MAP, multiple IMRT plans were created on the same planning CT, and each plan was individually optimized with a presumed (potential) prostate location. The number of presumed prostate locations was determined by the movement direction and magnitude of the prostate. . Because the prostate movements in the lateral direction were typically small, only discrete movement of 5 mm in the anterior (A), posterior (P), superior (S), and inferior (I) directions were considered when generating presumed prostate locations from the planned prostate position. Because the prostate shifts (e.g., ≥ 10 mm) were infrequent from our patient population, we decided not to include these shifts in this study. Hence, eight presumed prostate positions were

created for each patient by rigidly shifting the originally planned prostate position in the A-P and S-I direction using an in-house program. Those shifted prostate contours were referred to as A5, P5, S5, I5, A5S5, A5I5, P5S5, and P5I5, with the letter representing the shift direction and 5 referring to 5 mm shift. . For example, four shifted prostate contours, A5, P5, S5, and I5, are shown along with the planned prostate contour in Fig. 2.

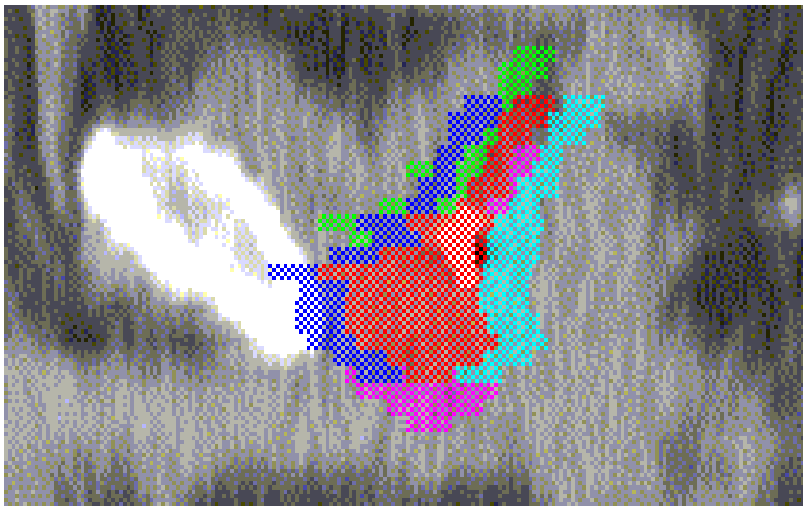


Fig. 2. Shifted prostate contours of A5, P5, S5, and I5 (represented in blue, cyan, green, and purple) from the planned contour in red.

These shifted prostate and original PLNs were used as the planning target volume for creating multiple IMRT plans, based on the guideline described in section II.A.

II.E. Online re-optimization adaptive planning strategy

For each fraction with > 3 mm prostate displacements, an online re-optimization adaptive radiotherapy (rART) plan was created on the corresponding MV-CBCT images. Since it was difficult to accurately contour the soft tissue organs on MV-CBCT images due to their limited

soft-tissue contrast, the contours of the prostate, bladder, and rectum was first transferred from planning CT to the MV-CBCT after a rigid image registration of the implanted markers and then manually edited if visible deformations in these organs were observed. The contours of the PLN and external of the patient body were transferred from the planning CT to the MV-CBCT after a rigid pelvic bone registration.

For comparison, the prostate (CTV) and PLNs were directly used as the planning target for rART planning without additional planning margins. A prescription isodose line was selected on each rART plan to ensure 95% of the prostate and 95% of the PLNs received the prescription doses. Similar dose constraints for the bladder and rectum as those in the clinical plan were applied in the process of DMPO within the Pinnacle TPS.

II.F. Iso-shifting planning strategy

The iso-shifting strategy was a well-adapted clinical method for IMRT treatment of prostate cancer under daily image guidance. For MV-CBCT IGRT, this strategy was implemented by shifting the treatment couch according to the registration of the implanted markers inside the prostate on the MV-CBCT and planning CT images. To compare with the MAP strategy, simulated iso-shifting plans were also created on the MV-CBCT images by shifting the planning isocenter while keeping the same beam configurations as used in the original IMRT plans.

II.G. Plan comparison

Because the axial field of view (FOV) for MV-CBCT images was 256×256 , an in-house program was used to extend the FOV in the MV-CBCT images to match the dimensions of the planning CT (512×512) to recover any missing body tissue, which affected beam attenuation

and dose calculation. Those processed images were input back to the Pinnacle system via DICOM and set as the primary images for contouring and dose calculation. Because the accuracy of the dose calculation of using CBCT images was subject to the cupping artifacts and CT density inaccuracy as well as the limited FOV of our current MV-CBCT imaging system, a constant CT density of 1 g/cm^3 was assigned to all tissues enclosed by the external contour, which was transferred to the MV-CBCT after the bony-based image registration.

To validate our MAP strategy, an MAP-IMRT plan was compared with the corresponding iso-shifting and rART plans (as described in previous sections) based on the defined endpoint doses to the targets and OARs delineated on the MV-CBCT images. The doses to 95% of the target volumes (D95) and doses to 5% of the rectum and bladder (D5) were compared for all 17 fractions. Student t-tests were used to compare these defined endpoints.

III. RESULTS

III.A. Image guidance

For these 6 patients, MV-CBCT images were only acquired weekly with daily orthogonal portal imaging to minimize radiation dose to the patients. A total of thirty three MV-CBCTs were available for this study. After dual image registrations of each CBCT and the corresponding planning CT, we found seventeen fractions with the prostate shifts greater than 3 mm in any directions. The distribution of these prostate movements with respect to the pelvic bones is shown in Fig. 3. As expected, lateral prostate shifts were smaller than 2 mm in 16 of 17 fractions, and the prostate shifts greater than 3 mm occurred mostly in either the A-P or S-I directions, or both directions.

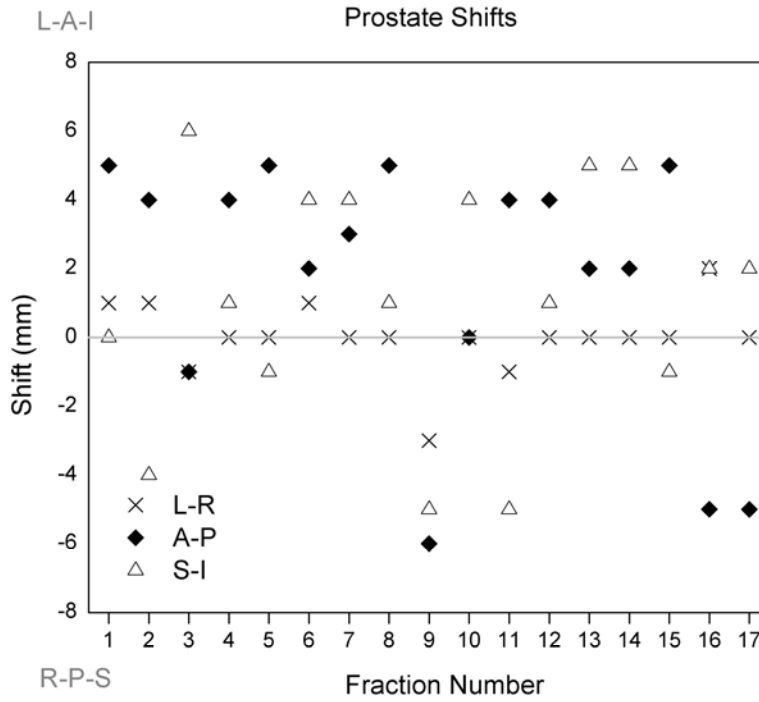


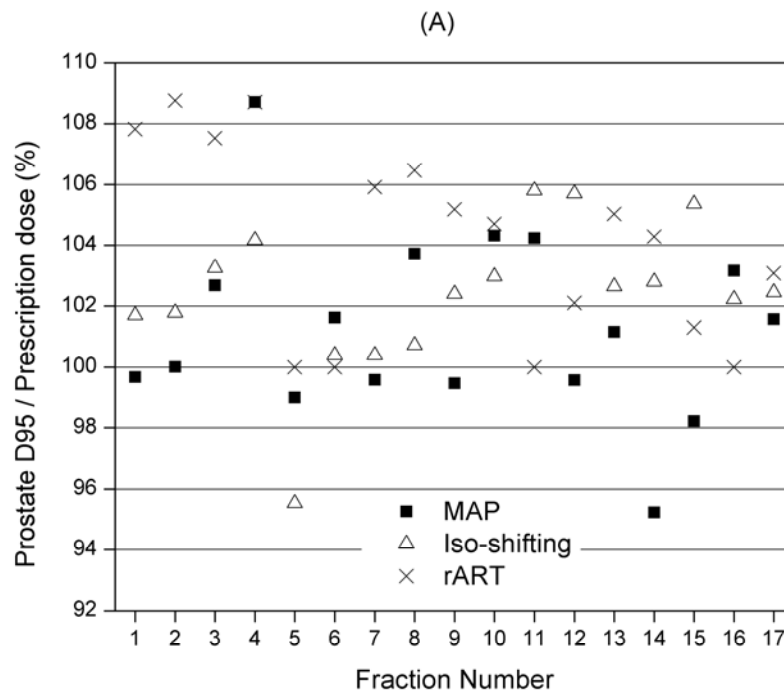
Fig. 3. Prostate shifts for 17 fraction used for dosimetric evaluation. The prostate movements along the three axes are plotted for each fraction. The positive shifts are in the left, anterior, and inferior direction, respectively.

III.B. Dose comparison using MV-CBCT

For the prostate, $D_{95} > 97\%$ of the prescription dose was observed in 16, 16, and 17 of 17 fractions for the MAP, iso-shifting, and rART verification plans (see Fig. 4A). The average (\pm SD) D_{95} of the prostate were $101.3 \pm 3.1\%$, $102.4 \pm 2.4\%$, and $104.2 \pm 3.2\%$ for the MAP, iso-shifting, and rART plans, respectively. The mean D_{95} of the prostate between the MAP and iso-shifting plans was not statistically different ($p = 0.089$). The mean D_{95} of the MAP plans was statistically different from that of rART plans ($P < 0.05$). The mean D_{95} of the iso-shift plans was also statistically different ($P, 0.05$).

For PLNs, D95 > 97% of the prescription dose was observed in 10, 3, and 17 of 17 fractions for the MAP, iso-shifting, and rART verification plans (see Fig. 4B). The average D95 of PLNs were $97.1 \pm 2.7\%$, $94.0 \pm 3.3\%$, and $100.9 \pm 1.4\%$ of the prescription dose for the MAP, iso-shifting, and rART plans, respectively. The mean D95 of PLNs among the MAP, iso-shift, and rART plans were statistically different ($p < 0.05$).

Overall, the use of the MAP strategy with 9 IMRT plans can achieve similar dose coverage to the prostate but improved dose coverage to PLNs compared to conventional isocenter shifting approach. The online re-optimization method was the best solution to independent motion of the prostate and PLNs.



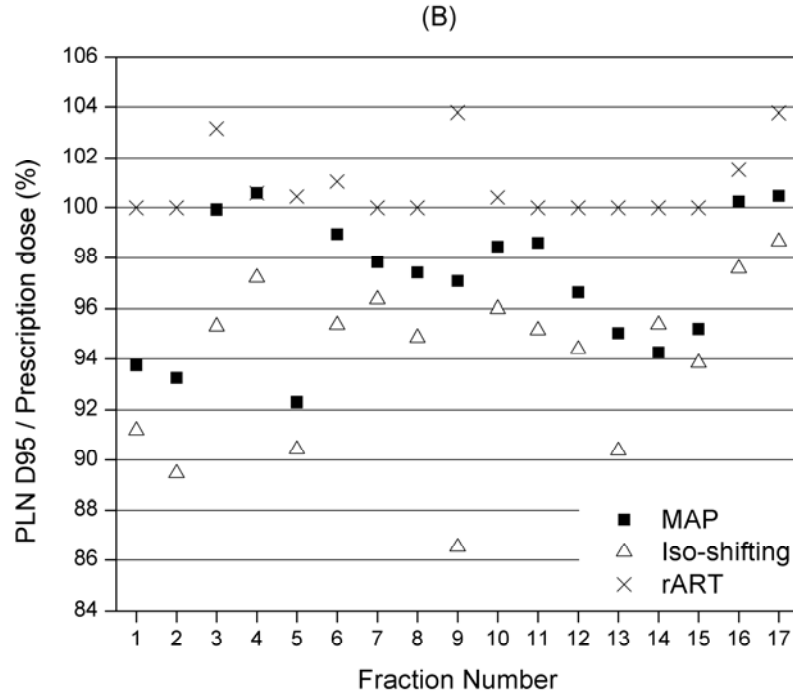


Fig. 4. (A) Prostate D95 and (B) PLN D95 for 17 fractions with large prostate displacements. The dosimetric values are normalized to prescription doses.

The average (\pm SD) D5 of the rectum was 45.78 ± 5.75 Gy, 45.44 ± 4.64 Gy, and 44.64 ± 2.71 Gy, and the average (\pm SD) D5 of the bladder was 45.18 ± 2.70 Gy, 46.91 ± 3.04 Gy, and 45.67 ± 3.61 Gy for the MAP, iso-shifting, and rART verification plans, respectively.

IV. DISCUSSIONS

In this work, we have retrospectively evaluated the MAP strategy that can potentially be used to compensate for independent motion of the prostate and pelvic lymph nodes in the whole pelvic radiotherapy of high-risk prostate cancer. The MAP technique with nine IMRT plans has been shown to maintain similar dose coverage to the prostate but to improve dose coverage to PLNs, compared to those achieved using the conventional iso-shifting method. For our local practice,

the translational shifts of the isocenter are made based on the locations of three markers, implanted inside the prostate before the radiotherapy treatment course, shown on the MV-CBCT images and those on the planning CT images.

Designed as an off-line strategy, the MAP technique is straightforward and practical. Compared to conventional IGRT process, the similar workflow and time is expected for implementing the MAP approach for daily treatment. Although another image registration based on the bony structures is required, it can be automatically and quickly achieved on most current equipped IGRT software. With much effort put into preparation of more IMRT plans beforehand, we expect to save treatment time and effort during the treatment compared with online re-optimization methods.^{17,20,21,24,26,27,30} The implementation of the re-optimization approach requires dedicated time and involvements of the attending physician, physicist, and machine therapists. Many steps are needed for a newly optimized plan to be loaded into the record and verify (R&V) system and to be approved for treatment delivery. The use of the MLC adaptation method^{18,19,22} can quickly create a high-quality adaptive plan on the sequencer, but a new function is required to be added into the R&V system. Therefore, the most current practice for prostate IGRT still uses the method of the isocenter shifting, based on the implanted marker or soft-tissue matching. Li et. al. have proposed a method referred to as adaptive images guided radiation therapy (AIGRT)³¹ and attempted to combine online re-optimization and re-position (isocenter-shifting). However, this approach still faces issues of the re-optimization mentioned above, and so for the method of using a knowledge base of prior treatments to generate new prostate IMRT plans³².

One major limitation our study was the use of MV CBCT images for daily contouring and dose calculation. Directly contouring soft-tissue organs on the available MV-CBCT remains difficult

due to its inherent low soft-tissue contrast compared to simulation CT or even kilo-voltage (KV) CBCT. This was also the reason that we did not include the seminal vesicles in this study, which were part of the planning target volume in the original plan. The accuracy of the dose calculation using CBCT images was subject to the cupping artifacts and CT density inaccuracy as well as the limited FOV of our current MV-CBCT imaging system. Although we circumvented these issues by rigidly transferring the contours from the simulation CT to MV-CBCT and assigning homogeneous density within the external contour, the accuracy of these methods needs to be further investigated. The use of large field of view (FOV) kV-CBCT images or daily diagnostic quality CT (e.g. CT on rails) is thus warranted for future studies of the MAP strategy.

Because multiple IMRT plans were created with limited number of presumed prostate locations, target coverage was compromised if daily target positions were not perfectly matched to those presumed positions. This situation was in part due to zero planning margins applied to the prostate for creating multiple IMRT plans in this study. We expect the target coverage may be improved by adding small margins (e.g. 2 mm) to the targets, which can compensate for inter- and/or intra-fraction target deformation and rotations, or for unmatched target locations. At the same time, the number of MAP-IMRT plans may be further reduced with a small planning margin applied for the target volumes. This hypothesis may warrant a future study on the MAP technique.

To fully take advantage of IMRT for patient receiving WPRT, the adequate dose coverage to the prostate and pelvic nodal volumes are essential. The results of this study indicated that the MAP strategy with 9 IMRT plans can achieve similar dose coverage to the prostate but improved dose coverage to pelvic lymph nodes when compared with the conventional iso-shifting strategy. The

concept of the MAP technique could be potentially extended to other sites involving target volumes with independent motion patterns.

V. CONCLUSIONS

Without requiring new software and hardware, the MAP strategy is straightforward and can be directly applied to clinical practice. Although it may take extra effort in preparation of multiple plans, the use of the MAP technique with 9 IMRT plans can partly compensate for most frequent independent movements of two target volumes in WPRT treatment of patients with immediate- and high-risk prostate cancer.

ACKNOWLEDGEMENTS

This research is supported in part by the United States Army Medical Research and Material Command (USAM/RMC, PC073349) and in part by a research grant from Siemens Medical Solutions.

Reference:#

1. S.A. Seaward, V. Weinberg, P. Lewis, et al., "Improved freedom from PSA failure with whole pelvic irradiation for high-risk prostate cancer," *Int. J. Radiat. Oncol. Biol. Phys.* **42**(5), 1055-62 (1998).
2. M. Roach, III, M. DeSilvio, C. Lawton, et al., "Phase III trial comparing whole-pelvic versus prostate-only radiotherapy and neoadjuvant versus adjuvant combined androgen suppression: Radiation Therapy Oncology Group 9413," *J. Clin. Oncol.* **21**(10), 1904-11 (2003).

3. R. Jacob, A.L. Hanlon, E.M. Horwitz, et al., "Role of prostate dose escalation in patients with greater than 15% risk of pelvic lymph node involvement," *Int. J. Radiat. Oncol. Biol. Phys.* **61**(3), 695-701 (2005).
4. M. Roach, 3rd, M. DeSilvio, R. Valicenti, et al., "Whole-pelvis, "mini-pelvis," or prostate-only external beam radiotherapy after neoadjuvant and concurrent hormonal therapy in patients treated in the Radiation Therapy Oncology Group 9413 trial," *Int. J. Radiat. Oncol. Biol. Phys.* **66**(3), 647-53 (2006).
5. M.T. Spiotto, S.L. Hancock, and C.R. King, "Radiotherapy after prostatectomy: improved biochemical relapse-free survival with whole pelvic compared with prostate bed only for high-risk patients," *Int. J. Radiat. Oncol. Biol. Phys.* **69**(1), 54-61 (2007).
6. A.A. Aizer, J.B. Yu, A.M. McKeon, et al., "Whole pelvic radiotherapy versus prostate only radiotherapy in the management of locally advanced or aggressive prostate adenocarcinoma," *Int. J. Radiat. Oncol. Biol. Phys.* **75**(5), 1344-9 (2009).
7. P. Milecki, M. Baczyk, J. Skowronek, et al., "Benefit of whole pelvic radiotherapy combined with neoadjuvant androgen deprivation for the high-risk prostate cancer," *J Biomed Biotechnol* **2009**, 625394 (2009).
8. G. Mantini, L. Tagliaferri, G.C. Mattiucci, et al., "Effect of whole pelvic radiotherapy for patients with locally advanced prostate cancer treated with radiotherapy and long-term androgen deprivation therapy," *Int. J. Radiat. Oncol. Biol. Phys.* **81**(5), e721-6 (2011).
9. L.K. Morikawa and M. Roach, 3rd, "Pelvic nodal radiotherapy in patients with unfavorable intermediate and high-risk prostate cancer: evidence, rationale, and future directions," *Int. J. Radiat. Oncol. Biol. Phys.* **80**(1), 6-16 (2011).

10. A. Wang-Chesebro, P. Xia, J. Coleman, et al., "Intensity-modulated radiotherapy improves lymph node coverage and dose to critical structures compared with three-dimensional conformal radiation therapy in clinically localized prostate cancer," *Int. J. Radiat. Oncol. Biol. Phys.* **66**(3), 654-62 (2006).
11. G. Sanguineti, M.L. Cavey, E.J. Endres, et al., "Does treatment of the pelvic nodes with IMRT increase late rectal toxicity over conformal prostate-only radiotherapy to 76 Gy?," *Strahlenther Onkol* **182**(9), 543-9 (2006).
12. F. Alongi, C. Fiorino, C. Cozzarini, et al., "IMRT significantly reduces acute toxicity of whole-pelvis irradiation in patients treated with post-operative adjuvant or salvage radiotherapy after radical prostatectomy," *Radiother. Oncol.* **93**(2), 207-12 (2009).
13. C. Cozzarini, C. Fiorino, N. Di Muzio, et al., "Significant reduction of acute toxicity following pelvic irradiation with helical tomotherapy in patients with localized prostate cancer," *Radiother. Oncol.* **84**(2), 164-70 (2007).
14. H.A. Shih, M. Harisinghani, A.L. Zietman, et al., "Mapping of nodal disease in locally advanced prostate cancer: rethinking the clinical target volume for pelvic nodal irradiation based on vascular rather than bony anatomy," *Int. J. Radiat. Oncol. Biol. Phys.* **63**(4), 1262-9 (2005).
15. K.M. Langen and D.T. Jones, "Organ motion and its management," *Int. J. Radiat. Oncol. Biol. Phys.* **50**(1), 265-78 (2001).
16. P. Xia, P. Qi, A. Hwang, et al., "Comparison of three strategies in management of independent movement of the prostate and pelvic lymph nodes," *Med. Phys.* **37**(9), 5006-13 (2010).
17. A.B. Hwang, J. Chen, T.B. Nguyen, et al., "Irradiation of the prostate and pelvic lymph nodes with an adaptive algorithm," *Med. Phys.* **39**(2), 1119-24 (2012).

18. L.E. Court, R.B. Tishler, J. Petit, et al., "Automatic online adaptive radiation therapy techniques for targets with significant shape change: a feasibility study," *Phys. Med. Biol.* **51**(10), 2493-501 (2006).
19. Y. Feng, C. Castro-Pareja, R. Shekhar, et al., "Direct aperture deformation: an interfraction image guidance strategy," *Med. Phys.* **33**(12), 4490-8 (2006).
20. Q. Wu, G. Ivaldi, J. Liang, et al., "Geometric and dosimetric evaluations of an online image-guidance strategy for 3D-CRT of prostate cancer," *Int. J. Radiat. Oncol. Biol. Phys.* **64**(5), 1596-609 (2006).
21. A. de la Zerda, B. Armbruster, and L. Xing, "Formulating adaptive radiation therapy (ART) treatment planning into a closed-loop control framework," *Phys. Med. Biol.* **52**(14), 4137-53 (2007).
22. E. Ludlum, G. Mu, V. Weinberg, et al., "An algorithm for shifting MLC shapes to adjust for daily prostate movement during concurrent treatment with pelvic lymph nodes," *Med. Phys.* **34**(12), 4750-6 (2007).
23. W.Y. Song, E. Wong, G.S. Bauman, et al., "Dosimetric evaluation of daily rigid and nonrigid geometric correction strategies during on-line image-guided radiation therapy (IGRT) of prostate cancer," *Med. Phys.* **34**(1), 352-65 (2007).
24. E.E. Ahunbay, C. Peng, G.P. Chen, et al., "An on-line replanning scheme for interfractional variations," *Med. Phys.* **35**(8), 3607-15 (2008).
25. W. Fu, Y. Yang, N.J. Yue, et al., "A cone beam CT-guided online plan modification technique to correct interfractional anatomic changes for prostate cancer IMRT treatment," *Phys. Med. Biol.* **54**(6), 1691-703 (2009).

26. A. Mestrovic, A. Nichol, B.G. Clark, et al., "Integration of on-line imaging, plan adaptation and radiation delivery: proof of concept using digital tomosynthesis," *Phys. Med. Biol.* **54**(12), 3803-19 (2009).
27. X.A. Li, F. Liu, A. Tai, et al., "Development of an online adaptive solution to account for inter- and intra-fractional variations," *Radiother. Oncol.* **100**(3), 370-4 (2011).
28. O. Morin, A. Gillis, J. Chen, et al., "Megavoltage cone-beam CT: system description and clinical applications," *Med. Dosim.* **31**(1), 51-61 (2006).
29. J. Pouliot, A. Bani-Hashemi, J. Chen, et al., "Low-dose megavoltage cone-beam CT for radiation therapy," *Int. J. Radiat. Oncol. Biol. Phys.* **61**(2), 552-60 (2005).
30. R. Mohan, X. Zhang, H. Wang, et al., "Use of deformed intensity distributions for on-line modification of image-guided IMRT to account for interfractional anatomic changes," *Int. J. Radiat. Oncol. Biol. Phys.* **61**(4), 1258-66 (2005).
31. T. Li, D. Thongphiew, X. Zhu, et al., "Adaptive prostate IGRT combining online re-optimization and re-positioning: a feasibility study," *Phys. Med. Biol.* **56**(5), 1243-58 (2011).
32. V. Chanyavanich, S.K. Das, W.R. Lee, et al., "Knowledge-based IMRT treatment planning for prostate cancer," *Med. Phys.* **38**(5), 2515-22 (2011).

#

**Alignment focus of Daily Image Guidance for Concurrent Treatment
Of Prostate and Pelvic Lymph Nodes**

Samah Ferjani, Ph.D., Guangshun Huang, Ph.D., Qingyang Shang, Ph.D.,
Kevin L. Stephans, M.D., Yahua Zhong, M.D., Peng Qi, Ph.D.,
Rahul D. Tendulkar, M.D., and Ping Xia, Ph.D.

Department of Radiation Oncology, Cleveland Clinic, Cleveland, OH 44195

Corresponding author:

Ping Xia, PhD

Cleveland Clinic
9500 Euclid Ave. - T28
Cleveland, OH 44195

Phone number: (216) 444-1938

Fax number: (216) 444-8934

Email: xiap@ccf.org

Shortened running title: **Daily Imaging Alignment Focus**

Acknowledgment

This research was supported by the United States Army Medical Research and Materiel Command (USAMRMC) (Grant No. W81XWH-080-0358). A part of the results was presented at the 54th annual meeting of the American Association of Physicists in Medicine, Charlotte, NC.

55 **Conflict of Interest Notification:** None

56

57

58

59

60

61

62

63

64

65

66

67

68

69

70

71

1 **Summary**

2 The independent movement of the prostate and lymph nodes challenges the choice of
3 daily imaging registration focus. Based on 124 CBCT images with planning margins of
4 8mm/6mm posterior to the prostate and 5 mm to the pelvic lymph nodes (PLN), this
5 study demonstrated that aligning to the prostate is an effective strategy, still delivering
6 adequate dose to the PLN; aligning to the pelvic bone may underdose to the prostate in
7 1/3 of fractions.

8

Alignment focus of Daily Image Guidance for Concurrent Treatment Of Prostate and Pelvic Lymph Nodes

Abstract

Purpose: To determine the dosimetric impact of daily imaging alignment focus on the prostate soft tissue versus the pelvic bones for the concurrent treatment of the prostate and pelvic lymph nodes (PLN), and to assess whether multi-leaf collimator (MLC) tracking or adaptive planning (ART) is necessary with the current clinical planning margins of 8mm/6mm posterior to the prostate and 5mm to the PLN.

Methods and Materials: A total of 124 kilo-voltage cone-beam computed tomography (kV-CBCT) images from six patients were studied. For each KV-CBCT, four plans were retrospectively created using an iso-center shifting methods with two different alignment focuses (prostate, PLN), MLC shifting method, and the ART method. The selected dosimetric endpoints were compared among these plans.

Results: For the iso-shift-contour, iso-shift-bone, MLC-shift, and ART plans, D99 of the prostate was $\geq 97\%$ of the prescription dose in 97.6%, 73.4%, 98.4%, and 96.8% of 124 fractions, respectively. Accordingly, D99 of the PLN was $\geq 97\%$ of the prescription dose in 98.4%, 98.4%, 98.4%, and 100% of 124 fractions, respectively. For the rectum, D5 exceeded 105% of the planned D5 (and D5 of ART plans) in 11% (4%), 10% (2%), and 13% (5%) of 124 fractions, respectively. For the bladder, D5 exceeded 105% of the planned D5 (and D5 of ART) plans in 0% (2%), 0% (2%), and 0% (1%) of 124 fraction, respectively.

Conclusion: For concurrent treatment of the prostate and PLN, with a planning margin to the prostate of 8mm/6mm posterior and a planning margin of 5mm to the PLN, aligning to the prostate soft tissue can achieve adequate dose coverage to the both target volumes; aligning to the pelvic bone would result in underdosing to the prostate in 1/3 of fractions. With these planning margins, MLC tracking and ART methods have no dosimetric advantages.

Introduction

Concurrent radiation treatment of the prostate and pelvic lymph nodes (PLN) is technically challenging because of the independent movement of the target volumes. Image-guided radiotherapy, especially in-room computed tomography (CT) such as kilovoltage cone beam CT (KV-CBCT) and CT-on-rails, has not only greatly improved the precision of patient positioning (1, 2) but also lead to possibility of adaptive radiotherapy (3-5). While the prostate is movable, the PLN are thought to be relatively fixed in close proximity to vascular structures (6), which are presumably fixed with respect to the pelvic bony anatomy. Simultaneously delivering IMRT to the prostate and PLN may require a large planning margin for one of the clinical target volumes (CTV), depending on the focus of daily image alignment (7) (8).

For concurrent treatment of the prostate and PLN, an ideal approach would be the real time adaptive radiotherapy (ART). The group from Medical College of Wisconsin has shown that with the CT-on-rails system and an adaptive morphing algorithm, the real time ART approach for prostate-only treatment requires a minimum of 8 minutes (9). Although real time ART is promising, the logistics and special requirements of the hardware and software may hamper the use of this method clinically. One of the greatest challenges is the requirement of real-time segmentation of the target volumes and sensitive structures, demanding significant time and effort from physicians. Assuming a minimum deformation of the prostate, our group proposed a multi-leaf collimator (MLC) tracking method (10) to compensate for inter-fractional movement of the prostate while concurrently treating the PLN, without requirement of real-time target volume

delineation and dose calculation (11). The MLC tracking method shifts the positions of the selected the MLC leaf pairs to track the prostate movement while keeping the positions of the other MLC leaf pairs unchanged.

With the current clinical planning margins of 8mm/6mm posterior to the prostate and 5mm to the PLN, the purpose of this study is to use clinically acquired CBCT images to determine the dosimetric impact of daily imaging alignment focus on the prostate soft tissue versus the pelvic bones (a surrogate for the PLN) for the concurrent treatment of the prostate and PLN, and to assess whether the MLC tracking or ART planning has dosimetric advantage.

Materials and Methods

Patient Selection, Treatment Planning and Delivery

Six patients, who received concurrent IMRT for the prostate and PLN under KV-CBCT imaging guidance, were randomly selected for this retrospective study. The study was approved by our local Institutional Review Board. Only 124 KV-CBCT, acquired by using an onboard imager from a commercial linear accelerator (Synergy S, Elekta), were suitable for our study to cover the volumes of PLN. The CBCTs with the longitudinal field of view of 25.6 cm and the superior border extended beyond L5-S1 vertebra were selected. The CBCT was acquired at 155 cm from the radiation source at a size of the detector panel of 41 cm x 41 cm. For each KV-CBCT, contours of the prostate, bladder and rectum were manually delineated by a physician. Because of the limited soft tissue

contrast in the CBCT images and the relatively fixed relationship between the PLN and the pelvic bones (8), PLN contours were transferred from the planning CT to the daily CBCT after a rigid bone image registration. For each CBCT, three verification plans and one ART plan were generated. To overcome unstable Hounsfield numbers in CBCTs due to the scattering, a density of 1g/cm^3 was assigned to all tissue and a zero density was assigned to the outside region of the body external in CBCTs (12).

In the initial IMRT plans, generated using the PinnacleTM treatment planning system (version 9.0, Philips Radiation Oncology System, Madison, Wisconsin), the iso-center was typically placed at the center of the entire treatment volume (including both targets), above the prostate. The planning margins for the prostate was 8mm/6mm and the planning margin for the PLN was 5 mm, following the Radiation Therapy Oncology Group (RTOG) consensus (13). All IMRT treatments were delivered with a step-and-shoot method using 10MV photons with a standard seven beam arrangement. In order to conduct a fair comparison with the verification plans, the clinical IMRT plans were recalculated without heterogeneity correction.

Image registrations

According to the previously proposed algorithm (10), the prostate displacement (relative to the pelvic bone) was measured by a dual image registration method: first aligning the KV-CBCT with the planning CT by the pelvic bones, and then aligning to the contour of the prostate. These dual imaging registrations were restricted with translation shifts only to reflect a common clinical practice during daily treatment. The registrations were

conducted manually by aligning the prostate contours from the planning CT and the CBCT with visual inspection to achieve the greatest overlap. Assuming that the pelvic lymph nodal volumes were fixed with respect to the pelvic bones, the difference of these two imaging registrations provided the prostate displacement.

Verification plans based on CBCT

Three types of verification plans were created for each CBCT. The first type of verification plan applied the beam configuration and parameters from the original IMRT plan to each CBCT with the treatment iso-center shifted based on the bony registration, referred to as iso-shift-bone plan. The second type of verification plan shifted the iso-center to match the daily prostate displacement based on the soft tissue registration. This plan is referred to as the iso-shift-contour plan. The third, referred to as the MLC-shift plan, was based on the MLC shifting algorithm proposed by our previous publication (10). With this MLC-shifting method, the displacement of the prostate was compensated without affecting the dose distributions to PLN. The algorithm was implemented with an in-house program which automatically identified MLC leaf pairs that were collimated to the prostate in the planning CT and adjusted the positions of these leaf pairs for each segment of the IMRT plan to compensate for the inter-fraction prostate motion in relative to the pelvic bones. Meanwhile, the MLC leaves that were conformal to the PLN were unchanged. Because the MLC-shifting method was not intended to create new IMRT plans but shift the selected MLC leaves, the planning margins for the prostate were kept the same as the original IMRT plans (8mm/6mm posterior). The newly created MLC-shift plans were then exported into to the Pinnacle planning system and applied to the

corresponding KV-CBCT for dose calculation.

Adaptive Radiotherapy (ART) plans

Based on each daily CBCT, a new IMRT plan was generated to simulate adaptive planning using the same number of beams and beam directions from the corresponding initial IMRT plan. The planning objectives from the original IMRT plan were also used as a starting point for plan optimization. Further adjustments in planning objectives were permitted in order to achieve the adequate dose coverage to the prostate and PLN and similar dose volume histograms (DVHs) of OARs as the original IMRT plan. Because the volume changes in the rectum and bladder, small deviations in DVHs of these OARs were permitted. In this study, the original IMRT plans and the ART plans were used as two benchmarks to evaluate the effectiveness of the three verification plans.

Results

Prostate and PLN

For a selected patient, who received concurrent irradiation of 50Gy for the prostate and the PLN, Figure 1 shows the detailed isodose distributions for the original IMRT plan, iso-shift-contour, iso-shift-bone, MLC-shift, and ART plans. Figures 2a-b show the corresponding dose volume histograms for the prostate, PLN, bladder, and rectum. In Figures 2a-b, in order to obtain an adequate dose coverage to the PLN, the DVH of the prostate in the ART plan was slightly better than other plans. For 124 CBCTs, a quantitative analysis of the dosimetric impact of alignment to the prostate versus the

pelvic bones for the prostate and the PLN from the three verification plans is shown in Table 1. In this study, because of residual positioning errors and limitation of dose calculation in CBCTs, we used a criterion of $D99 \geq 97\%$ of the prescribed dose to evaluate verification plans. Using this criterion, we found that 97.6%, 73.4%, and 98.4% of the fractions met the criterion in the iso-shift-contour, iso-shift-bone, and MLC-shift plans respectively. Using $D99$ of the prostate $\geq 97\%$ of the original IMRT $D99$ of the prostate as a criterion, 94.4%, 70.2%, and 96.8% of 124 fractions met the criterion in the iso-shift-contour, iso-shift-bone and MLC-shift plans, respectively. Using $D99$ of the prostate $\geq 97\%$ of the ART $D99$ of the prostate as a criterion, 93.5% of 124 fractions met the criterion in both iso-shift-contour and MLC-shift plans while only 67.7% met the criterion for the iso-shift-bone plans.

For the PLN, using a criterion of $D99$ of the PLN $\geq 97\%$ of the prescribed dose, we found that 98.4% of the fractions met the criteria for all three verification plans. Using $D99$ of the PLN $\geq 97\%$ of the planned $D99$ as a criterion, 98% of 124 fractions met the criterion in the iso-shift-contour, iso-shift-bone, and MLC-shift plans, respectively. Choosing $D99$ of the PLN $\geq 97\%$ of the ART $D99$ as a criterion, 96.8%, 95.2%, and 94.4% of the fractions met the criteria for the iso-shift-contour, iso-shift-bone, and MLC-shift methods, respectively.

Organs at risk

Figures 3a-b show $D5$ of the bladder and rectum normalized to corresponding $D5$ of the original IMRT plans for the iso-shift-contour, iso-shift-bone, and MLC-shifting plans.

Because of the daily changes of the bladder and rectum, we chose to evaluate D5 for all verification plans and we also allowed D5 deviate within 105% from the planned D5. For the bladder, the three verification plans had $D5 \leq 105\%$ of the planned dose in all fractions. For the rectum, 11%, 10%, and 13% of the fractions in iso-shift-contour, iso-shift-bone, and MLC-shift plans had $D5 \geq 105\%$ of the planned doses, respectively.

Figures 4a-b show the D5 of the bladder and rectum for all three types of verification plans normalized to corresponding D5 of the ART plans. Figure 4a shows that 2%, 2%, and 1%, of fractions from the iso-shift-contour, iso-shift-bone, and MLC-shifting plans had $D5 \geq 105\%$ of the ART D5 of the bladder, respectively. In Figure 4b, 4%, 2%, and 5%, of the fractions from the iso-shift-contour, iso-shift-bone, and MLC-shifting plans had $D5 \geq 105\%$ of the ART D5 of the rectum, respectively.

Effect of Magnitude of Prostate Displacements

Figure 5a shows the daily prostate D99 for iso-shift-contour, iso-shift-bone, and MLC-shifting plans normalized to the prostate D99 of the initial IMRT plan as a function of the prostate displacement magnitude. In 83% (103/124) fractions, the prostate motion magnitude was $\leq 0.74\text{cm}$ with the remaining 17% (21/124) fractions having $\geq 0.74\text{cm}$ prostate displacement. The magnitude of 0.74cm is equivalent 0.5cm inter-fraction prostate movement in both superior-inferior and anterior-posterior directions with 0.2cm movement in the lateral directions. In 83% (103 fractions), 94.2%, 76.7%, and 97% of the fractions received D99 of the prostate $\geq 97\%$ of the planned D99 of the prostate for the iso-shift-contour, iso-shift-bone, and MLC-shift methods, respectively. For the prostate

displacement $\geq 0.74\text{cm}$, 95.2 % (20/21) fractions had D99 of the prostate $\geq 97\%$ of the planned D99 for the iso-shift-contour and MLC-shift plans, but only 38%(8/21) of the fractions met the criterion for the iso-shift-bone plans.

Figure 5b plots the daily D99 of the PLN normalized to the planned D99 of the PLN for iso-shift-contour, iso-shift-bone, and MLC-shifting plans as a function of the prostate displacement magnitude. Among the fractions (103/124) that have the prostate displacement magnitude $\leq 0.74\text{cm}$, 99% (102/103) fractions achieved D99 of the PLN $\geq 97\%$ of the planned D99 PLN for the iso-shift-contour and MLC-shift methods, and 98% (101/103) of the fractions met this criterion for the iso-shift-bone method. For the prostate displacement magnitude $\geq 0.74\text{cm}$, 95.2% (20/21) of the fractions met the criterion for all three verification plans for the PLN.

Discussion

With image alignment focuses to the prostate soft tissue and to the pelvic bones for 124 KV-CBCTs, we evaluated conventional iso-center shifting, MLC tracking, and ART methods for concurrent treatment of the prostate and PLN with a planning margin of 8mm/6mm posterior to the prostate and a 5mm to the PLN. With these planning margins, our results indicated that aligning to the prostate soft tissue on daily KV-CBCT was an effective strategy and aligning to the pelvic bone would result in underdosing to the prostate in 1/3 of fractions. Without daily KV-CBCT or other daily imaging guidance methods to localize the prostate, it is necessary to enlarge the planning margin greater than 8 mm/6 mm posterior around the prostate, particularly in the superior-inferior and

213 anterior-posterior directions. This study, however, did not design to study the planning
214 margins without daily IGRT.

215
216 Furthermore, with the current clinical margins, we found that the ART or MLC tracking
217 method has no dosimetric advantages over iso-shift method with the alignment to the
218 prostate. A separate study is ongoing to further investigate dosimetric advantages for
219 ART or MLC tracking method if the planning margins are further reduced. In this study,
220 the pelvic bones were used as a surrogate for the PLN motion although we did not
221 thoroughly investigate validity of the use of this surrogate. Based on our knowledge,
222 there is no publication to contraindicate this assumption.

223
224 Recently, the Duke group (14) published their approach of combining replanning and
225 repositioning adaptive strategy using daily or weekly CBCT for prostate only treatment.
226 Using 5mm uniform planning margin and daily imaging alignment to the prostate soft
227 tissue, they found that D99 of the prostate received $\leq 98\%$ of the prescription dose in
228 13% of fractions. Real-time replanning or their proposed adaptive imaging guided
229 radiotherapy can remedy underdose of the prostate in these 13% of fractions. In
230 comparison, using the planning margin of 8mm/6mm posterior, we did not observe
231 underdose of the prostate in this large number of fractions (13%). Instead, our results
232 showed that when aligning daily images to the prostate, D99 of the prostate was $\geq 97\%$
233 of the prescription doses in 98% of fractions although we used slightly lower dosimetric
234 endpoint (97% of the prescription dose in the present study vs. 98% of the prescription

dose in the reference (14)). Whether our result would remain the same when using the more restrict Duke criterion needs further quantification.

With 5mm planning margin to the PLN, Hus et. al. from Stanford University simulated the effect of prostate displacement relative to the PLN (8). In their study, the PTV of the PLN still received 95% of the planned doses after randomly shifting the iso-center in any direction of the posterior, anterior, superior, and inferior by 4mm to 6mm. In the present study, using the same planning margin of 5mm to the PLN, we found that aligning to the prostate contour did not underdose the PLN, in agreement with the result of Hus et. al. (8). The difference between the Stanford study and our study is that the Stanford group used planning CTs to simulate prostate motions while our study directly used clinically acquired CBCTs for dose calculation.

One criticism to the present study is that we used criteria of D99 of the prostate and D99 of PLN $\geq 97\%$ of the prescription dose or 97% of the planned D99 dose to evaluate the verification plans. Because of several limitations in using CBCT to verify daily dose, we allowed D99 of the prostate to be $\geq 97\%$ of the prescription dose instead of $\geq 100\%$ of the prescription dose. The limitations of using CBCT to verify daily dose included that only the translational shifts were considered to correct the inter-fraction prostate motion; tissue heterogeneity correction was not applied; inter- and intra-observer variations on the prostate contours were not investigated. Since obtaining the precise Hounsfield Numbers for each CBCT (15) is challenge, we chose to use homogeneity tissue calculation methods in the CBCT verification plans for this study.

258

259 If we use the prescription dose as a criterion while aligning to the prostate soft tissue,
260 only 84% fractions had D99 of the prostate meet the criterion. If a criterion of greater
261 than 97% of the prescription dose was used, this number increased to 98%. Similarly with
262 5mm planning margin to the PLN and with alignment focus to the pelvic bones, only
263 80% fractions had D99 of the PLN meet the prescription dose. If a criterion of greater
264 than 97% of prescription dose was used, this number increased to 98%. Clinically, it
265 would be desirable to have D99 of the both targets in all fractions greater than the
266 prescription dose. We believe that these results did not indicate that the planning margins
267 are inadequate while a proper imaging alignment focus was applied. These results rather
268 indicated the limitations of directly using CBCT for dose verification, at least in our
269 approaches of using CBCT.

270

271 Separating the magnitude of inter-fraction prostate motion into two groups, we found that
272 for the prostate motion $\leq 0.74\text{cm}$, aligning to the pelvic bone would result in inadequate
273 dose to the prostate in 30% of the fractions despite of a planning margin of 8 mm/6 mm
274 posterior. For fractions with the prostate motion $\geq 0.74\text{cm}$, the situation was worse,
275 underdosing the prostate in 72% of the fractions. To our surprise, the PLN would receive
276 adequate dose in nearly all fractions (98%) independent of the image alignment focus.
277 One possible explanation to this result is that the conformity of the iso-dose line to the
278 PLN is not as high as that to the prostate. Similarly, the MLC shift method also achieved
279 good dose coverage to the PLN.

280

In the era of imaging guidance, the planning margins of 8mm/6mm posterior for the prostate appear generous. A separate study is ongoing to further investigate potential the planning margins reduction if ART or MLC tracking is applied. Another limitation of the study is that the number of patients is small due to the limited longitudinal field of view of the available CBCTs and due to the retrospective nature of the study. Future study is needed to confirm our findings with more number of patients and to investigate whether directly using a diagnostic quality CT as the verification CT can overcome the observed limitation of using CBCT for dose verification.

Conclusion

We have demonstrated that for the concurrent treatment of the prostate and PLN aligning to the prostate soft tissue on daily KV-CBCT is an effective strategy with our clinical planning margins; aligning to the pelvic bone would result in underdosing to the prostate in 1/3 of fractions. Whether MLC tracking method or ART can reduce the planning margins requires further investigation.

References

1. Yoo S, Yin FF. Dosimetric feasibility of cone-beam CT-based treatment planning compared to CT-based treatment planning. *Int J Radiat Oncol Biol Phys* 2006;66:1553-1561.
2. Fu W, Yang Y, Yue NJ, *et al.* A cone beam CT-guided online plan modification technique to correct interfractional anatomic changes for prostate cancer IMRT treatment. *Phys Med Biol* 2009;54:1691-1703.
3. Yan D, Lockman D, Brabbins D, *et al.* An off-line strategy for constructing a patient-specific planning target volume in adaptive treatment process for prostate cancer. *Int J Radiat Oncol Biol Phys* 2000;48:289-302.
4. Wu QJ, Thongphiew D, Wang Z, *et al.* On-line re-optimization of prostate IMRT plans for adaptive radiation therapy. *Phys Med Biol* 2008;53:673-691.
5. Nuver TT, Hoogeman MS, Remeijer P, *et al.* An adaptive off-line procedure for radiotherapy of prostate cancer. *International Journal of Radiation Oncology Biology Physics* 2007;67:1559-1567.
6. Shih HA, Harisinghani M, Zietman AL, *et al.* Mapping of nodal disease in locally advanced prostate cancer: Rethinking the clinical target volume for pelvic nodal irradiation based on vascular rather than bony anatomy. *International Journal of Radiation Oncology Biology Physics* 2005;63:1262-1269.
7. Shimizu S, Osaka Y, Shinohara N, *et al.* Use of Implanted Markers and Interportal Adjustment with Real-Time Tracking Radiotherapy System to Reduce Intrafraction Prostate Motion. *International Journal of Radiation Oncology Biology Physics* 2011;81:E393-E399.

- 320 8. Hsu A, Pawlicki T, Luxton G, *et al.* A study of image-guided intensity-modulated
321 radiotherapy with fiducials for localized prostate cancer including pelvic lymph
322 nodes. *International Journal of Radiation Oncology Biology Physics*
323 2007;68:898-902.
- 324 9. Peng C, Chen G, Ahunbay E, *et al.* Validation of an online replanning technique
325 for prostate adaptive radiotherapy. *Phys Med Biol* 2011;56:3659-3668.
- 326 10. Ludlum E, Mu G, Weinberg V, *et al.* An algorithm for shifting MLC shapes to
327 adjust for daily prostate movement during concurrent treatment with pelvic lymph
328 nodes. *Med Phys* 2007;34:4750-4756.
- 329 11. Xia P, Qi P, Hwang A, *et al.* Comparison of three strategies in management of
330 independent movement of the prostate and pelvic lymph nodes. *Med Phys*
331 2010;37:5006-5013.
- 332 12. Price RA, Murphy S, McNeeley SW, *et al.* A method for increased dose
333 conformity and segment reduction for SMLC delivered IMRT treatment of the
334 prostate. *Int J Radiat Oncol Biol Phys* 2003;57:843-852.
- 335 13. Lawton CA, Michalski J, El-Naqa I, *et al.* RTOG GU Radiation oncology
336 specialists reach consensus on pelvic lymph node volumes for high-risk prostate
337 cancer. *Int J Radiat Oncol Biol Phys* 2009;74:383-387.
- 338 14. Li T, Thongphiew D, Zhu X, *et al.* Adaptive prostate IGRT combining online re-
339 optimization and re-positioning: a feasibility study. *Phys Med Biol* 2011;56:1243-
340 1258.

341 15. Bissonnette JP, Balter PA, Dong L, *et al.* Quality assurance for image-guided
342 radiation therapy utilizing CT-based technologies: a report of the AAPM TG-179.
343 *Med Phys* 2012;39:1946-1963.
344
345
346

Captions

Figure 1: Detailed Isodose distributions for the prostate and PLN from the original IMRT plan, iso-shift contour, iso-shift bone, MLC-shifting plan, and ART plans in the axial, sagittal, coronal view. The solid red with the red line is the contour of the prostate. The solid pink with the pink line is the contour of the pelvic lymph nodes. The yellow line is the contour of the bladder. The brown line is the contour of the rectum. The blue line is the iso-dose line of 50 Gy, and the green line is the iso-dose line of 45 Gy.

Figure 2: Dose volume histograms for the prostate, PLN, bladder, and rectum for a selected original IMRT plan, iso-shift contour, iso-shift bone, MLC-shift, and ART plans.

Figure 3: (a) D5 of the bladder, (b) D5 of the rectum. Both calculated based on daily KV-CBCT for the iso-shift contour, iso-shift bone, and MLC-shift methods and normalized to the corresponding original IMRT dose.

Figure 4: (a) D5 of the bladder, (b) D5 of the rectum. Both calculated based on daily KV-CBCT for the iso-shift contour, and iso-shift bone, MLC-shift methods and normalized to the corresponding ART dose.

Figure 5: (a) D99 of the prostate, (b) D99 of the PLN. Both normalized to the corresponding original IMRT dose, versus the magnitude of the prostate displacement for, the iso-shift contour, iso-shift bone, and MLC-shift methods.

370

371

372

373

374

375

376

377

378

Table 1: Percentage of 124 fractions have D99 of the prostate and PLN greater than 97% of the prescription dose, 97% of the original planned D99, or 97% of ART planned D99 in iso-shift (contour and pelvic bones), MLC-shift, and ART plans.

	Iso-shift-contour method (%)		Iso-shift-bone method (%)		MLC-shift method (%)		Adaptive planning method (%)	
	Prostate	PLN	Prostate	PLN	Prostate	PLN	Prostate	PLN
D99> 97% of the prescription dose	97.6	98.4	73.4	98.4	98.8	98.4	98.6	100
D99> 97% of the original IMRT D99	94.4	98.4	70.2	97.6	96.8	98.4	98.6	99.2
D99> 97% of the adaptive method	93.6	96.8	67.7	95.2	93.51	94.4		

Figure 1

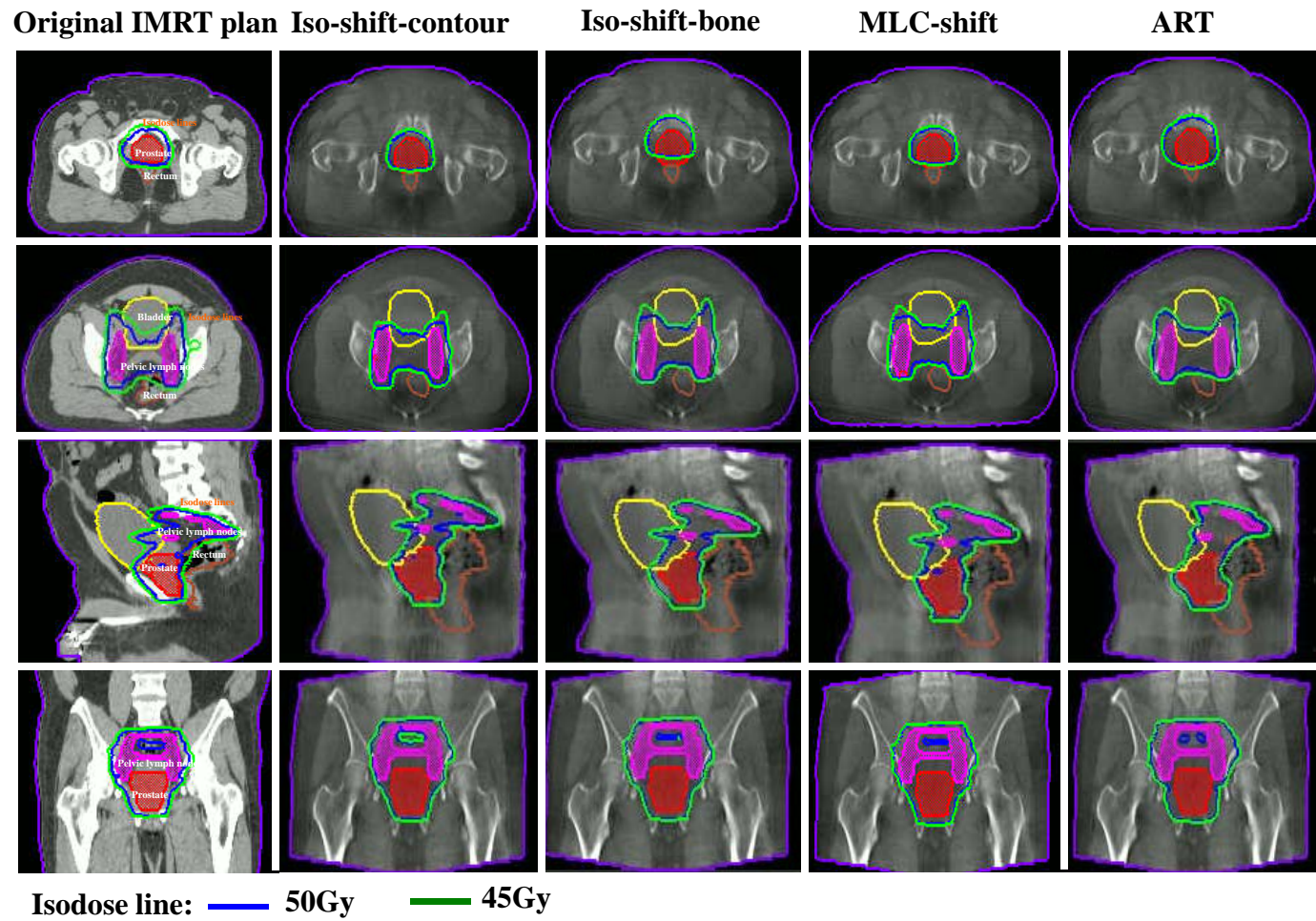
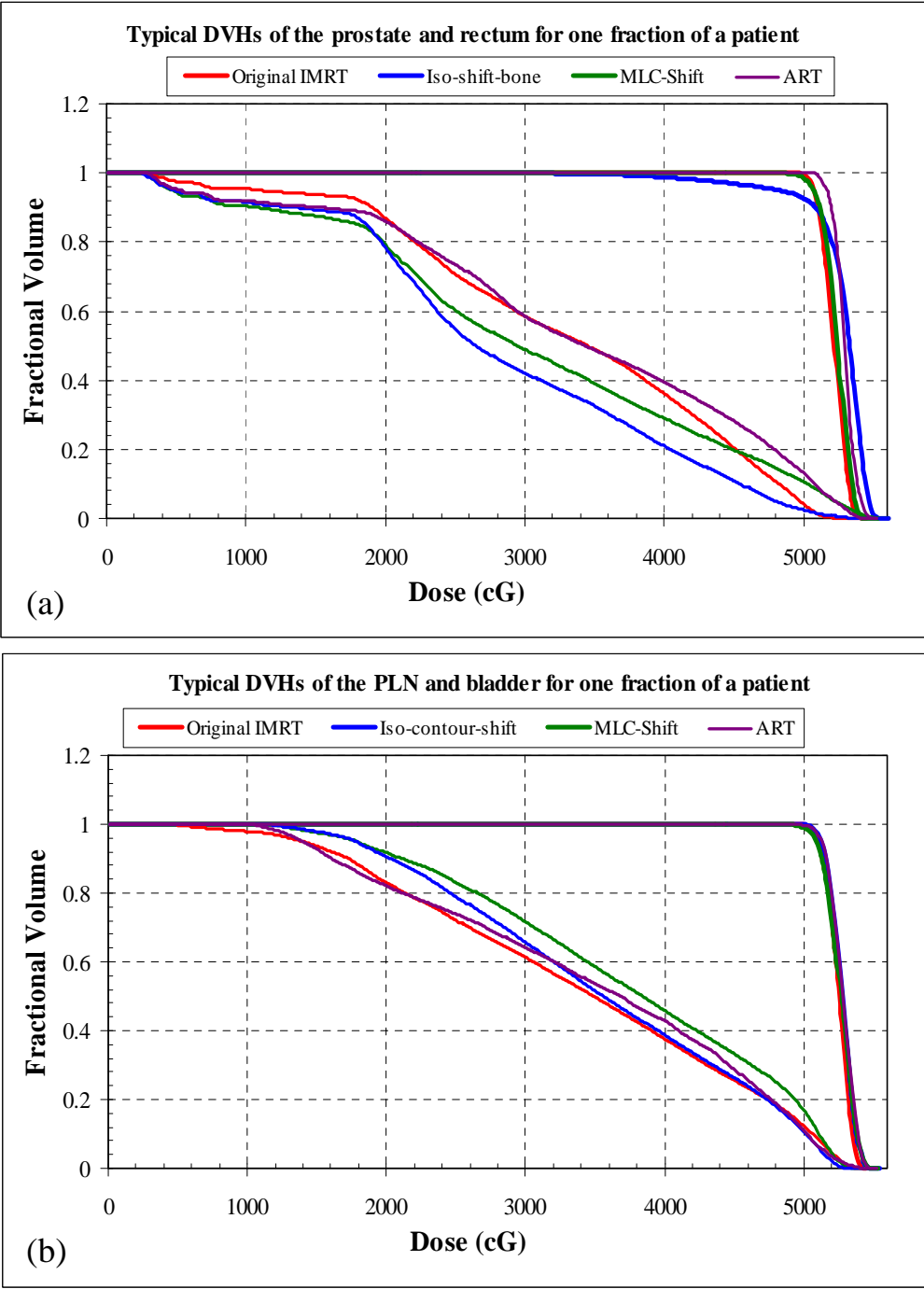


Figure 2Figure 3



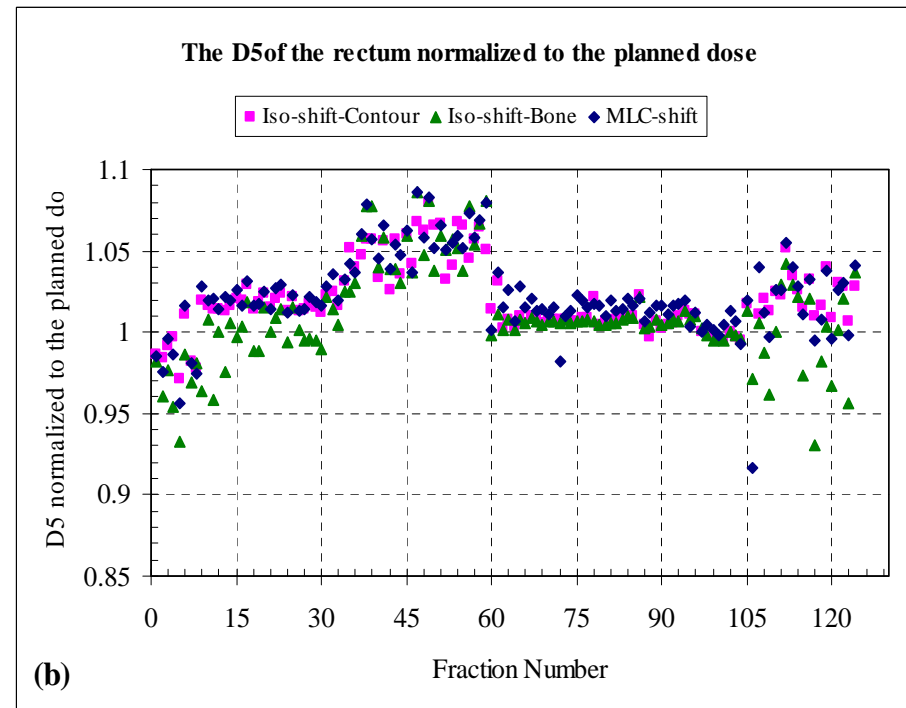
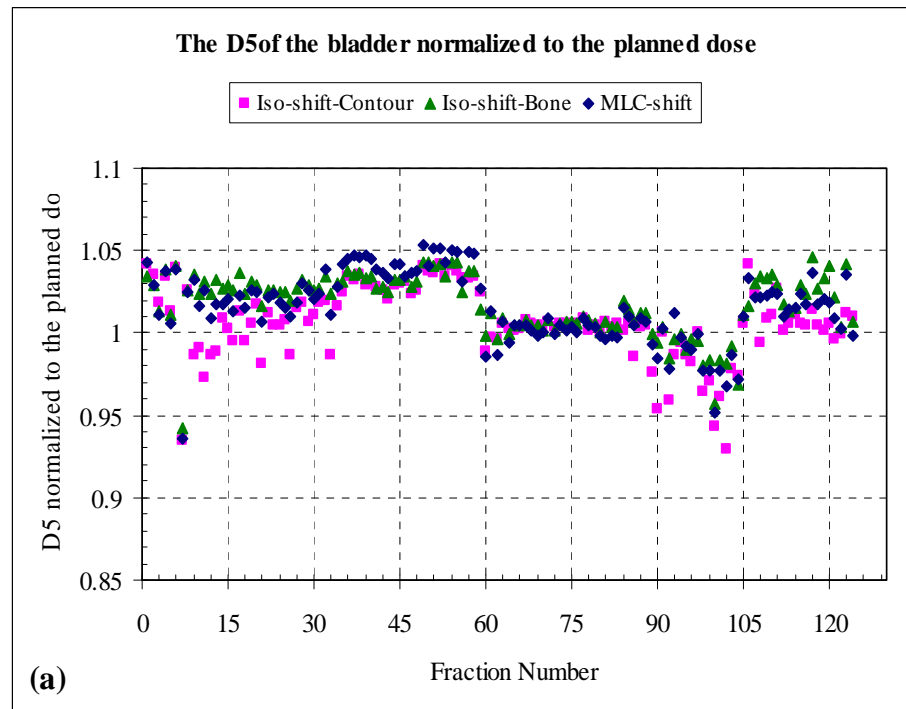
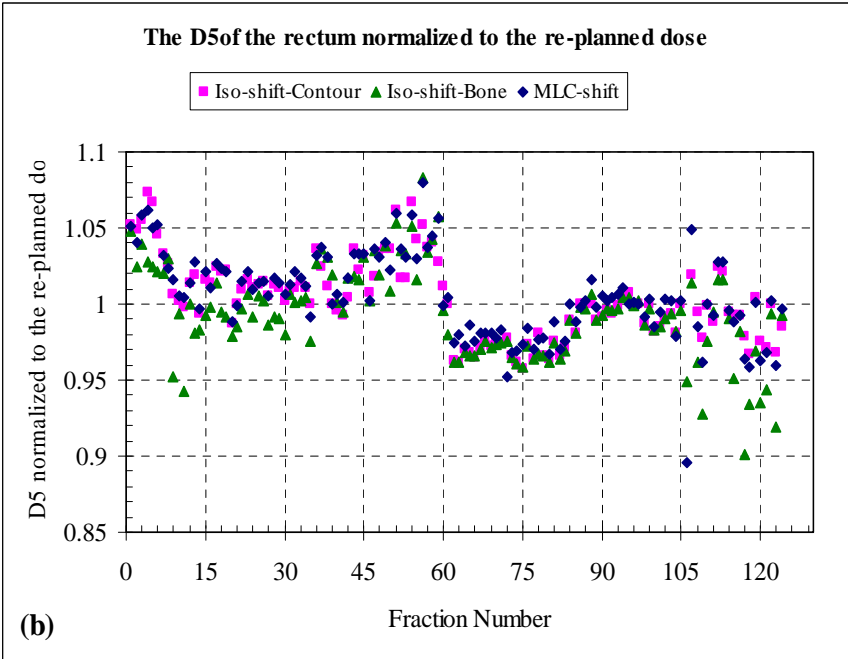
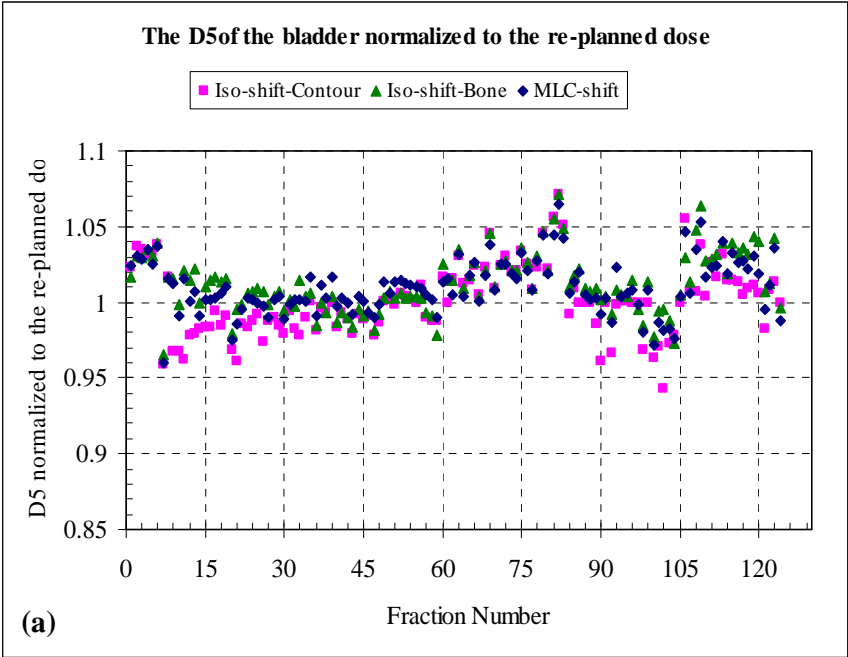
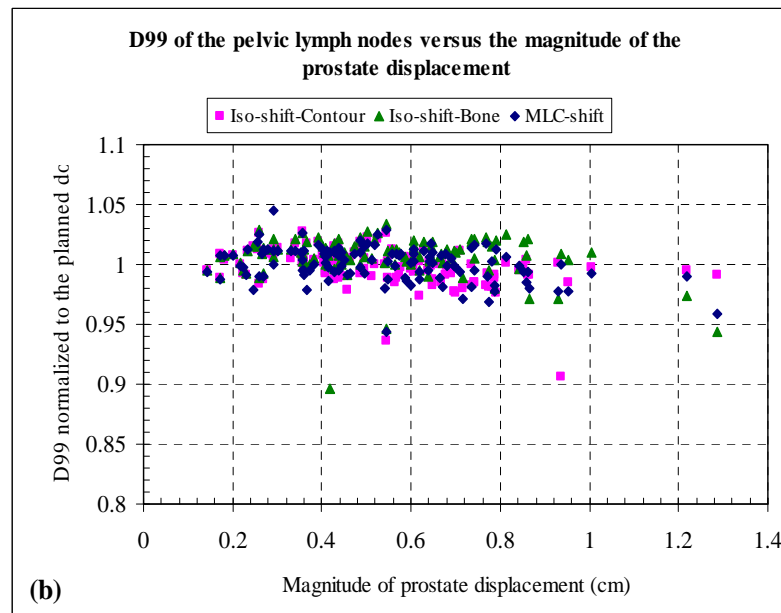
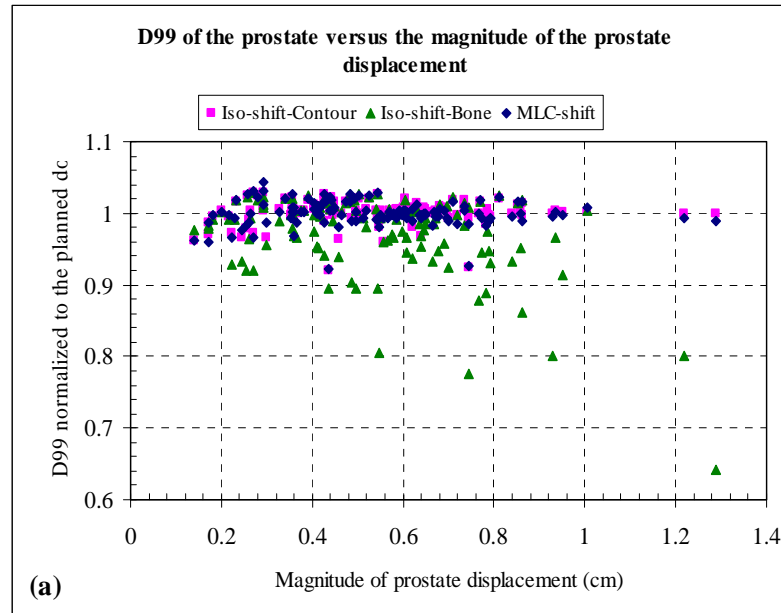


Figure 4Figure 5





Planning Margins Validation for Concurrent Treatment of Prostate and Pelvic Lymph Nodes under Daily Image Guided Delivery

Samah Ferjani, Kevin L. Stephans, Rahul Tendulkar, and Ping Xia
Department of Radiation Oncology, Cleveland Clinic, Cleveland, OH 44195

Purpose: To validate prostate planning margins for concurrent treatment of the prostate and pelvic lymph nodes (PLN) under daily kilo-voltage cone beam (KV-CBCT) imaging guidance while applying MLC and iso-center shifting methods to compensate for inter-fractional prostate motion.

Methods and Materials: Ninety-four daily KV-CBCTs from five patients, who received IMRT treatment with a clinical planning margin to the prostate of 8mm/6mm posterior (M(8,6)), and 5mm to the PLN, were selected. Three additional IMRT plans were created for each patient with the prostate planning margins of 6mm/4mm posterior (M(6,4)), 4mm/2mm posterior (M(4,2)) and 2mm uniform margin (M(2,2)). The PLN planning margin remained 5mm. Subsequently, each plan was applied to the daily KV-CBCT using MLC and iso-center shifting methods. Daily D95 of the prostate and D95 of the PLN, and D5 of the rectum and D5 of the bladder were evaluated for adequate planning margins.

Results: For both the MLC and iso-center shifting methods, D95 of the prostate was $\geq 97\%$ of the prescription dose in 97.8% (100%), 98.9% (97.9%), 95.8% (97.9%), and 93.7% (96.8%) of 94 fractions, for M(8,6), M(6,4), M(4,2), and M(2,2) respectively. Accordingly, D95 of the PLN was $\geq 97\%$ of the prescription dose in 98.9% (100%), 100% (98.9%), 98.9% (98.9%), and 100% (98.9%), for M(8,6), M(6,4), M(4,2), and M(2,2) respectively. For the rectum, D5 exceeded 105% of the original IMRT D5 for the MLC-shift (and iso-center shift) plans in 16% (14.9%), 14.9% (16.4%), 5.4% (12.2%) and 4.3% (12.2%) for these four planning margins respectively. For the bladder, D5 exceeded 105% of the original IMRT D5 for the MLC-shift (and iso-center shift) plans in 0% (1.1%), 6.4% (3.2%), 13.9% (4.3%), and 8.6% (4.3%), respectively.

Conclusion: With 5 mm planning margin to the PLN, both MLC tracking and iso-center shifting method can reduce the prostate planning margin to 4mm/2mm posterior while achieving adequate targets coverage.

Appendix I: Accepted as a poster presentation at the Annual Meeting of American Association of Physicists in Medicine at Charlotte, NC, July 29-Aug 2, 2012.

Using Shifting Planned Dose Matrix to Evaluate Daily Dose Changes For IMRT Prostate Treatment

S. Ferjami, G Huang, Q. Shang, and P. Xia

Purpose: Summation of the daily DVH from the KV-cone beam CT (KV-CBCT) to obtain a composite dose volume histogram (DVH) is challenge. Directly translating the planned dose matrix according to the measured daily prostate displacements provided a common reference frame for a composite DVH from daily DVHs. The purpose of this study is to evaluate the shifting planned dose matrix method when compared to the dose recalculation method using daily KV-CBCT.

Methods and Materials: Six patients, who received concurrent IMRT treatment for the prostate and pelvic lymph nodes with 124 daily CBCTs, were selected for this study. Contours for each CBCT were transferred from the planning CT after soft tissue registration for the prostate and after bony registration for the pelvic lymph nodes. Using the same planning beam configurations, we re-calculated doses for these CBCTs after shifting to the corrected treatment isocenters. The planned dose matrix translation was performed by an in house program written in MATLAB and incorporated with the Computational Environment for Radiotherapy Research (CERR) software. The corresponding daily DVH was obtained by shifting the planned dose matrix according to the shifts of the treatment iso-center. To compare these two methods, selected endpoint doses for the tumor targets and sensitive structures were extracted from these DVHs.

Results: For the prostate displacement less than 1.5 cm, the dose matrix shifting method resulted in 93% and 98% fractions within 5% differences from the recalculation method for D95 of the prostate and pelvic lymph nodes, respectively. These numbers, however, reduced to 58% and 71% when 2% dose difference criterion was used.

Conclusion: Allowing 5% daily dose difference, shifting planned dose matrix provides an effective means to evaluate daily dose changes for concurrent IMRT treatment for the prostate and pelvic lymph nodes. The utility of this tool is to provide a common coordinate frame to obtain a composite dose distribution.

Sensitivity of MatriXX 2D Array in Detection of MLC Leaf Positioning Errors

Qingyang Shang and Ping Xia

Purpose: MLC leaf positioning errors significantly impact the accuracy of IMRT delivery. The aim of this study was to investigate the detection sensitivity of a commercial MatriXX 2D ion chamber array for MLC leaf positioning errors

Methods: Systematic MLC leaf positioning errors (± 1 , ± 2 , ± 3 mm) were purposely introduced on the one side of leaf bank in a square field ($10 \times 10 \text{ cm}^2$) and a clinical IMRT prostate plan with 5 fields (0° , 50° , 100° , 260° , 310°), using a clinical treatment planning system (TPS). To test the effect of the detector resolution (7.62 mm), the center of the square field was shifted to different locations at 1 mm intervals in relationship to the detector positions. Both treatment plans, with and without leaf positioning errors, were delivered and measured with a commercial MatriXX device. To eliminate potential beam modeling errors from the TPS, the Gamma index of each measured field was directly calculated between planar doses with and without errors.

Results: For the square field, the Gamma indices of 3%/3mm were 99.8% and 98.8% for 1 mm and 2 mm leaf positioning errors, respectively; the Gamma indices of 2%/2mm were 98.8% and 97.5% for 1mm and 2 mm errors, respectively. The Gamma index was independent of the error positions relative to the detector positions. For the clinical prostate treatment plan, the average Gamma indices of 3%/3mm for 5 fields were 100%, 99.8%, and 98.6% for 1 mm, 2 mm, and 3 mm errors, respectively; the average Gamma indices of 2%/2mm were 99.8%, 98.3%, and 96.6% for 1 mm, 2 mm, and 3 mm errors, respectively.

Conclusion: With the Gamma index of 3%/3mm having a passing rate of 99%, the MatriXX 2D array can detect 2 mm leaf positioning errors for a single square field, and 3 mm errors for multiple segment fields.

Effect of MLC leaf width on treatment adaptation and accuracy for concurrent irradiation of prostate and pelvic lymph nodes

Qingyang Shang, Peng Qi, Samah Ferjani, and Ping Xia^{a)}

Department of Radiation Oncology, Cleveland Clinic, Cleveland, Ohio 44195

(Received 21 February 2013; revised 26 March 2013; accepted for publication 15 April 2013; published 6 May 2013)

Purpose: The aim of the study was to evaluate the impact of multileaf collimator (MLC) leaf width on treatment adaptation and delivery accuracy for concurrent treatment of the prostate and pelvic lymph nodes with intensity modulated radiation therapy (IMRT).

Methods: Seventy-five kilovoltage cone beam CTs (KV-CBCT) from six patients were included for this retrospective study. For each patient, three different IMRT plans were created based on a planning CT using three different MLC leaf widths of 2.5, 5, and 10 mm, respectively. For each CBCT, the prostate displacement was determined by a dual image registration. Adaptive plans were created by shifting selected MLC leaf pairs to compensate for daily prostate movements. To evaluate the impact of MLC leaf width on the adaptive plan for each daily CBCT, three MLC shifted plans were created using three different leaf widths of MLCs (a total of 225 adaptive treatment plans). Selective dosimetric endpoints for the tumor volumes and organs at risk (OARs) were evaluated for these adaptive plans. Using the planning CT from a selected patient, MLC shifted plans for three hypothetical longitudinal shifts of 2, 4, and 8 mm were delivered on the three linear accelerators to test the deliverability of the shifted plans and to compare the dose accuracy of the shifted plans with the original IMRT plans.

Results: Adaptive plans from 2.5 and 5 mm MLCs had inadequate dose coverage to the prostate ($D_{99} < 97\%$, or $D_{\text{mean}} < 99\%$ of the planned dose) in 6%–8% of the fractions, while adaptive plans from 10 mm MLC led to inadequate dose coverage to the prostate in 25.3% of the fractions. The average $V_{56\text{Gy}}$ of the prostate over the six patients was improved by 6.4% (1.6%–32.7%) and 5.8% (1.5%–35.7%) with adaptive plans from 2.5 and 5 mm MLCs, respectively, when compared with adaptive plans from 10 mm MLC. Pelvic lymph nodes were well covered for all MLC adaptive plans, as small differences were observed for D_{99} , D_{mean} , and $V_{50.4\text{Gy}}$. Similar OAR sparing could be achieved for the bladder and rectum with all three MLCs for treatment adaptation. The MLC shifted plans can be accurately delivered on all three linear accelerators with accuracy similar to their original IMRT plans, where gamma (3%/3 mm) passing rates were 99.6%, 93.0%, and 92.1% for 2.5, 5, and 10 mm MLCs, respectively. The percentages of pixels with dose differences between the measurement and calculation being less than 3% of the maximum dose were 85.9%, 82.5%, and 70.5% for the original IMRT plans from the three MLCs, respectively.

Conclusions: Dosimetric advantages associated with smaller MLC leaves were observed in terms of the coverage to the prostate, when the treatment was adapted to account for daily prostate movement for concurrent irradiation of the prostate and pelvic lymph nodes. The benefit of switching the MLC from 10 to 5 mm was significant ($p \ll 0.01$); however, switching the MLC from 5 to 2.5 mm would not gain significant ($p = 0.15$) improvement. IMRT plans with smaller MLC leaf widths achieved more accurate dose delivery. © 2013 American Association of Physicists in Medicine. [<http://dx.doi.org/10.1118/1.4803499>]

Key words: multileaf collimator (MLC), leaf width, treatment adaptation, IMRT, prostate

I. INTRODUCTION

The introduction of the multileaf collimator (MLC) has streamlined the radiotherapy process and enabled intensity modulated radiation to be the mainstay of radiotherapy. Several studies on the dosimetric impact of the MLC leaf width have been conducted and have confirmed the advantage of the smaller leaf width in terms of plan conformity and organ at risk (OAR) sparing.^{1–10} Based on the sampling theory, Bordfeld *et al.*¹¹ predicted that the optimal leaf width, which equals to the optimal dose sampling distance, is ap-

proximately the beam penumbra (20%–80%) divided by 1.7. For a 10 MV photon beam from a Varian linear accelerator, the beam penumbra for field sizes of 5×5 to 20×20 cm² at 10 cm depth varies from 7 to 9 mm. For concurrent treatment of the prostate and pelvic lymph nodes (PLN), for which 10 MV photon beams are often used in our institution, the predicted optimal MLC leaf width is about 4–5.5 mm. This theoretical prediction is generated from a physical point of view without considering specific clinical applications. Many planning studies have compared different MLC leaf widths for specific cancer sites. Particularly, for prostate cancer

treatment, Kubo *et al.*¹ reported the use of 1.7–3 mm MLCs could achieve better protection of the bladder and rectum than the use of 10 mm MLC for prostate-only treatment. Abe *et al.*⁶ observed improvement in plan conformity and reduction in the rectal dose of 3 over 5 mm MLC for intraprostatic dose painting plans. However, the differences between these two leaf widths were relatively small. Kesteren *et al.*⁸ conducted a Pareto front comparison between 5 and 10 mm MLCs for VMAT treatment planning. They found using 5 mm MLC provided better conformity index, dose homogeneity, and OAR sparing. Wang *et al.*⁹ compared the dosimetric impact of MLC leaf width of 4 mm (mMLC) and 10 mm for stereotactic IMRT of prostate treatment, and demonstrated that both the bladder and rectum had consistent reductions in all dose indices for mMLC, and the target dose inhomogeneity was improved in the mMLC plans as well. Wu¹⁰ studied the effect of 5 and 10 mm MLCs on prostate treatment planning. They showed that narrower leaves had a slight improvement in the TCP and NTCP, and gave slightly better sparing of OARs.

Under image-guidance, treatment adaptation has been frequently applied. However, the impact of MLC leaf width on treatment adaptation has not been extensively studied. For prostate-only treatment, a classical strategy for treatment adaptation is to shift the treatment isocenter to follow the prostate movement. For concurrent treatment of the prostate and pelvic lymph nodes, with the strategy of shifting the isocenter, a large planning margin on one of the targets may be required, depending on how daily images are aligned. Our group previously proposed an adaptive algorithm of shifting MLC leaves to cope with the independent movement of the two targets and to avoid increasing planning margin for either target.^{12,13} This method adapted MLC portals to compensate for daily prostate movement while maintaining the dose to pelvic lymph nodes. For prostate movement in the longitudinal direction, the accuracy of the compensation was limited by the width of the MLC leaf, and over- or undercompensation for the prostate movement may be resulted depending on the magnitude of the movement and the leaf width of the MLC. It was the motivation of this study to investigate how different leaf widths can affect the over- or undercompensation. Intuitively, finer MLC leaf width can achieve better accuracy for the compensation. However, the clinical relevance of the dosimetric differences between different MLCs is not clear. Moreover, to the best of our knowledge, no study has been published thus far that assesses the impact of MLC leaf width on delivery accuracy of the treatment plan, especially for concurrent treatment of the prostate and pelvic lymph nodes. The aim of this study was to evaluate the relative significance of MLC leaf width for treatment adaptation and delivery accuracy for concurrent treatment of the prostate and pelvic lymph nodes with daily acquired verification images.

II. MATERIALS AND METHODS

II.A. Patient selection and treatment planning

Six patients, who received concurrent treatment of prostate and pelvic lymph nodes, were selected for this retrospective

TABLE I. Characteristics of three MLCs used in this study.

	Novalis TX	Artiste	Synergy
Leaf width (mm)	2.5(central 32 pairs) and 5(outer 28 pairs)	5	10
Number of leaf pairs	60	80	40
Maximum field size (cm ²)	40 × 22	40 × 40	40 × 40

study. For daily image guidance, each patient had kilovoltage cone beam CTs (KV-CBCT). Ten to fifteen CBCT images were randomly selected for each patient, and a total of 75 daily verification images were included. On each daily CBCT, the prostate, bladder, and rectum were manually contoured by a physician. The pelvic lymph nodes were only contoured on the planning CT, and were then transferred to the daily CBCT after rigid bony registration, since the nodal volumes were relatively stable in relation to the pelvic bones.

Three MLC leaf widths were evaluated in this study, including 2.5, 5, and 10 mm from the linear accelerators of Novalis TX (Varian), Artiste (Siemens), and Synergy (Elekta) available at our institution. The characteristics of each MLC are summarized in Table I. In particular, the Novalis TX linear accelerator has 32 pairs of leaf with 2.5 mm leaf width in the central 8 cm of field, and 14 pairs of leaf with 5 mm width on the outer 7 cm of field on each side. In this work, the treatment plan isocenter was adjusted so that the prostate volume was placed within the central portion of the field for the Novalis TX machine. The leaf pairs used to conform to the prostate volume were from the central 2.5 mm leaves, and the resultant variations in dose distributions were solely due to the effect of the 2.5 mm leaf width.

Three IMRT treatment plans with the same beam arrangements and planning parameters, but having different MLC leaf widths, were generated for each patient. The IMRT plans were created with the Pinnacle treatment planning system (Pinnacle 9.0, Philips Radiation Oncology System, Madison, WI), using a step-and-shoot method and a typical seven-beam arrangement with the collimator angle setting at 0°. The planning margins for these patients were 6 mm posterior and 8 mm elsewhere. The beam energy was 10 MV for the Synergy and Novalis TX machines, and was 15 MV for the Artiste machine. The patients were prescribed to 2 Gy per fraction to the prostate and 1.8 Gy per fraction to pelvic lymph nodes for 28 fractions (a total dose of 56 Gy to the prostate and 50.4 Gy to the nodal volumes) for the first phase of treatment followed by a boost treatment for the prostate only. To investigate the MLC width effect on the method which was designed for treating two targets with independent movements, our study was focused on the initial IMRT plan.

Since the Hounsfield Units (HU) in CBCT are inaccurate and unreliable for dose calculation, the electron density of the CBCT was overridden with 1 g/cm³ for voxels inside the patient external body contour and 0 (air) for voxels outside the external contour. To eliminate dose variations originating from inhomogeneity, the electron density of the planning CT was also overridden with 1 g/cm³ within the external contour.

II.B. Image registration

A dual image registration was used to obtain daily prostate shift relative to the pelvic bones. Each daily CBCT was registered to the planning CT by using: (a) bony registration, which aligned the pelvic bones in both images and (b) contour registration, which aligned the prostate contours in both images. By subtracting the shifts from bony registration, patient positioning setup errors were removed, and the prostate shifts relative to the pelvic bones were determined. The dual image registration was performed in the same treatment planning system (Pinnacle 9.0) with translational shifts only, reflecting a common clinical practice of correcting only translational errors.

II.C. Treatment adaptation by shifting MLC

The treatment adaptation was accomplished based on a MLC leaf shifting algorithm proposed by Ludlum *et al.*¹² The algorithm adjusted the IMRT portals by shifting selected MLC leaf pairs to compensate for daily prostate movement, while maintaining the dose to pelvic lymph nodes. When the prostate movements were in the lateral and/or anterior/posterior directions, the shifts of the MLC leaf pairs depended only on the prostate movement projected in the plane perpendicular to the beam angle; when the prostate movement was in the superior/inferior direction, both the magnitude of the movement and the MLC leaf width affected the change of the portals. Depending on the leaf width of the MLC, the smallest prostate movement that could be precisely compensated by the MLC shifting method was the width of the MLC.

To investigate the effect of the MLC leaf width in compensating for the prostate movement in the longitudinal direction, a specific MLC shifted plan was created for each of the three MLCs for each daily CBCT (a total of 225 treatment plans). The original plan information, including beam configurations, MLC leaf positions, jaw positions, beam isocenter, contours of region of interest, etc., was exported from the treatment planning system and loaded into an in-house program. The program automatically identified the MLC leaf pairs encompassing the prostate and adapted their positions for each IMRT segment based on the daily prostate shift in three directions. Meanwhile, the positions of the MLC leaf pairs that expose radiation to pelvic lymph nodes were unchanged. The shifted MLC plan was then input back to the treatment planning system for dose calculation and dose volume histogram (DVH) analysis.

To quantify the MLC leaf width effect, selective dosimetric endpoints for the tumor volumes and OARs were evaluated for each patient. These endpoints included the dose to 99% (D99) of the prostate and pelvic lymph nodes, the mean dose, D_{mean} , of the prostate and PLN, volume of the targets that receive the prescription dose ($V_{56\text{Gy}}$ for the prostate and $V_{50.4\text{Gy}}$ for PLN). For OARs, the dose received by 5% of the rectum (D5) and bladder (D5) and the mean dose to these OARs D_{mean} were calculated from the DVHs of the regions of interest.

II.D. Plan delivery accuracy assessment (experiment)

Since the positions of the MLC leaf pairs were adjusted outside the treatment planning system or treatment console, the deliverability of the MLC shifted plan needed to be tested on the specific linear accelerators. MLC shifted plans that compensated for hypothetical prostate movements of 2, 4, and 8 mm in the longitudinal direction were created for each MLC leaf width using the in-house program. Because the magnitudes of the prostate movements were not necessary to be a multiple of the MLC leaf width, approximations were made to shift the MLC shapes by the nearest number of leaf widths. For example, for prostate movement of 2 mm in the longitudinal direction, only shifting one pair of MLC leaf with 2.5 mm leaf width (referred to as 2.5 mm MLC) could compensate the prostate motion. No shifting plans were generated for 5 and 10 mm MLC. Therefore, compensating for prostate movements of 2, 4, and 8 mm in the longitudinal direction resulted in three different MLC shifted plans using 2.5 mm MLC, two different shifted plans using 5 mm MLC, and one shifted plan using 10 mm MLC. This approximation may result in over- or undercompensation for the shifted plans. To evaluate the effect of MLC leaf width on delivery accuracy of the shifted plans, we also conducted measurements using the MatriXX 2D array device (IBA Dosimetry GmbH, Schwarzenbruck, Germany). The measured planar doses were compared to the calculated planar doses by using the gamma index and absolute dose difference.

III. RESULTS

III.A. Dosimetric evaluation

III.A.1. Prostate shifts in the longitudinal direction

Daily prostate shifts in the longitudinal direction obtained from the dual image registration for all 75 fractions are shown in Fig. 1(a). The average of the absolute magnitudes is 3.2 ± 2.0 mm, ranging from 7.5 mm inferiorly to 8 mm superiorly. Figure 1(b) shows the means and standard deviations of patient specific shifts in the longitudinal direction.

III.A.2. Target coverage

All dosimetric endpoints of the shifted plans were normalized to the planned values of the initial IMRT plan for each MLC, so the variations of the original plan quality due to the use of different MLCs were removed. The differences in the dosimetric endpoints were primarily from the leaf width effect of the MLC shifted plans. The treatment adaptation was based on the actual prostate shifts in three directions.

Figure 2 shows D99 of the prostate and pelvic lymph nodes (CTVs not PTVs) of the shifted plans using three MLCs when normalized to the planned D99 of the initial IMRT plans. Specifically, we found that D99 of the prostate is less than 97% of the planned D99 in 5 out of 75 fractions (6.7%) for 2.5 mm MLC shifted plans, 6 out of 75 fractions (8%) for 5 mm MLC shifted plans, and 19 out of 75 fractions (25.3%) for 10 mm MLC shifted plans. The differences in the

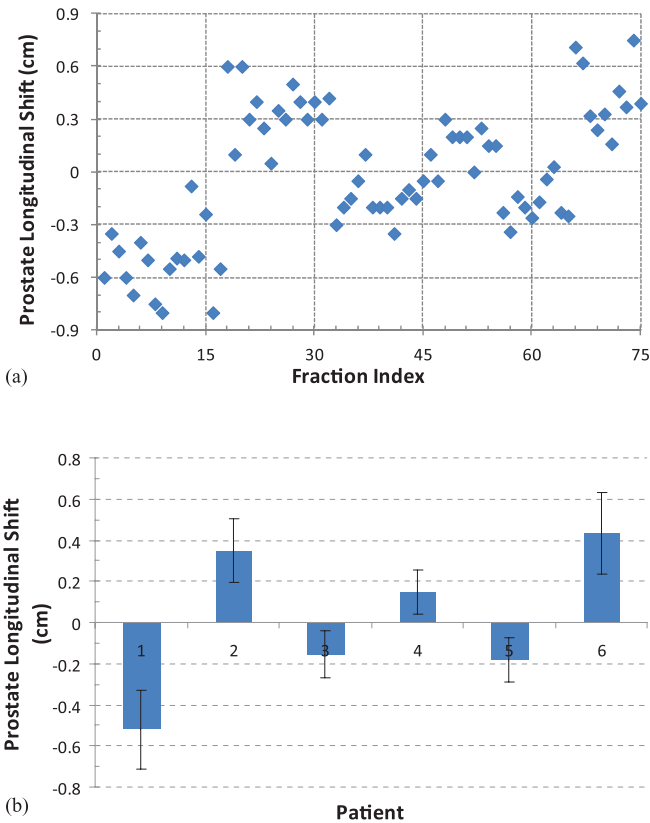


FIG. 1. Prostate shifts in the longitudinal direction. (a) Daily prostate shifts for all fractions. (b) The means and standard deviations of patient specific shifts. Positive and negative shifts correspond to the prostate shifts in the inferior and superior directions, respectively.

number of fractions in which D99 is less than 97% of the planned D99 were significant ($p \ll 0.01$) between 5 and 10 mm MLC shifted plans, but insignificant ($p = 0.15$) between 2.5 and 5 mm MLC shifted plans. For pelvic lymph nodes, all shifted plans using 2.5 and 5 mm MLCs received D99 of the PLN greater than 97% of the planned D99 of PLN, while 71 fractions (94.7%) of shifted plans using 10 mm MLC met this criterion. The quantitative analysis of D99 and D_{mean} of the prostate and pelvic lymph nodes for the three MLC leaf widths is summarized in Table II.

Figure 3 shows the average volumes of the prostate and pelvic lymph nodes receiving the prescription dose for each patient. The index is $V_{56\text{Gy}}$ for the prostate and $V_{50.4\text{Gy}}$ for PLN, both normalized to the planned volumes. It was observed that both 2.5 and 5 mm MLC shifted plans had an aver-

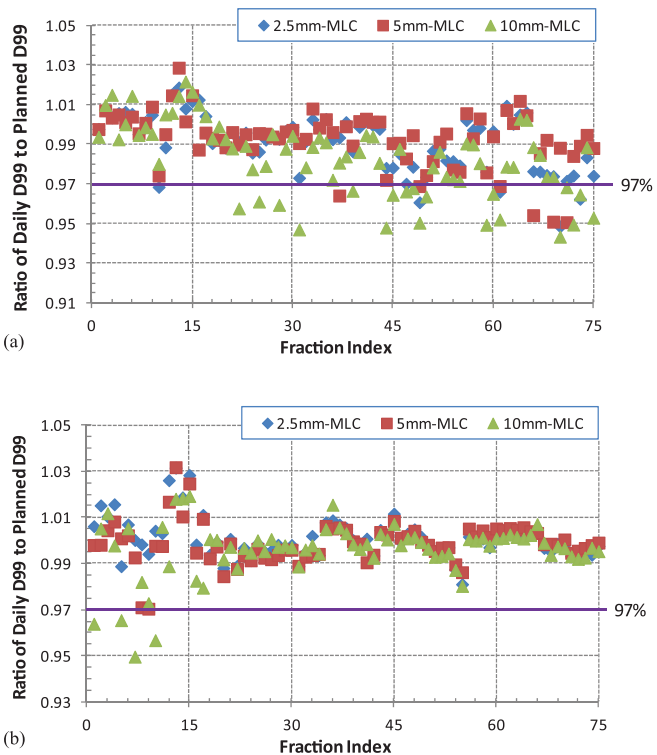


FIG. 2. Daily D99 of (a) the prostate and (b) pelvic lymph nodes. D99 is expressed as a ratio of the daily dose to the planned dose.

age $V_{56\text{Gy}}$ of the prostate greater than 93% of the planned volumes for all patients, while for patient 4 and patient 6, 10 mm MLC shifted plans had significantly ($p \ll 0.01$) lower $V_{56\text{Gy}}$ (85.6% and 62.2%, respectively) of the prostate (Table III). For pelvic lymph nodes, all patients had an average $V_{50.4\text{Gy}}$ greater than 97% of the planned volumes for all shifted plans using the three MLC leaf widths. The p -values for 2.5 and 10 mm MLC shifted plans were 0.27, indicating there was no significant difference for lymph nodes coverage between the two. Table III lists the mean and standard deviation of $V_{56\text{Gy}}$ for the prostate and $V_{50.4\text{Gy}}$ for PLN for each patient. The overall means of $V_{56\text{Gy}}$ for the prostate were 98.6%, 98.0%, and 92.2% for 2.5, 5, and 10 mm MLC shifted plans, respectively. $V_{56\text{Gy}}$ decreased by about 6% when the MLC was switched from 5 to 10 mm.

Figure 4 shows a typical daily DVH of the prostate and pelvic lymph nodes, as well as the bladder and rectum for the three MLCs. The DVH curve for the prostate using 5 mm MLC was hidden behind the curve using 2.5 mm MLC,

TABLE II. The dosimetric comparison of D99 and D_{mean} of the prostate and pelvic lymph nodes for 2.5, 5, and 10 mm MLC shifted plans.

MLC leaf width (mm)	Prostate CTV		Pelvic lymph nodes CTV	
	D99 > 97% of the planned dose (%)	D_{mean} > 99% of the planned dose (%)	D99 > 97% of the planned dose (%)	D_{mean} > 99% of the planned dose (%)
2.5	93.3	94.7	100	94.7
5	92	96	100	94.7
10	74.7	74.7	94.7	94.7

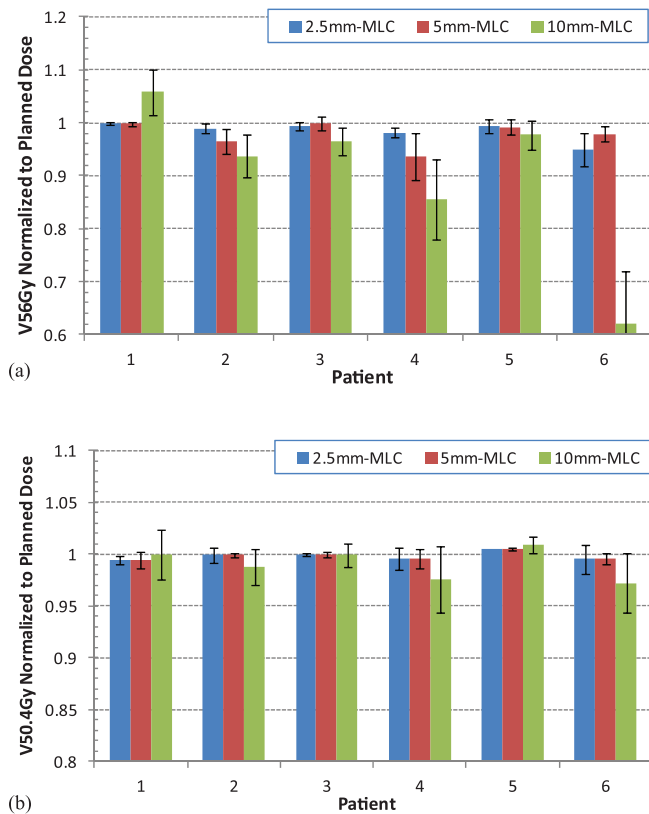


FIG. 3. Average volume of (a) the prostate and (b) pelvic lymph nodes receiving the prescription dose for each patient. Error bar indicates one standard deviation.

indicating that using these two MLCs resulted in very similar prostate dose coverage.

III.A.3. OAR sparing

Figure 5 shows a ratio of daily D5 to the planned D5 of the bladder and rectum. Using 105% of the planned D5 as a threshold, all fractions of 2.5 and 5 mm MLC shifted plans were within this threshold for D5 of the bladder and 10 mm MLC shifted plans had 14 fractions (18.7%) that exceeded the threshold. After a close examination of the data, we found that these fractions were from one patient, who consistently had smaller bladder volumes (about 20%–30% of the planned volume) during the treatment course. For this patient, the drastic

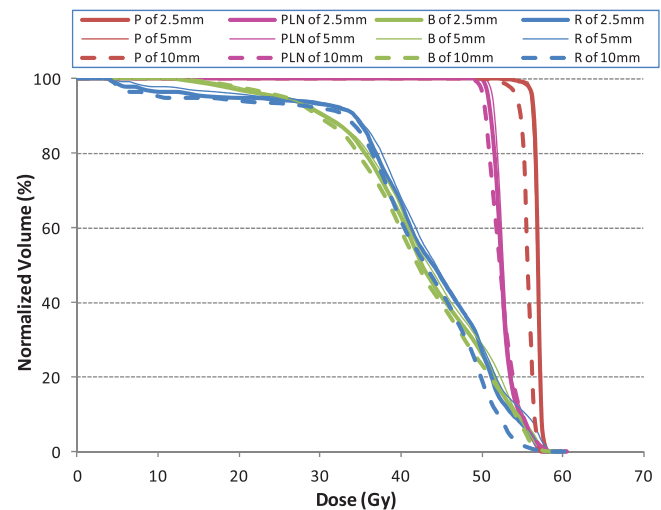


FIG. 4. Typical DVHs of the targets and OARs for one fraction of a patient. P for prostate, PLN for pelvic lymph nodes, B for bladder, and R for rectum.

changes in the bladder volume induced larger and more frequent longitudinal shifts. The imperfect compensation in this direction due to the finite leaf width may result in the increase of the D5 of the bladder. Furthermore, the smaller daily bladder volume may contribute to the increase of the daily D5 of the bladder. For D5 of the rectum, 93.3% of the fractions met the 105% criterion for all shifted plans using the three MLCs.

Figure 6 shows for each patient the average D_{mean} of the bladder and rectum, which are comparable for all shifted plans using the three MLCs.

III.B. Deliverability and accuracy

For three hypothetical shifts of 2, 4, and 8 mm in longitudinal directions, the MLC shifted plans and the original IMRT plans of a patient were delivered on the three linear accelerators to test the deliverability of the shifted plans and to compare the dose accuracy of the shifted plans with the original IMRT plans. The 3%/3 mm gamma index between the measured and calculated plans is shown in Table IV. It was noted that each shifted plan achieved a passing rate similar to the original plan although the shifted plan associated with the smallest MLC leaf width (2.5 mm) had the highest passing

TABLE III. The average volumes of the prostate and pelvic lymph nodes receiving the prescription dose for each patient.

Patient no.	$V_{56\text{Gy}}$ of the prostate			$V_{50.4\text{Gy}}$ of pelvic lymph nodes		
	2.5 mm (%)	5 mm (%)	10 mm (%)	2.5 mm (%)	5 mm (%)	10 mm (%)
1	99.8 \pm 0.3	99.8 \pm 0.3	105.8 \pm 4.2	100.0 \pm 0.4	99.4 \pm 0.8	100.0 \pm 2.4
2	98.9 \pm 1.0	96.5 \pm 2.3	93.7 \pm 4.0	99.4 \pm 0.7	99.9 \pm 0.1	98.7 \pm 1.7
3	99.3 \pm 0.8	99.8 \pm 1.3	96.5 \pm 2.6	100.0 \pm 0.2	100.0 \pm 0.3	100.0 \pm 1.1
4	98.1 \pm 1.0	93.6 \pm 4.4	85.6 \pm 7.5	99.6 \pm 1.1	99.6 \pm 0.9	97.5 \pm 3.2
5	99.3 \pm 1.2	99.2 \pm 1.4	97.7 \pm 2.7	100.0 \pm 0.0	100.5 \pm 0.1	100.9 \pm 0.8
6	94.9 \pm 3.1	97.9 \pm 1.4	62.2 \pm 9.8	98.5 \pm 1.4	99.5 \pm 0.6	97.2 \pm 2.8
Overall	98.6 \pm 2.0	98.0 \pm 3.0	92.2 \pm 14.3	99.6 \pm 0.9	99.8 \pm 0.6	99.1 \pm 2.4

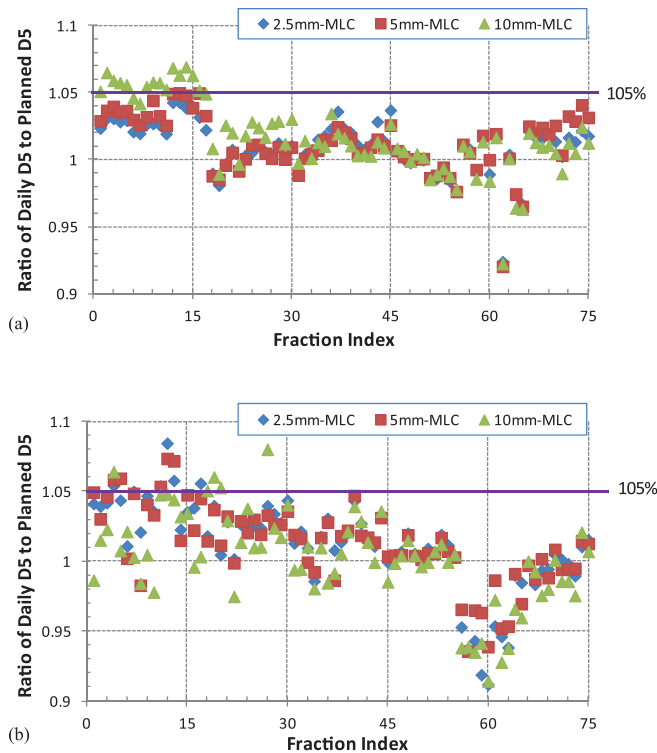


FIG. 5. Daily D5 of the (a) bladder and (b) rectum. D5 is expressed as a ratio of the daily dose to the planned dose.

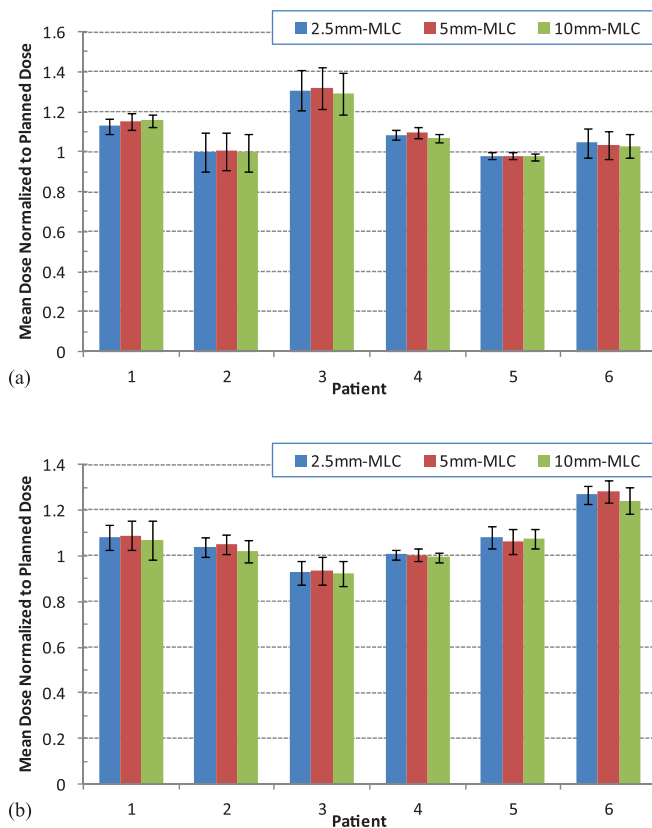


FIG. 6. Mean dose of the (a) bladder and (b) rectum as a ratio of the daily dose to the planned dose. Error bar represents one standard deviation.

TABLE IV. Gamma passing rate (3%/3 mm) between the measured and calculated plans for the original IMRT plans and MLC shifted plans corresponding to prostate movements of 2, 4, and 8 mm in the longitudinal direction.

	Original (%)	2 mm (%)	4 mm (%)	8 mm (%)
2.5 mm MLC	99.6	99.3	99.3	99.5
5 mm MLC	93.0	...	93.3	92.8
10 mm MLC	92.1	92.6

rate while the shifted plan associated with the largest MLC leaf width (10 mm) had the lowest passing rate.

Figure 7 shows the isodose line differences and absolute dose differences between the measured and calculated planar doses for the original and MLC shifted plans for the Novalis TX machine (2.5 mm MLC). For prostate movements of 2, 4, and 8 mm in the longitudinal direction, the corresponding adaptive plans shifted MLC leaves by one leaf width, two leaf widths, and three leaf widths, respectively. Dose differences mainly occurred in high dose gradient regions, and the patterns were similar among all shifted plans. The results observed were similar for plans with 5 and 10 mm MLCs in the Artiste and Synergy machines.

Table V shows the percentage of pixels whose point dose differences between the measurement and calculation were less than 3% and 5% of the maximum dose for the original IMRT plans and the MLC shifted plans of the three MLC leaf widths. For a specific MLC leaf width, the percentages of pixels with point dose differences being less than 3% or 5% were almost the same for the original IMRT plan and the MLC shifted plans, indicating that the shifted plans achieved similar accuracy as the original plan.

IV. DISCUSSION

The dosimetric impact of MLC leaf width on treatment planning has been investigated by several groups. Smaller MLC leaf widths improve dose conformity, tumor coverage, and critical organ sparing significantly, especially when the tumor volume is relatively small, or the tumor is adjacent to (or partially overlapping with) critical structures.^{4,7} However, the benefits are small and the clinical relevance remains to be proven.

In this study, the effect of MLC leaf width on treatment adaptation for concurrent treatment of the prostate and pelvic lymph nodes using the MLC leaf shifting algorithm was studied by comparing dosimetric endpoints of different MLC leaf widths. The daily dose distribution is a combined result of the

TABLE V. The percentages of pixels with dose differences between the measurement and calculation being less than 3% and 5% of the maximum dose.

	Original (%)		2 mm (%)		4 mm (%)		8 mm (%)	
	<3	<5	<3	<5	<3	<5	<3	<5
2.5 mm MLC	85.9	94.8	86.6	95.1	86.2	94.5	86.1	95.1
5 mm MLC	82.5	92.8	84.3	92.8	83.4	92.8
10 mm MLC	70.5	88.5	67.4	86.0

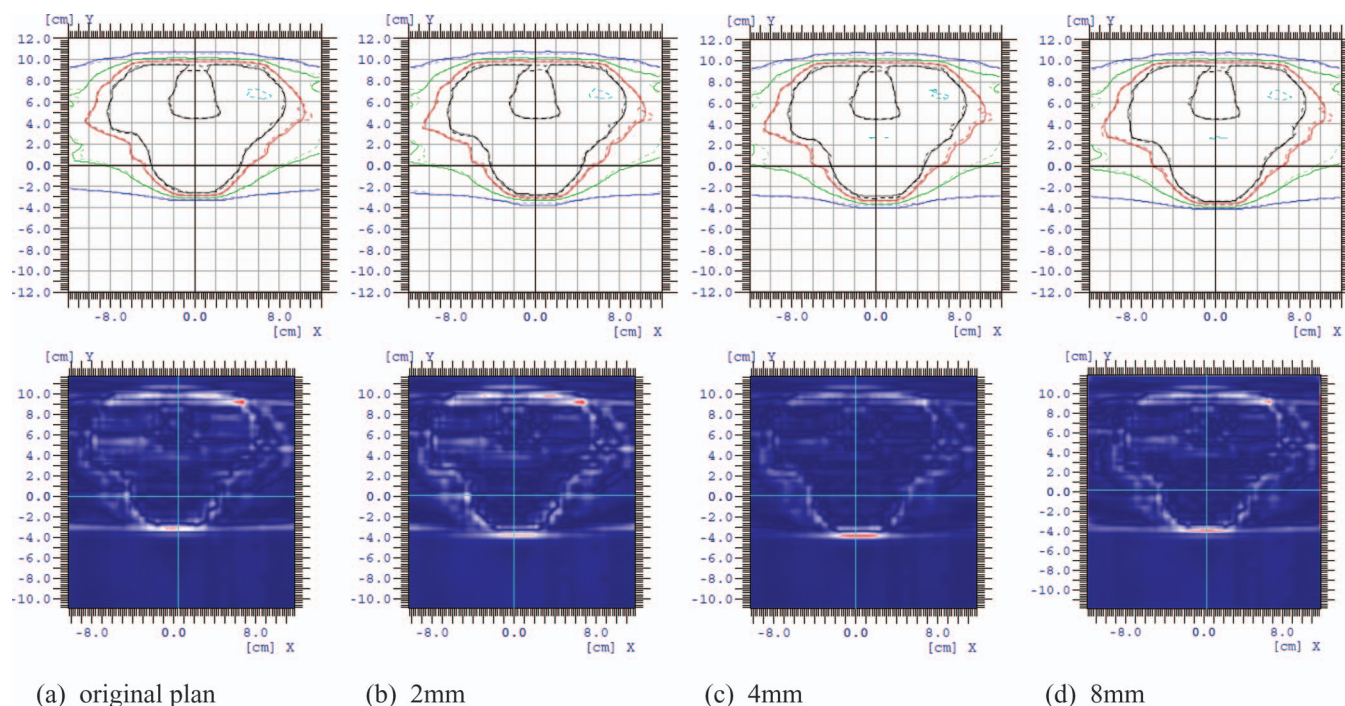


FIG. 7. Isodose line differences and absolute dose differences between the measured and calculated planar doses for the original and shifted plans corresponding to prostate movements of 2, 4, and 8 mm in the longitudinal direction for the Novalis TX machine.

original plan quality and the effect of the treatment adaptation in compensating for the prostate movement. To isolate the impact of MLC leaf width on the adaptive method from the initial plan quality, all dosimetric endpoints were normalized to the corresponding planned values in order to minimize the influence originated from the variation of plan quality. Therefore, the differences resulting from the dose distributions suggested the effect of leaf width on the treatment adaptation algorithm alone.

The treatment adaptation was based on the actual prostate shifts in three directions. Since the MLC leaves were always shifted by the nearest number of leaf widths to compensate the prostate movement in the longitudinal direction, over- or undercompensation may be resulted depending on the magnitude of the movement in this direction and the leaf width of the MLC for the adaptive plans. The dosimetric and delivery impacts of the MLC leaf width for the prostate and pelvic lymph nodes were studied. For this group of patients with the absolute magnitude of the prostate movement in the longitudinal direction of 3.2 ± 2.0 mm, adaptive plans from 2.5 and 5 mm MLCs had inadequate dose coverage to the prostate ($D_{99} < 97\%$, or $D_{\text{mean}} < 99\%$ of the planned dose) in 6%–8% of the fractions, while adaptive plans from 10 mm MLC led to inadequate dose coverage to the prostate in 25.3% of the fractions (Table II). The average $V_{56\text{Gy}}$ of the prostate over the six patients was improved by 6.4% (1.6%–32.7%) and 5.8% (1.5%–35.7%) with 2.5 and 5 mm MLC adaptive plans, respectively, when compared with 10 mm MLC adaptive plans (Table III). The benefit of switching the MLC from 10 to 5 mm was significant ($p \ll 0.01$); however, switching the MLC from 5 to 2.5 mm would not significantly improve the prostate coverage ($p = 0.15$). According to Bortfeld

et al.,¹¹ the optimal leaf width in a MLC treatment is of the order of the 20%–80% penumbra width divided by 1.7. For a typical 10 MV beam with a penumbra width of 7–9 mm (measured from our Novalis TX machine), the optimal leaf width is in the range of 4–5.5 mm. This prediction sets a theoretical limit for the MLC leaf width from a physical point of view. Further reduction of the leaf width does not lead to physical improvements of the dose distribution. Our observation of adaptive plans from 5 mm MLC achieved better results than adaptive plans from 10 mm MLC while similar benefit as adaptive plans from 2.5 mm MLC agreed well with this theoretical prediction by Bortfeld *et al.*¹¹

The dose coverage to pelvic lymph nodes was not affected by MLC leaf width, as small differences were observed for D_{99} , D_{mean} , and $V_{50.4\text{Gy}}$ among the three types of MLC shifted plans. This is understandable because the MLC leaf shifting method does not change the positions of the MLC leaf pairs covering the nodal volumes, which is due to the fact that pelvic lymph nodes are relatively stable in relation to the pelvic bones. The MLC leaf width had negligible effect on the pelvic lymph nodes from adaptive plans. This observation may not apply to the classical isocenter shifted plans.

OAR sparing had a small difference among adaptive plans from 2.5, 5, and 10 mm MLCs. This seems implausible as many other planning studies have shown that smaller MLC has beneficial impact on critical organ sparing. However, it should be noted that in our study the dosimetric endpoints were normalized to the corresponding values of the initial IMRT plan for each MLC width. The OAR sparing differences among MLCs, as well as other aspects of the plan qualities, were eliminated. Our other studies have shown that the MLC leaf shifting method delivered comparable doses to the

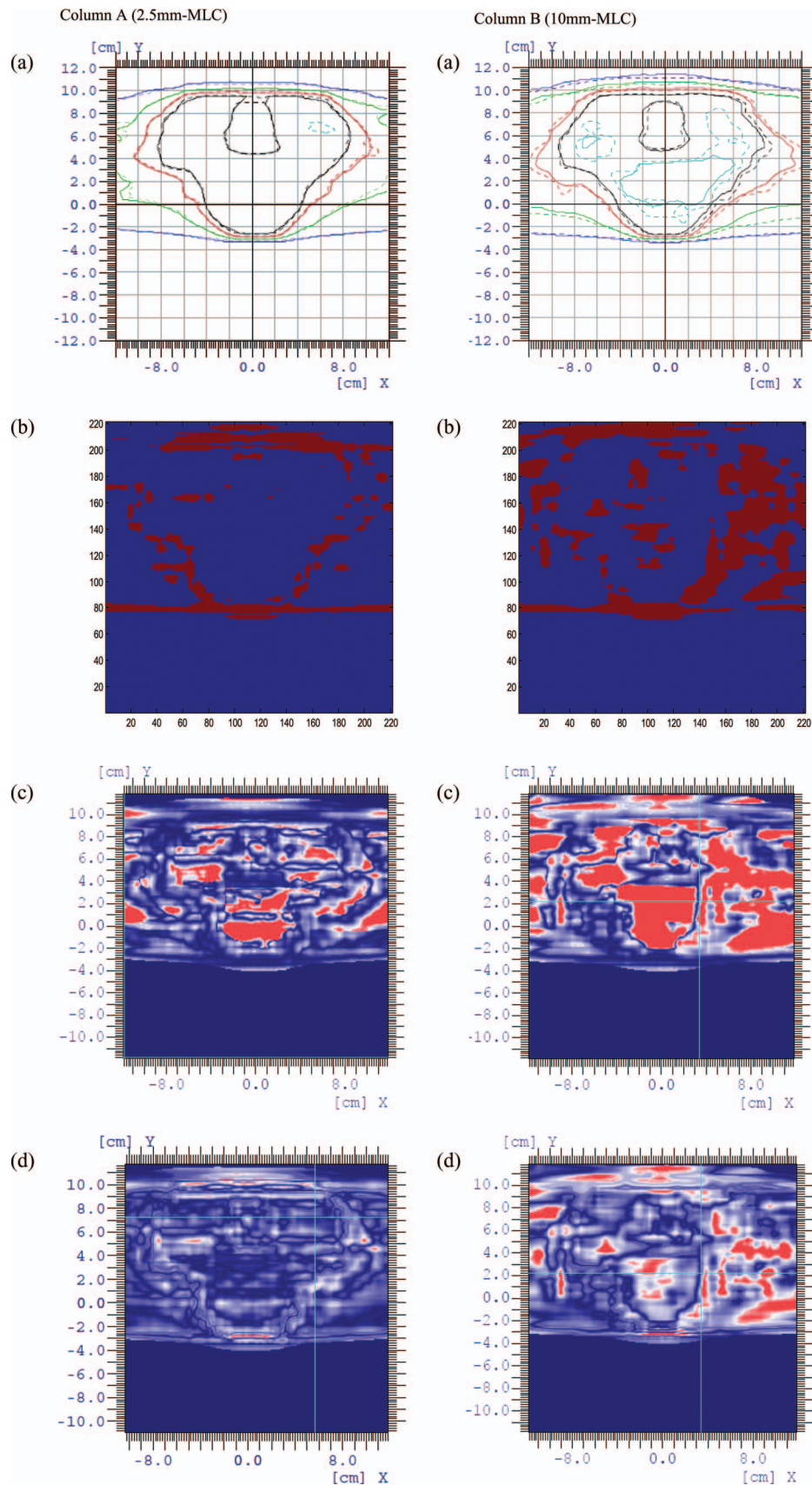


FIG. 8. Dose metrics, including (a) isodose line differences, (b) absolute dose differences (3%), (c) DTA (3 mm), and (d) gamma index (3%/3 mm) between measurements and calculations of the original IMRT plans from (A) 2.5 mm MLC and (B) 10 mm MLC. Areas in bright color indicate points in the planar dose that fail the criterion of each dose metric.

bladder and rectum as the method of shifting the isocenter, either by aligning to the pelvic bones or aligning to the prostate contour. This study further indicated that similar OAR sparing could be achieved with adaptive plans from 2.5, 5, and 10 mm MLCs using the MLC leaf shifting method.

The MLC shifted plans can be accurately delivered on all three linear accelerators, which was suggested by a gamma passing rate above 90% for each MLC leaf width. It was noted that the percentage of pixels with point dose differences greater than 3% or 5% increased as the MLC leaf width increased (Table V). Figure 8 shows the isodose line differences, absolute dose differences (3%), DTA (3 mm), and gamma index (3%/3 mm) between the measurement and calculation of the original IMRT plans from 2.5 and 10 mm MLCs. Areas in bright color indicate points in the planar dose that fail the criterion of each dose metric. It was observed that points with dose differences greater than 3% were located mainly at the high dose gradient regions, indicating that the MLC leaf width could have a direct impact on dose distributions in these regions. In general, IMRT plans from 2.5 mm MLC have a better plan conformity and faster dose fall-off in the high dose gradient regions when compared to IMRT plans from 10 mm MLC, as shown by the planning isodose line differences in Fig. 8(a). Therefore, the percentage of points with dose differences greater than 3% was lower for plans from 2.5 mm MLC [Fig. 8(b)]. Less steep dose gradient associated with plans from 10 mm MLC also led to lower DTA (3 mm) passing rate in regions where dose differences were greater than 3% [Fig. 8(c)]. As an overall result, IMRT plans from 10 mm MLC had a relatively lower gamma (3%/3 mm) passing rate than plans from 2.5 mm MLC [Fig. 8(d) and Table IV]. In conclusion, IMRT plans with smaller MLC leaf widths achieved more accurate dose delivery.

The presented results were for the concurrent treatment of the prostate and pelvic lymph nodes. Tumors with similar characteristic of independent movements but smaller volumes might benefit more when using 2.5 or 5 mm MLCs.

This adaptive algorithm is currently not applicable clinically because it will require a new feature in the Record and Verify system to allow the user to change the MLC leaf positions prior to treatment at the treatment console. It is our attempt to verify that this adaptive algorithm has a potential for a quick adaptation although other logistic issues such as the pretreatment quality assurance remain to be resolved. The advantage of this MLC leaf shifting algorithm is that it does not require a real time dose calculation, because the leaf opening for each leaf pair is unchanged while the small changes in the off-axis factors introduced by shifting the MLC leaves contribute a negligible change to the dose distribution, which has been investigated in the previous publication.¹²

V. CONCLUSIONS

According to our analysis, dosimetric advantages associated with smaller MLC leaves were observed in terms of the

coverage to the prostate when the treatment was adapted to account for daily prostate movement for concurrent irradiation of the prostate and pelvic lymph nodes. Smaller MLC leaves also achieved higher delivery accuracy. A MLC with 5 mm leaf width might be sufficient since any improvement with a 2.5 mm MLC was relatively small.

ACKNOWLEDGMENTS

This research is supported in part by the United States Army Medical Research and Materiel Command (USAMRMC, PC073349). The authors would also like to thank Dr. Long Huang and Dr. Han Liu for their assistance in plan delivery and measurement.

^{a)} Author to whom correspondence should be addressed. Electronic mail: xia@ccf.org; Telephone: (216) 444-1938; Fax: (216) 444-8934.

¹ H. D. Kubo, R. B. Wilder, and C. T. E. Pappas, "Impact of collimator leaf width on stereotactic radiosurgery and 3D conformal radiotherapy treatment plans," *Int. J. Radiat. Oncol., Biol., Phys.* **44**, 937–945 (1999).

² J. E. Monk, J. R. Perks, D. Doughty, and P. N. Plowman, "Comparison of a micro-multileaf collimator with a 5-mm-leaf-width collimator for intracranial stereotactic radiotherapy," *Int. J. Radiat. Oncol., Biol., Phys.* **57**, 1443–1449 (2003).

³ J. B. Fiveash, H. Murshed, J. Duan, M. Hyatt, J. Caranto, J. A. Bonner, and R. A. Popple, "Effect of multileaf collimator leaf width on physical dose distributions in the treatment of CNS and head and neck neoplasms with intensity modulated radiation therapy," *Med. Phys.* **29**, 1116–1119 (2002).

⁴ M. S. Ding, F. Newman, C. H. Chen, K. Stühr, and L. E. Gaspar, "Dosimetric comparison between 3DCRT and IMRT using different multileaf collimators in the treatment of brain tumors," *Med. Dosim.* **34**, 1–8 (2009).

⁵ J. H. Chang, K. M. Yenice, K. L. Jiang, M. Hunt, and A. Narayana, "Effect of MLC leaf width and PTV margin on the treatment planning of intensity-modulated stereotactic radiosurgery (Imsrs) or radiotherapy (Imsrt)," *Med. Dosim.* **34**, 110–116 (2009).

⁶ E. Abe, T. Mizowaki, Y. Norihisa, Y. Narita, Y. Matsuo, M. Narabayashi, Y. Nagata, and M. Hiraoka, "Impact of multileaf collimator width on intraprostatic dose painting plans for dominant intraprostatic lesion of prostate cancer," *J. Appl. Clin. Med. Phys.* **11**, 144–154 (2010).

⁷ J. Y. Jin, F. F. Yin, S. Ryu, M. Ajlouni, and J. H. Kim, "Dosimetric study using different leaf-width MLCs for treatment planning of dynamic conformal arcs and intensity-modulated radiosurgery," *Med. Phys.* **32**, 405–411 (2005).

⁸ Z. van Kesteren, T. M. Janssen, E. Damen, and C. van Vliet-Vroegindeweij, "The dosimetric impact of leaf interdigitation and leaf width on VMAT treatment planning in Pinnacle: Comparing Pareto fronts," *Phys. Med. Biol.* **57**, 2943–2952 (2012).

⁹ L. Wang, B. Movsas, R. Jacob, E. Fourkal, L. Chen, R. Price, S. Feigenberg, A. Konski, A. Pollack, and C. Ma, "Stereotactic IMRT for prostate cancer: Dosimetric impact of multileaf collimator leaf width in the treatment of prostate cancer with IMRT," *J. Appl. Clin. Med. Phys.* **5**, 29–41 (2004).

¹⁰ V. W. Wu, "Effects of multileaf collimator parameters on treatment planning of intensity-modulated radiotherapy," *Med. Dosim.* **32**, 38–43 (2007).

¹¹ T. Bortfeld, U. Oelfke, and S. Nill, "What is the optimum leaf width of a multileaf collimator?," *Med. Phys.* **27**, 2494–2502 (2000).

¹² E. Ludlum, G. W. Mu, V. Weinberg, M. Roach, L. J. Verhey, and P. Xia, "An algorithm for shifting MLC shapes to adjust for daily prostate movement during concurrent treatment with pelvic lymph nodes," *Med. Phys.* **34**, 4750–4756 (2007).

¹³ P. Xia, P. Qi, A. Hwang, E. Kinsey, J. Pouliot, and M. Roach, "Comparison of three strategies in management of independent movement of the prostate and pelvic lymph nodes," *Med. Phys.* **37**, 5006–5013 (2010).

Appendix L

Multi-adaptive Plan (MAP) IMRT to Accommodate Independent Movement of the Prostate and Pelvic Lymph Nodes

Ping Xia, Peng Qi, Jean Pouliot, and Mack Roach

Purpose: Concurrent irradiation of the prostate and pelvic lymph nodes is technically challenging due to treating one moving target and one immobile target. Real time planning would be an ideal method, but this method is not clinically feasible due to many technical and logistical challenges. The purposes of this project are to propose a new management strategy and to compare this strategy with the conventional isocenter shifting method using retrospectively created real time plans as a benchmark.

Methods/Materials: The proposed new management strategy, referred to as Multiple Adaptive Plans (MAP), is to create a pool of plans for several most likely prostate locations. Since the prostate often moves in the anterior/posterior and superior/inferior directions, for each patient, nine MAP plans are considered to accommodate prostate movements of 0.5 cm in one or two of these directions. Without requiring any additional hardware or software, the MAP strategy is to choose a plan from the pool that most closely matches to the “prostate position of the day”. This prostate position can be determined by dual image registrations: one aligned to the implant markers in the prostate and the other aligned to the pelvic bones. To validate effectiveness of this strategy, from treatment data of six patients, seventeen daily megavoltage cone beam CTs (MV-CBCT) that demonstrated large prostate movements of 0.4 cm to 0.8 cm were selected for this study. For each patient, based on the detected prostate movements, one of 9 MAP plans was retrospectively selected for treatment. The selected MAP plan was then applied to the corresponding MV-CBCT to calculate the dose delivery. Based on these MV-CBCTs, iso-center shifting plans and retrospective real-time plans were also created for these treatment days. Using these real-time plans as the benchmark, the recalculated MAP plans and the conventional iso-center shifting plans were compared in terms of dosimetric values of the prostate, pelvic lymph nodes, bladder, and rectum.

Results: Of these fractions, the MAP, iso-center shifting, and real-time planning techniques resulted in similar dose coverage to the prostate. Correspondingly, 95% of the prostate volume would receive a daily dose > 97% of the prescription dose in 15, 16, and 16 fractions. The above techniques would result in 95% of the pelvic lymph node volume receiving a daily dose > 97% of the prescription dose in 12, 6, and 13 fractions, respectively. The average doses to 5% and 50% of the bladder (D5, D50), relative to the planned endpoint doses, would be 93.7% (62.0%), 97.1% (63.2%), and 92.2% (62.9%), respectively. The average D5 (D50) of the rectum relative to the planned endpoint doses would be 92.9% (59.6%), 92.5% (58.7%), and 89.8% (55.8%), respectively.

Conclusion: Using of the MAP technique with 9 pre-created plans, which accommodate for independent prostate shifts, can achieve our treatment goals for the treatment of high-risk prostate cancer.

Impact: The proposed MAP strategy can be directly applied into clinical practice immediately although it may require extra effort in treatment planning. Our future research will seek a solution to minimize this planning effort.